12-2018

Longitudinal and Temporal Comparison of Beach Sand on the Rio Grande Delta System

Samantha B. Moore
The University of Texas Rio Grande Valley

LONGITUDINAL AND TEMPORAL COMPARISON OF BEACH SAND ON THE RIO GRANDE DELTA SYSTEM

A Thesis

by

SAMANTHA B. MOORE

Submitted to the Graduate College of
The University of Texas at Rio Grande Valley
In partial fulfillment of the requirements for the degree of

MASTER OF SCIENCE

December 2018

Major Subject: Ocean, Coastal, and Earth Sciences

LONGITUDINAL AND TEMPORAL COMPARISON OF BEACH SAND ON THE RIO GRANDE DELTA SYSTEM

A Thesis
by
SAMANTHA B. MOORE

COMMITTEE MEMBERS

Dr. Elizabeth Heise
Chair of Committee

Dr. Jude Benavides
Committee Member

Dr. Christopher Gabler
Committee Chair

December 2018

ABSTRACT

Moore, Samantha B., Longitudinal and Temporal Comparison of Beach Sand on the Rio Grande Delta System. Master of Science (MS), December, 2018, 88 pp., 3 tables, 23 figures, references, 33 titles.

The Rio Grande is the 5th longest river in North America and defines a significant extent of the United States-Mexico border. This study addresses how the composition of sand forming the Rio Grande river delta into the Gulf of Mexico at Boca Chica Beach is changed by input of additional sand transported northward by longshore current along the Mexican coastline. Second, we also investigated how the sand composition was modified going across the jetty from Boca Chica Beach to South Padre Island. We also verified the temporal relationship between the sands at Boca Chica Beach and South Padre Island. Detrital zircon geochronology was used to characterize the provenance of the sands. In general, most of the nine samples studied yielded U-PB age distributions that indicated a mixed Rocky Mountain and Mexican volcanic provenance signature. Six of eight sands were indistinguishable at 95% confidence from the Rio Grande River reference sample

DEDICATION

The completion of my master studies would not have been possible without the love and support of my family. My husband, Joe W. Moore III, my father, Mike Baker, my mothers, Luan Baker and Helen Baker, and my daughter, Sophia, wholeheartedly inspired, motivated and supported me to accomplish this degree. Thank you for your love and patience.

ACKNOWLEDGMENTS

I will always be grateful to Dr. Elizabeth Heise, chair of my thesis committee, for all her mentoring and advice. From research design, and data processing, to manuscript editing, she encouraged me to complete this process through her infinite patience and guidance. My thanks go to my dissertation committee members: Dr. Jude Benavides, and Dr. Christopher Gabler. Their advice, input, and comments on my dissertation helped to ensure the quality of my intellectual work.

I would also like to thank Dr. Marty Grove from Stanford University and Dr. David Kimbrough from San Diego State University for allowing me to use their machines to run my samples. Also, I would like to acknowledge the many volunteers, especially Romeo Rubiano and Isaiah Dorsey, for helping me collect samples throughout the length of my project. Lastly, I would like to thank Erick Tripp for helping with me creating GIS maps for my project.

TABLE OF CONTENTS

LIST OF TABLES

LIST OF FIGURES

CHAPTER I

INTRODUCTION

Overview of a Delta

Deltas are depositional structures formed under the dynamic conditions associated with river transport into a standing body of water. Deltaic morphology is influenced by geological setting, the flux of sediment delivery, the particle distribution of the sediment, hydrodynamic processes acting along the river/ocean interface, and many other factors (Woodroffe, 2003). Formation and growth of a delta requires that the flux of sediment down a river exceeds the rate of sediment removal by nearshore processes (Woodroffe, 2003). Rivers are the principal sources of sediment for most deltas, however the extent to which river processes dominate the geomorphology of a delta depends on the relative influence of tides and waves as well as the rate of coastal subsidence and the frequency and intensity of large storm events (Woodroffe, 2003). Formation of a large delta will cause the adjacent coastline to both prograde and subside. This implies that sediments must be delivered by the river faster than they are dispersed by waves, tides and ocean currents (Masselink and Hughes, 2003).

According to Galloway's classification of deltas, there are three different types of deltas (Masselink and Hughes, 2003). Figure 1 schematically illustrates Galloway's classification with examples of each type of delta. The first type of delta shown in Figure 1 are the fluvial-dominated deltas which are characterized by large catchments, river discharge into protected seas with minimal nearshore wave energy, and a small tidal prism. The second type are the wave-

dominated deltas characterized by the exposure to open-ocean swell. Wave processes shape deltas where fluvial dominance is reduced, either because of anthropogenic affects, or as part of a delta cycle where distributaries are abandoned (Woodroffe, 2003). Shore-parallel sandy ridges are characteristic of deltas that are subject to strong wave action (Woodroffe, 2003). Sand is moved alongshore and form spits where waves approach the shore obliquely (Woodroffe, 2003). The third type of delta are the tide-dominated deltas characterized by a tidal prism larger than the fluvial discharge. These types of deltas commonly occur along tectonically-passive trailing edge coastlines (Davis and Fitzgerald, 2004).

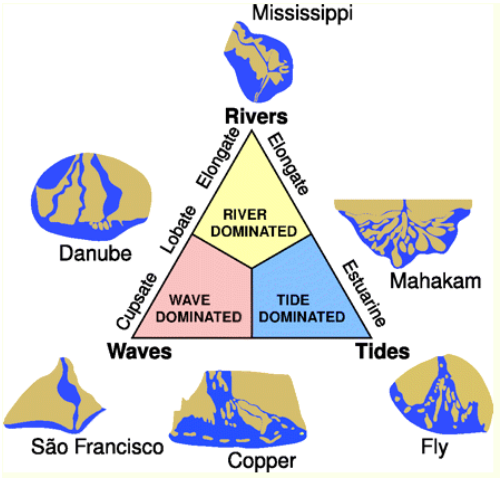

Figure 1 *Galloway's (1975) classification of fine-grained deltas, where the three main types are fluvial-, tide- and wave-dominated. Photo courtesy of Seybold et al., 2007*

Most deltas exhibit three morphological features: the delta plain, delta front and prodelta (Masselink and Hughes, 2003). The delta plain is the sedimentary platform that mantles recent coastal progradation, which is the growth of a river delta farther out into the sea over time. The delta plain consists of distributary channels that emanate from the trunk river, overbank environments, levees, crevasse splays and flood basins (Davis and Fitzgerald, 2004). The delta front is the active interface of the delta and the ocean. Most of the sediment from the distributary channels are deposited on the delta front, which then forms a distributary mouth bar. This entails

depositing the coarse sediment first (Masselink and Hughes, 2003). The morphology of the bar depends on the hydrodynamic behavior of the river effluent, and any modification caused by waves and/or tides. The prodelta is very far from the distributary mouth, so only fine grain sediments are deposited here (Masselink and Hughes, 2003). Not all deltas include a prodelta, and when present they are located in water depths beyond the regional wave base and are unaffected by tides (Masselink and Hughes, 2003).

It is important to note that Galloway's classification scheme is limited to medium to fine-grained sediment that forms all of the World's major deltas (Masselink and Hughes, 2003). Two types of deltas not included in Galloway's classification are fan- and braid-deltas. These are coarse-grained deltas, and consist of mostly gravels, cobbles, and boulders (Masselink and Hughes, 2003). These commonly occur on tectonically-active leading-edge coastlines (Davis and Fitzgerald, 2004). A fan delta is composed of the coarsest sediment, largely cobbles and boulders, and occur where a subaerial fan feeds directly into coastal waters. A braid delta is composed of a slightly finer and better sorted sediment mix, mostly largely gravels and cobbles, that is delivered by braided rivers that cross a narrow coastal plain before reaching the coastline (Masselink and Hughes, 2003).

Mississippi River Delta System

The Mississippi River delta system is one of the largest and well-studied in the United States. It drains a large catchment (over 3×10^6 km^2) and empties into the Gulf of Mexico. Wave energy is generally relatively low along the coast and tidal energy is almost completely overwhelmed by meteorological variations in water level (Woodroffe, 2003).

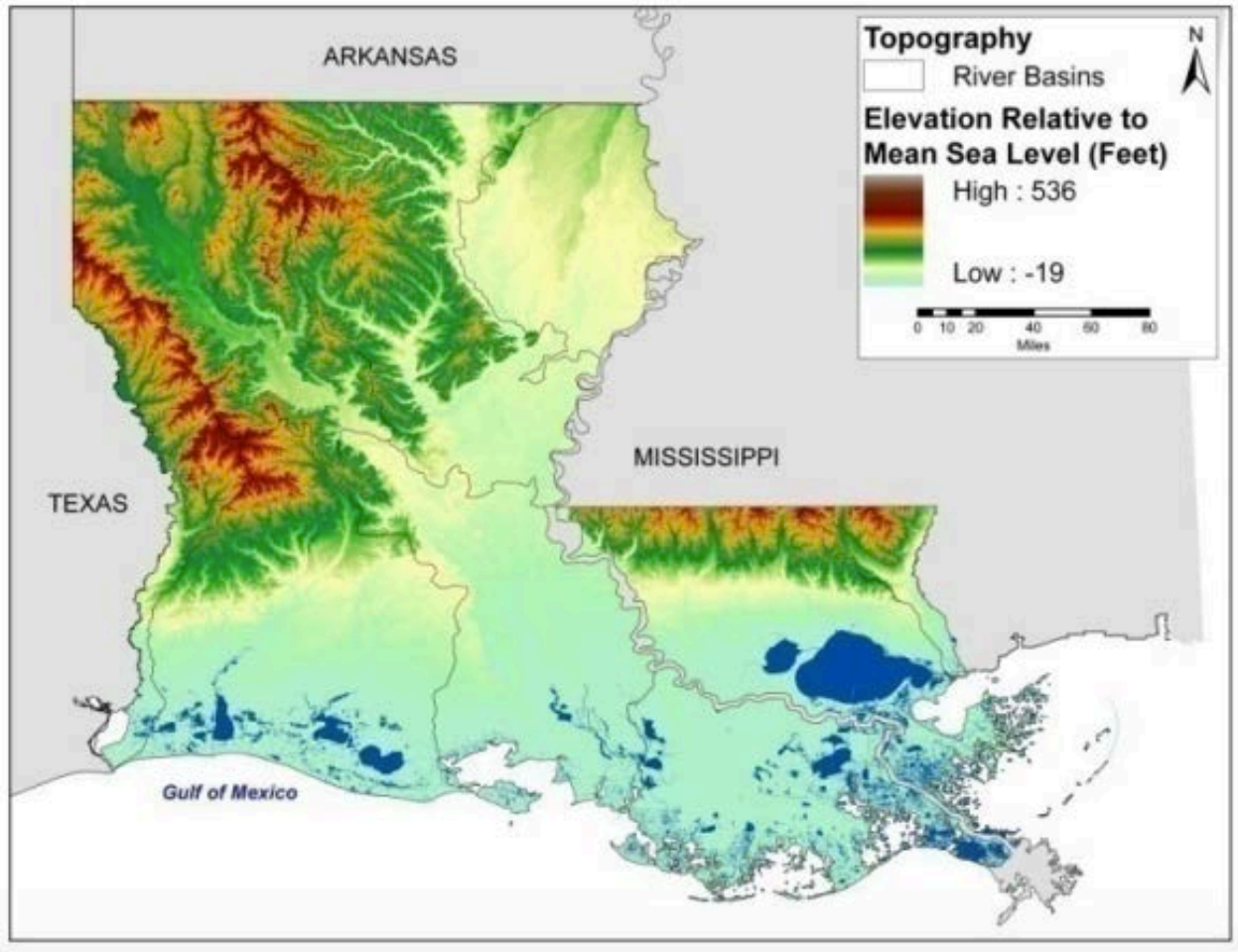

Figure 2 *Topographic map of Louisiana. Shows that the topography is dominated by several upland areas, river valleys, and the Coastal zone (Bolourchi and McHie, 2010)*

The geomorphology of the Mississippi River delta lobes and subdelta cycles provide an excellent example of the dynamic processes that can occur at the moths of a river-dominated delta (Woodroffe, 2003). Louisiana and areas along the coast in Texas and Mississippi are the seat of deltaic sedimentation accumulation for a long period of time, which makes it complicated to pinpoint the exact start date of the Mississippi River delta system (Russell and Russell, 1955). The sedimentation of the delta results in a characteristic pattern consisting of: "(1) a framework of natural levees, with associated channel and crevasse deposits; (2) within this framework,

deposits of the marshes, lakes, and bays; (3) an outer margin of beach and bar deposits; and (4) deposits of the open Gulf beyond" (Russell and Russell, 1955).

It is difficult to pinpoint exact when the Mississippi River delta was initiated because the coastal regions of Mississippi, Louisiana and Texas have been the site of deltaic sedimentation accumulation throughout the Cenozoic (Russell and Russell, 1955). The ancient (Pleistocene) Gulf Coast featured two main types of sedimentation. The first sediment transport mode was glacially triggered. After a long period of erosional stability in the Gulf of Mexico watershed throughout the late Cenozoic, glaciation events that began in the Pleistocene caused streams to carry heavy loads of gravel and other sediment to the ocean. This heavy sediment flux overloaded the streams and caused them to evolve by branching so that the large flux of sediment could be more efficiently transported to the Gulf (Russell and Russell, 1955). The second type of sediment transport features fine-grained sediment. These are typified by the Mississippi River and its distributaries that meander and overflow their banks through crevasses during major floods to supply sediment to the intervening interdistributary bays (Woodroffe, 2003).

During recent geologic time and the accompaniment of the last rise in sea-level, the configuration of the Mississippi River delta system has changed rapidly through time (Russell and Russell, 1955). This dynamic behavior is due to the fact of limiting distributaries that extend from an apex at the junction of the Red and Mississippi Vermillion River and Bay on the west (Fig. 2). The active channel deposits primarily consists of fine sand and some coarser detritus. The average grain size and degree of sorting varies, especially at high-water stages. In the low-water stages, areas within active channels become loaded with well sorted sand (Russell and Russell, 1995). Areas farther away from active channels, such as marshes and stagnant bays, tend to have a concentration of finer grained silt and mud (Russell and Russell, 1995).

Rio Grande River Delta System

The Rio Grande flows along the border between southwestern Texas and northern Mexico and is the 5th longest river in North America (Benke and Cushing, 2005). The overall river is 2830 km long and drains a significant portion of the southern Rocky Mountains of New Mexico and southern Colorado, western Texas, and northeastern Mexico. The headwaters of the Rio Grande begin at Stony Pass, elevation 3838 m in the San Juan Mountains of south-western Colorado (Ewing and Gonzalez, 2016). Before 1850, the river flowed naturally into the delta region and begins as a clear spring- and snow-fed mountain stream (Benke and Cushing, 2005). After entering New Mexico, the river bisects the state and then flows in a generally south-eastern direction, it forms the shared border between Texas and Mexico before it empties into the Gulf of Mexico near Brownsville, Texas (Benke and Cushing, 2005). Along the way, the river picks up additional waters from the Sangre de Cristo Mountains, Rio Conchos, the Pecos River, runoff from the Sacramento Mountains area, Devils River, several short streams, the Rio Salado, and the Rio San Juan (Ewing and Gonzalez, 2016). Thus, the river derives its water flow from mountains in the north, in the west, and the southwest (Ewing and Gonzalez, 2016).

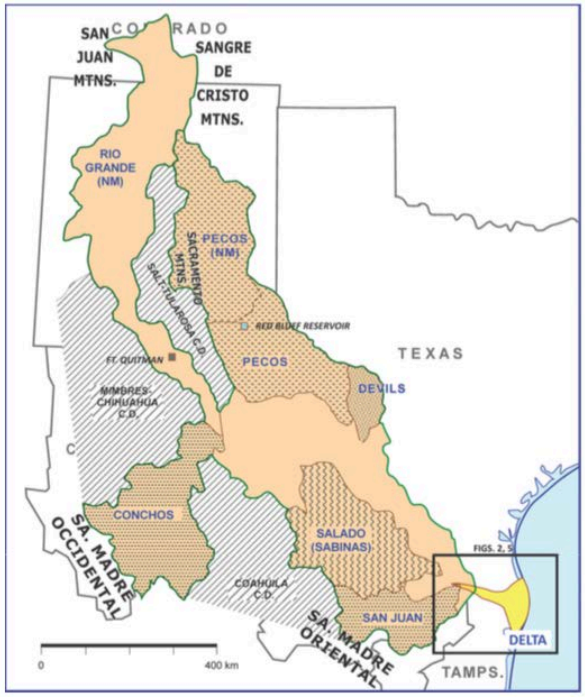

Figure 3 *Drainage areas of the Rio Grande/Rio Bravo delta system. Ewing and Gonzalez, 2016*

As the Rio Grande flows, it goes through seven physiographic provinces including the Southern Rocky Mountains (SR), Colorado Plateau (CO), Basin and Range (BR), Great Plains (GP), Coastal Plain (CP), Sierre Madre Occidental (SC), and Sierra Madre Oriental (SO) (see Fig. 3; Benke and Cushing, 2005). Historically, the Rio Grande in the southern part of New Mexico was a pebbly sand bedload stream. Presently sand and silt predominate because coarser sediment is trapped within the Elephant Butte Dam (Benke and Cushing, 2005). With the additions of dams, diversions, weirs, and reduced flow caused by agricultural diversions, the Rio Grande is one of the most impacted rivers in the world (Benke and Cushing, 2005).

Rio Grande Delta

The Rio Grande delta (also referred to as the Rio Bravo in Mexico) was constructed along the coast of the southernmost Texas and northern Tamaulipas (Figure 3). The modern delta formed primarily between 8000 and 3000 years BP as a result of a large sediment flux carried by

the Rio Grande during the Holocene Climatic Optimum (Ewing and Gonzalez, 2016). It is presently one of the major deltas of North America (Ewing and Gonzalez, 2016). In spite of this, comparatively little sedimentologic research has been performed on the Rio Grande delta due to a combination of factors that include the difficulties of working across borders on an international stream (Ewing and Gonzalez, 2016). Presently, more than 600,000 people inhabit the Holocene delta and river plain (Ewing and Gonzalez, 2016).

The Rio Grande Delta Basin is extensive, covering over 360,000 km^2 (Fig. 4). Note that over half of the delta lies south of the present Rio Grande drainage (i.e., within Mexico; see Fig 4). The Holocene delta begins west of San Benito, Texas. At the longitude of Harlingen, the Holocene plain widens with numerous inactive distributaries marking the transitional zone to the Rio Grande Delta (Fig. 4; Ewing and Gonzalez, 2016). Further east, within ca. 50 km of the Gulf Coast, delta plain deposits occur for some 110 km in a north-south direction (Ewing and Gonzalez, 2016). The highly meandering old river channels, known locally as *resacas*, are bounded by sand-rich levees, and lie 3-5 m topographically above the surrounding interchannel areas. At the eastern side of the delta plain, a continuous shoreline and dune system marks the edge of the Gulf of Mexico (Ewing and Gonzalez, 2016). Strong and nearly continuous south-southeast prevailing winds move sand from south to north, around the protruding delta towards the convergence zone in central Padre Island to the north of the area (Ewing and Gonzalez, 2016).

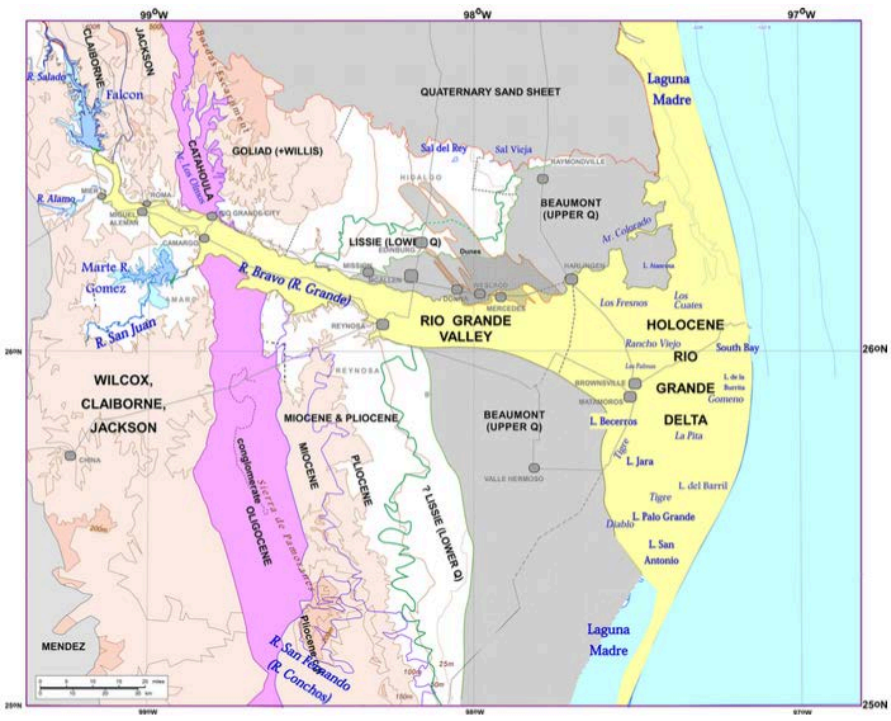

Figure 4 *Physiography and geologic systems of the Rio Grande Delta and the Lower Rio Grande Valley. Map from Ewing and Gonzalez, 2016*

Morphologically, the Rio Grande delta itself can be divided into two topographic domains, the upper and lower delta plain. The upper delta plain is an extension of the valley floodplain (Ewing and Gonzalez, 2016). The *resacas* are very prominent in this area and are the most distinctive part of the delta. Mainly because they are highly sinuous meandering channels (like the Rio Grande) sitting on a high sand-rich meanderbelt levee (Ewing and Gonzalez, 2016). The lower delta plain is geomorphically similar to the upper delta plain, except in general the land level is distinctly lower in elevation (Ewing and Gonzalez, 2016). Rather than *resacas* the interchannel areas in the lower delta plain are occupied by large shallow ephemeral lakes referred to as *esteros* (Ewing and Gonzalez, 2016). Most of these lakes are saline or brackish, and when they dry out they form expansive mudflats. Currently, more research is essential for the delta history as a whole.

Anthropogenic Impacts on the Rio Grande Delta System

The Rio Grande is one of the most impacted rivers in the world, and both water-quantity and water-quality issues are major concerns (Benke and Cushing, 2005). Numerous settlements were found along the Rio Grande in New Mexico by Spanish conquistadors in 1540 (Benke and Cushing, 2005). The region along the Texas-Mexico border showed a long history of human habitation as well. In 1598 Don Juan de Onate began settlements along the Rio Grande in the El Paso area (Benke and Cushing, 2005). Settlements developed along the river valley until 1680, when a Pueblo revolt drove the Spanish out of the upper Rio Grande (Benke and Cushing, 2005). By 1749 settlements established Reynosa, Camargo, and Mier by Jose de Escandon (Ewing and Gonzalez, 2016).

By the early 1800s Spanish control started to weaken throughout the region and permitted the onset of Anglo-American colonization began in Texas (Benke and Cushing, 2005). In 1836, Texas declared independence and claimed the Rio Grande from mouth to source (Benke and Cushing, 2005). At this time, the United States set up a fort opposite Matamoros, that is now known as Fort Brown (Ewing and Gonalez, 2016). While this fort was subsequently besieged by a Mexican army, two subsequent battles (Palo Alto and Resaca de la Palma) led to the defeat of the Mexican forces and ended the siege. As a result, Mexico conceded that the Rio Grande represented the boundary with Texas in the Treaty of Guadalupe Hidalgo in 1848. This agreement ended the Mexican War (Benke and Cushing, 2005).

Prior to 1904, land adjacent to the Rio Grande River was mostly used for ranching and limited agriculture including sugar cane plantations. Extension of the railroad to Brownsville ultimately connected the Rio Grande Valley with regions to the north (Ewing and Gonzalez, 2016). This development prompted towns and irrigation projects to sprout along the tracks. In

Texas, companies built steam operated pump houses to divert water from the Rio Grande River to their ranches, which could be miles away (Ewing and Gonzalez, 2016). Mexican irrigation was delayed by the revolution and its aftermath. However, by the 1930s, the Secretario de Recursos Hydraulicos began construction of two immense irrigation districts; one using water from Rio Bravo, and the other using water from Rio San Juan (Ewing and Gonzalez, 2016).

Flooding within the Rio Grande Valley has long been a major concern, especially since it had the potential to submerge large tracts of the Valley floor. To address this concern, a system of floodways was designed and built in 1924-1931 (Ewing and Gonzalez, 2016). On the Mexican side, a large set of dams was built to trap floodwaters, and a floodway designed to release them safely (Ewing and Gonzalez, 2016). On the Texas side, the floodways used the Arroyo Colorado as a natural drain, but added a 'North Floodway' from Mercedes to Raymondville then east (Ewing and Gonzalez, 2016).

Brazos Santiago Pass has been the subject of numerous studies by the U.S. Army Corps of Engineers. Studies have been recorded as early as in the 1850s and continuing to the present. These early studies monitored changes in width and depth of the natural channel and Laguna Madre (Morton and Pieper, 1975). As a result of these studies, jetty construction was proposed as the only means of maintaining a natural channel (Morton and Pieper, 1975). Construction began in the late 1920s (Meyer-arendt, 1987) and by 1936, a deep-water ship channel was built inland from the pass at Brazos Santiago towards Brownsville, now called the Brownsville Ship Channel (Ewing and Gonzalez, 2016). This 27-km long channel has been steadily deepened throughout the years, and is now at 13 m navigation depth (Ewing and

Figure 5 *The jetties in Isla Blanca Park on South Padre Island. Photo courtesy of Romeo Rubiano, 2015.*

Gonzalez, 2016). The Brownsville Ship Channel affected the connections from the Laguna Madre to the *esteros* of the Texas portion of the delta, which caused a number of the *esteros*' to become nearly dry (Ewing and Gonalez, 2016). The Lower Rio Grande Wildlife Refuge has recently started to restore those connections.

U.S. and Mexico signed a Water Treaty in 1944, and charged the International Boundary and Water Commission to construct a mainstream dam to regulate floods and water supply (Ewing and Gonzalez). Falcon Dam and a reservoir was constructed, and opened in 1953, and Amistad Dam in 1969 (Benke and Cushing, 2005). Along the Rio Grande, 5 dams have been built. The two mentioned above in the lower portion of the Rio Grande, in 1975 the Cochiti Dam was built in New Mexico (Benke and Cushing, 2005). Where the river then flows to the Elephant Butte Reservoir, completed in 1916, which happens to be the largest reservoir in New Mexico (Benke and Cushing, 2005). The Rio Grande flows south out of the Elephant Butte Reservoir to Caballo Reservoir (Benke and Cushing, 2005). The river continues south where it flows to Amistad and Falcon Dams. With all of the human impacts on the river, the Rio Grande failed to reach the Gulf of Mexico in much of 2002 and 2003 (Benke and Cushing, 2005). Also, the mouth of the river has been closed several times by sand bars transported south to north during times of low streamflow (Ewing and Gonzalez, 2016). Thus, the delta area has been extensively modified by human activity, which disrupted the natural stream flow and ecosystems (Ewing and Gonzalez, 2016).

Figure 6 *Falcon Dam and reservoir on the lower Rio Grande. Photo courtesy of Chronicle File.*

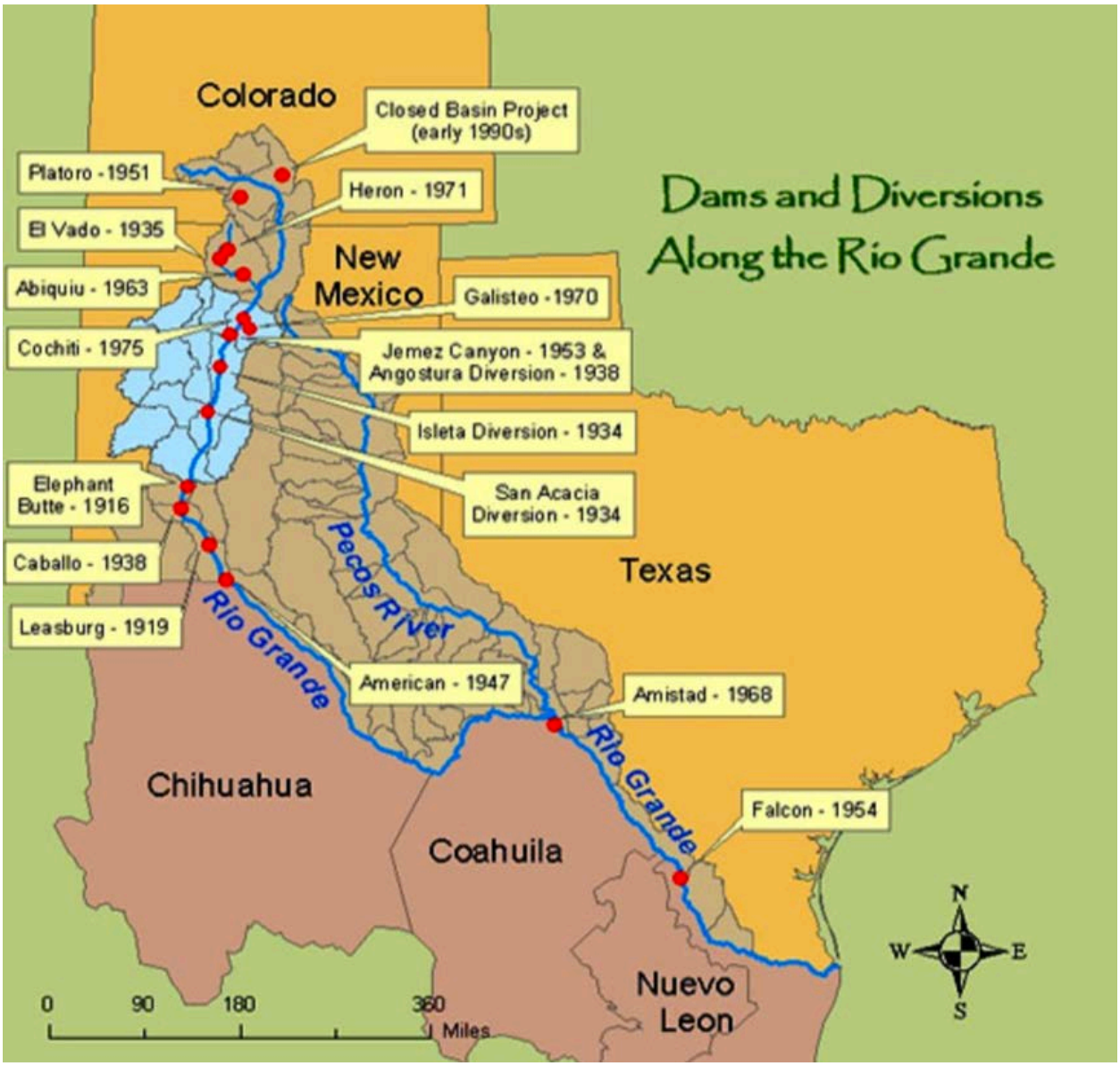

Figure 7 *Dams and diversions along the Rio Grande River. Map courtesy of Annenberg Learner.*

CHAPTER II

GOALS AND METHODS OF THE STUDY

Questions to be Addressed

The goals of this study were to evaluate anthropogenic effects upon the nature of sediment that occurs along the interface between the Rio Grande Delta and the Gulf of Mexico. Specific questions included:

(1) Was sand present on Boca Chica Beach immediately northeast of the present-day Rio Grande river mouth primarily derived from the Rio Grande River or from northeast-directed longshore sediment transport from Mexico?

(2) Is there a contrast in sedimentary provenance of the sand across the Jetties lining Brazos Santiago Pass between Boca Chica Beach and South Padre Island?

(3) Was the sand originating from Boca Chica Beach, dredging of the Brownsville Ship Channel, or erosion from the jetty itself helping to contribute to the composition on South Padre Island?

Question (1) was tested by obtaining river sand from the Rio Grande River, sand representative of that being transported northeastwards along the Mexican coast (Playa Bagdad), modern beach sand and sediment cored from Boca Chica Beach. Questions (2) and (3) were addressed by sampling additional sand excavated from the Brownsville Ship Channel, and by sampling modern beach sand and coring sediment from South Padre Island. The acquired sand samples

were characterized morphologically. Detrital zircon was extracted from the heavy concentrate of these sands and analyzed using laser ablation, inductively coupled plasma mass spectrometry (LA-ICP-MS) to assess sediment provenance. The latter is accomplished by using the measured U-Pb age distributions to "fingerprint" the provenance signal of the sands (e.g., Gehrels, 2012).

Sample Locations

Table 1 *Sample locations, site names, GPS coordinates, and sample masses*

Sample	Location	Site Name	Depth of sample	GPS Coordinates	Weight A (kg):	Weight B (kg):	Weight C (kg):
1	South Padre Island	Edwin King	Top of core	N 26° 11.396' W 097° 10.513'	0.4488	0.4606	
2	South Padre Island	Edwin King	Bottom of core ~15ft	N 26° 11.396' W 097° 10.513'	0.5307	0.5344	
3	South Padre Island	Isla Blanca Park-jetties	Surface sand	N 26° 04.344' W 097° 09'15.45"	0.33	0.2686	
4	Boca Chica Beach	Beach near Brazos Santiago Pass	Surface sand	N 26° 03.840' W 097° 09.022'	0.6253	0.5609	
5	Boca Chica Beach	Beach midpoint	Surface sand	N 26° 00.109' W 097° 09.050'	0.5572	0.5092	
6	Boca Chica Beach	Beach near mouth of Rio Grande	Surface sand	N 25° 57.396' W 097° 08.870'	0.5568	0.6328	
7	Boca Chica Beach	Beach near mouth of Rio Grande	Top of core	N 25° 57.396' W 097° 08.870'	0.4401	0.4528	
8	Boca Chica Beach	Beach near mouth of Rio Grande	Bottom of core ~15 ft	N 25° 57.396' W 097° 08.870'	0.6971	0.371	
9	Mexico	Playa Bagdad	Surface sand	N 25° 49.429' W 097° 09.119'	0.5076	0.4751	
10	Mexico	Rio Bravo	Surface sand	N 25° 50.981' W 097° 26.146'	0.6121	0.58	
11	Brownsville	Brownsville Ship Channel	Surface sand	N 26° 0'33.24" W 097° 16'30.74"	0.5613	0.5244	0.58

Table 1 summarizes details pertaining to the 11 samples collected for this project. Figure 8 is an image created in ArcGIS that shows the locations of the entire study area. Figure 9 is an image created from ArcGIS that shows the locations of the samples collected from the modern

Rio Grande River channel (Rio Bravo) and from along the Mexican coast (Playa Bagdad). Also shown are collection locations from Boca Chica Beach. Note that these are distributed between the mouth of the modern Rio Grande River and the jetties at Brazos-Santiago Pass. Figure 10 is a ArcGIS map that shows sample locations across Brazos-Santiago Pass while Figure 11 illustrates the location of sand from South Padre Island.

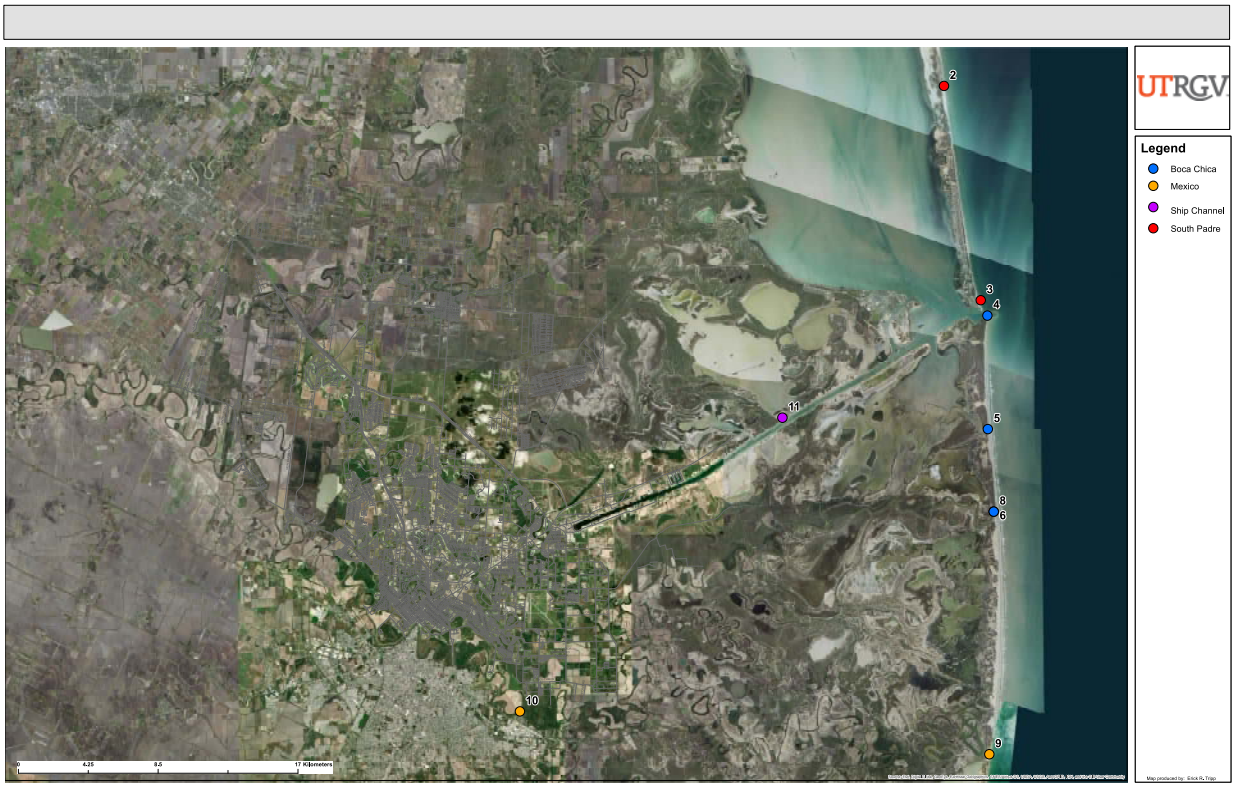

Figure 8 *Sample locations for the entire study. See Table 1. Map created by Erick Tripp*

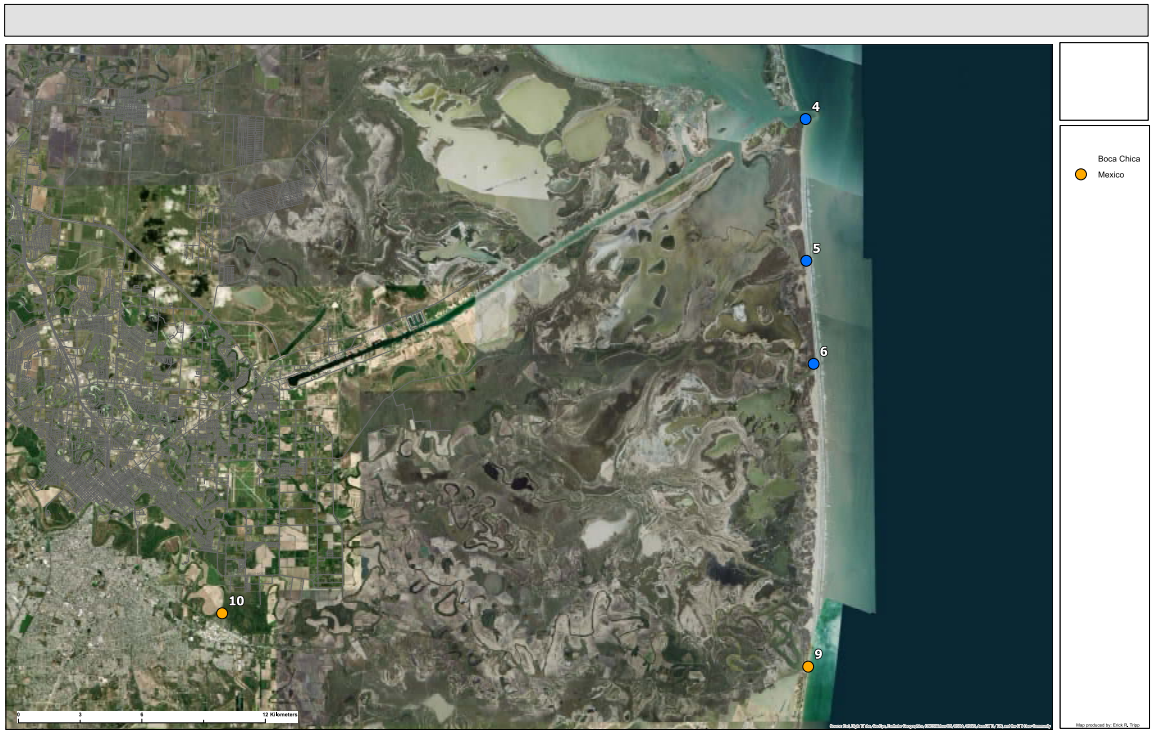

Figure 9 *Sample locations selected to address the provenance of sand on Boca Chica Beach. The yellow pins are in Mexico, and the red pins are Boca Chica Beach*

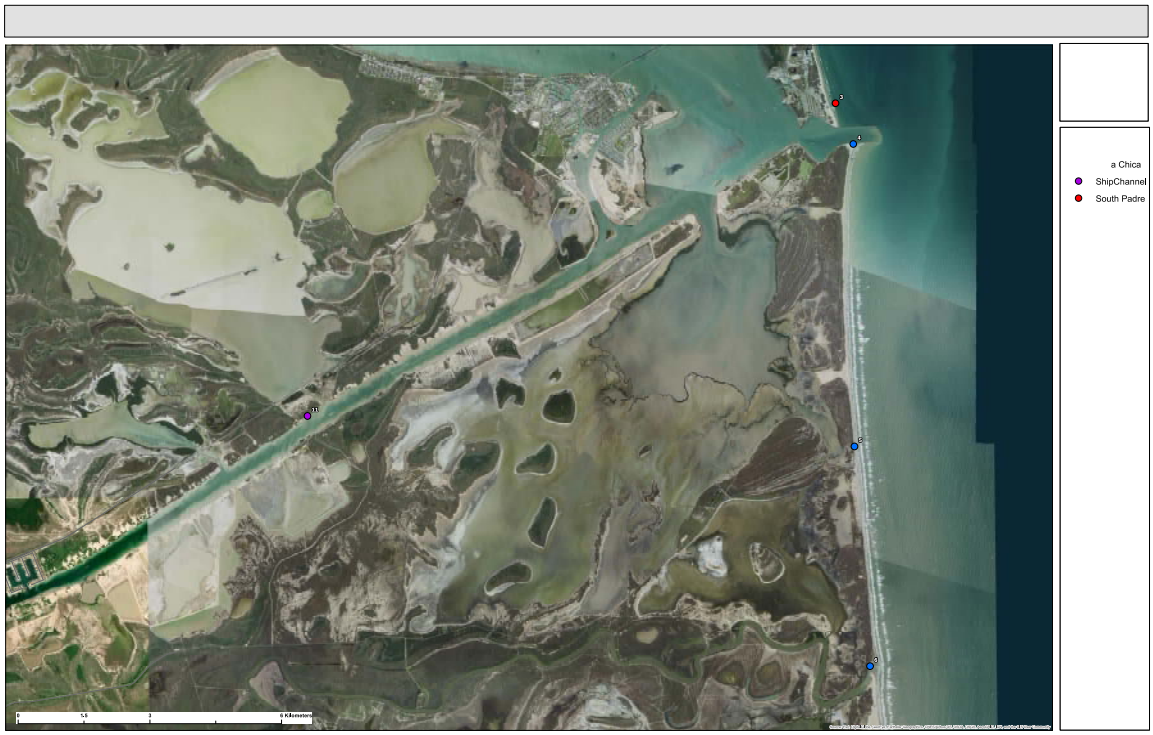

Figure 10 *Sample locations straddling Brazos Santiago Pass.*

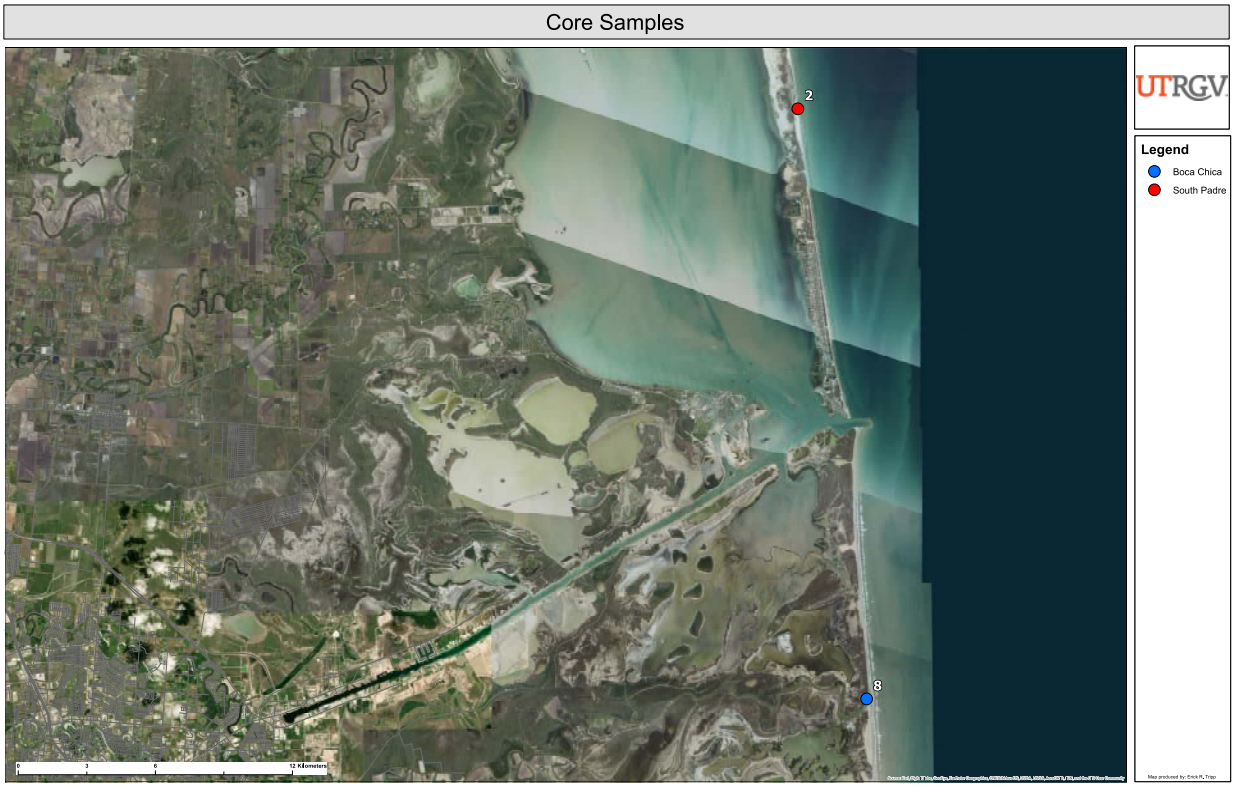

Figure 11 *Sample locations from Boca Chica Beach and South Padre Island where both surficial sand and cored sediment was obtained.*

Methodology

Collection of Surficial Samples

A hand-held GPS device was used to record the latitude and longitude of all samples. At each location, a scoopula was used to fill two sample bags which were then securely fastened at the top to prevent cross contamination (Fig. 12). With the Vibracorer samples, a sample was taken from the top of the core sample and from the bottom (see below).

Figure 22 *Surface sand samples collected at Boca Chica Beach.*

Sediment Coring

Sediment coring is a very valuable technique for the collection of subsurface information. The approach offers the means of acquiring sediment cores, as well as installing instrumentation in observation wells such as neutron moisture-meter access tubes and other types of point sampling devices (Shuter and Teasdale, 1989). The method is generally restricted to the drilling of unconsolidated materials or softer rocks (Shute and Teasdale, 1989). The drill responds differently in different types of lithologies which helps determine the type of sediment the drill is able to efficiently penetrate. In sand, drilling is relatively easy with a fast penetration rate. In sand and gravel, there may be a slight reduction in the penetration rate depending on the gravel size. In silt, silty clay, or clay the drilling rates slow down because of the stronger coupling of the auger with the more cohesive sediment (Shuter and Teasdale, 1989).

Below is the list of materials used for sampling collection:

1. WINK Vibracorer Drill
2. 6.5 h.p. Honda Motor
3. Flex Cable
4. Snipes
5. Tools (hammer, pipe wrenches, etc.)
6. Sample Tubes/Bags
7. Sample Caps
8. Gin Pole hoisting and pull-down system
9. Global Positioning Unit (GPS)
10. Rite-in-Rain Notebook
11. Safety Gear (hard hat, steel toed boots, googles, gloves, etc.)

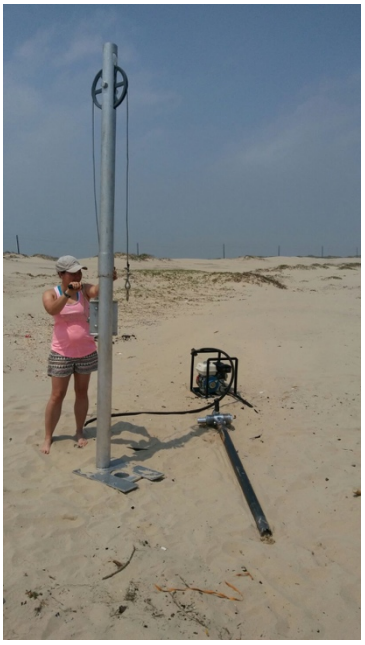

Figure 13 *Getting ready to hoist the Vibracorer to shake out the sample into a sample collection bag. Photo courtesy of Leticia Contreras, 2017.*

Although simple hand auger drilling is one of the best and economical form of methods for collecting uncontaminated samples (e.g., Fig 14), only shallow bore holes are feasible (Shuter and Teasdale, 1989). The Vibracorer was chosen for this study because of its demonstrated ability to efficiently penetrate a variety of substrates to greater depths (Fig 13). The WINK Vibracore Portable Drill was inventd by Fred Wink in 1981 is small, lightweight, simple to operate, and is widely employed by drilling industry for shallow penetration test holes. Just like the hand-operated auger, the Vibracorer can collect undisturbed core samples (vibracorer.com) The device uses vibration energy created from a 6.5 horsepower Honda engine to generate 7,000 to 12,000 acoustic vibrations per minute. This energy is transferred to the drill string. Since the Vibracorer works by vibration, instead of rotation or percussion as the hand auger, there is no need for drilling fluids, which contaminates the sample (vibracorer.com). The Vibracore drill system is very versatile and efficient. It can be used in many different types of sediment sampling; such as investigation of lake, river stream, delta and estuary sediments, tailings ponds investigations, sludge pond sampling, and dredging (vibracorer.com).

Figure 14 *Left photo: Former students using a hand auger. Photo courtesy of Dr. Elizabeth Heise. Photo on right: WINK Vibracorer. Photo courtesy of vibracorer.com*

The two sample sites, Boca Chica Beach and South Padre Island, were picked because of their placement in the Rio Grande delta system. Boca Chica Beach is located in the Lower Rio Grande Valley, where a secluded coastal environment is interspersed with miles of beach front, saline flats, mangrove marshes, shallow bays and unique dunes of wind-blown clay known as 'lomas' (U.S. Fish and Wildlife Service). The beach itself is only eight miles long and is protected by state and federal authorities as part of the Lower Rio Grande Valley National Wildlife Refuge (Oko, 2013). The City of South Padre Island, TX is located on the southernmost portion of the island approximately 13 kilometers north of the mouth of the Rio Grande. The city is approximately 8 kilometers long and 0.8 km wide at the widest points (Heise et al., 2008).

Figure 15 *Boca Chica Beach. Top picture is of the Gulf of Mexico. Bottom left is of the Vibracore and sand dunes. Bottom right- core samples from the Vibracore near the mouth of the river at Boca Chica Beach.*

The Vibracorer location on Boca Chica Beach was picked because of its proximity to the mouth of the river (Rio Grande River). Edwin King County Park on South Padre Island was picked because of its location outside of the city limit. The drill was set up by attaching the shoe bit to the bottom of the core barrel, the drill head was then attached and one end of the flex cable was added on. The other end of the flex cable was attached to the generator and then turned on. A test drill was performed first and was left about three quarters of the way into the ground to be used as an anchor for the wrench and pulley system. The drill head was detached from the core barrel and reattached on a second core barrel that was set up the same exact way as the test drill with the exception that a side ejector was also added. The drill was then sent down and measured periodically through the side ejector. Once the side ejector was submerged in the ground, another core barrel was added to the drill. Once the drill had gone down into the earth as far as it would

go or approximately 4.5 m (15 ft) the generator was turned off, and the flex cable was removed from the drill head. The wrench and pulley system was set up over the test drill core barrel. The drill was then pulled up out of the ground and unattached from the bottom as it was brought out. When the side ejector was removed, the flex cable was added back to the drill head. The core barrel was then pulled all the way out of the ground and the drill shoe was removed. A plastic sample bag was placed at the bottom of the barrel, and the drill was turned back on so that the sediment would shake out of the barrel and into the bag. The sample bag was then tied up and labeled. The rest of the drill was then taken apart and cleaned for the next drilling location. The methodology was adapted from the Wink Vibracorer manual to suit our needs on a beach.

Geochronology

U-PB geochronology was performed at the UA Laserchron Facility. Detrital zircon geochronology is a very powerful tool for determining the provenance and maximum depositional age of classic strata (Gehrels et al, 2006). This approachhas applications in structural geology, tectonics, stratigraphy, paleontology, and geochemistry. Zicron is a common accessory phase in igneous rocks and naturally contains radioactive ^{238}U, ^{235}U, and ^{232}Th (Faure and Mensing, 2005). As indicated in Figure 16, U-Th-Pb geochronology is based upon radioactive decay of multiple parent isotopes to different stable isotopes of Pb (Schoene, 2014). The U-Pb system is based upon the decay of U and Th to Pb, as follows:

$^{238}U \rightarrow {}^{206}Pb^*$ with half-life of 4.468 Ga
$^{235}U \rightarrow {}^{207}Pb^*$ with half-life of 0.704 Ga
$^{232}Th \rightarrow {}^{208}Pb^*$ with half-life of 14.01 Ga
(Gehrels, 2010)

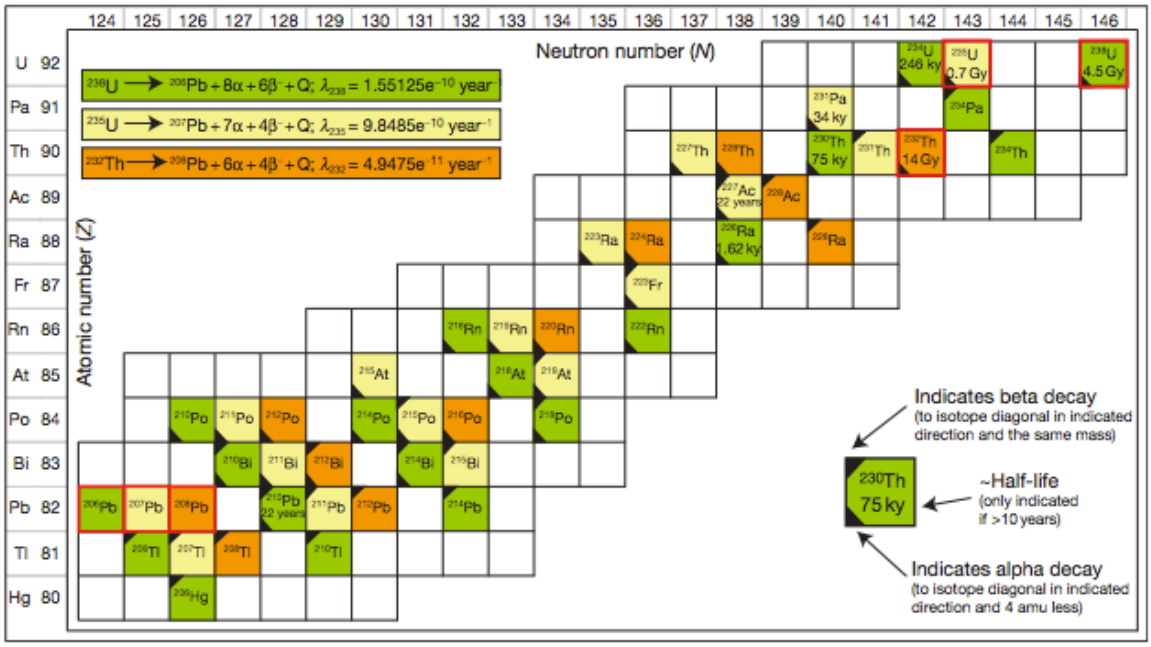

Figure 16 *An illustration of the U-Th-Pb decay chains. Each isotope occurring is color coded to its parent isotope, which are outlined in red. The stable daughter isotopes of Pb are also outlined in red. Photo courtesy of Schoene, 2014*

U and Th do not decay directly to Pb, but instead follows a sequence of alpha and beta decays that create a series of intermediate daughter isotopes, and always lead to the same stable isotope of Pb (Fig. 16; Shoene, 2014). Paired decay of ^{238}U and ^{235}U is particularly powerful because independent measures of U-Pb age are obtained that permit the concordance of the results to be assessed.

Zircon ($ZrSiO_4$) is a powerful mineral for U-Th-Pb geochronology because of the following properties (Schoene, 2014):

- High U concentration (commonly 100-1000 ppm)
- Moderate Th concentration (commonly 10-100 ppm)
- U and Th are tightly held
- Low common Pb during crystallization (ppt)
- Grows at 600-1100°C but retains Pb to >800°C
- Common in felsic and intermediate igneous rocks
- Chemically and mechanically resistant
- Contains other elements that yield complementary information

The abundance of detrital zircon in clastic sedimentary rocks combined with its resistance to chemical and physical weathering, contributes to the popularity and prolificacy of the U-Pb system for geochronology performed with sedimentary rocks (Gehrels, 2012).

The detrital zircons analyzed in this study were concentrated from the unconsolidated sands using a variety of hydrodynamic, magnetic, and density methods. Zircon (which has a density of 4 $^{g}/_{cm^3}$) behaves much differently than most common rock-forming minerals (Simpson et al., 2012). Low density minerals were removed from the sample by using a Gemini water table that operates on principles similar to gold panning. After drying the sample in an oven maintained at 50°C, ferromagnetic minerals such as magnetite and pyhrrotite were removed with a hand magnet. Lower magnetic susceptibility (paramagnetic) minerals were then removed using a Frantz Magnetic Separator using a setting of 0.7 Amp, 5° side tilt, and 20° forward tilt. Finally, minerals denser than 3.28 $^{g}/_{cm^3}$ were concentrated using heavy liquid (diiodemethane) with the aid of a separation funnel.

The steps outlined above yielded a highly concentrated aggregate of zircon for all of the samples investigated based upon observations performed with a 10x binocular microscope.

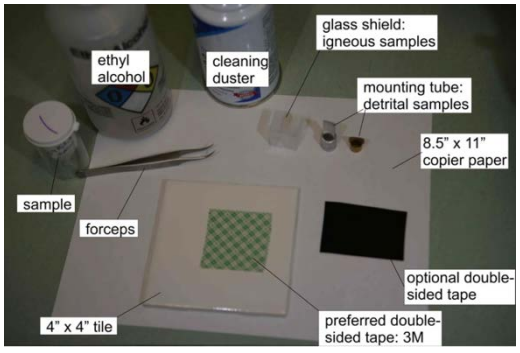

Figure 17 *Materials needed to mount the samples. Photo courtesy of Pullen and Pepper, 2009*

Aliquots from each of the zircon concentrates were mounted on double-sided sticky tape together with primary and secondary standards and potted in epoxy to from 1" diameter sample mounts (Gehrels, 2010) (Fig 17). Standard zircon SL (Sri Lanka standard zircon with a 564 Ma; Bernhardt, 2011) and secondary standard zircon R33 were added to the mounts to standardize the U-Pb measurements (e.g., Pullen and Pepper, 2009). The mounting techniques employed were designed to sample zircon that was

unfractionated according to size of shape (e.g., Gehrels et al., 2006). The surface of the epoxy plug is polished down with grit sandpaper to the point where two-thirds (2/3) of the average grain was preserved. A final polish is produced with a micron lapping film.

In this study, we employed Laser-Ablation Inductively Coupled Plasma Mass Spectrometer (LA-ICPMS) methods that permit rapid determination rapid determination of U-Th-Pb ages with micron-scale spatial resolution (Gehrels et al, 2006). Geochronologic analyses are conducted by ablating micron size particles from zircon using an Excimer (λ = 193 nm) laser and analyzing U-Th-Pb isotopes with a multi-collector ICPMS instrument (Fig. 18; Gehrels et al, 2006).

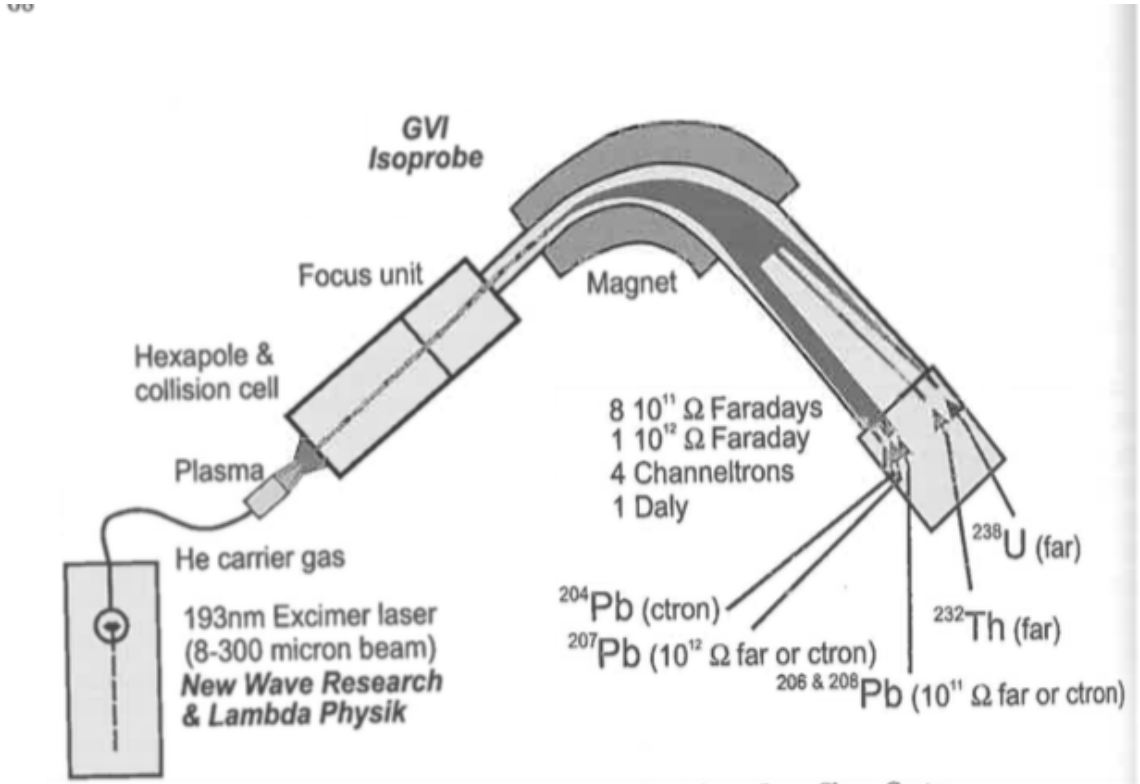

Figure 18 *Arizona LaserChron Centers Laser-Ablation Multicollector ICP Mass Spectrometry (LA-MC-ICPMS). This is a schematic of the Isoprobe showing the main compenents of the instrument. Photo courtesy of Grehels et. al, 2006*

The LA-MC-ICPMS was first applied to U-Pb geochronology in the 1990s, and the fundamental design of the instrumentation has changed little since that time (Gehrels et al, 2006). This method of U-Pb measurement is preferred for detrital studies because of its rapid analysis time, and affordability relative to other methods (Shoene, 2014) (Fig 18). Measurement of accurate $^{206}Pb/^{207}Pb$ and $^{206}Pb/^{204}Pb$ is relatively straightforward because of the limited fractionation of Pb isotopes during laser ablation and plasma ionization (Gehrels, 2010). The primary challenges in determining the ratios are as follows:

- Determination of $^{206}Pb/^{207}Pb$ with sufficient precision to determine a useful age, especially for young samples where ^{207}Pb abundance is relatively low,
- Generation of a ^{204}Pb signal that is of sufficient intensity that can be measured reliably.
- Reduction of Pb and Hg backgrounds such that small Pb signals can be measured accurately. (Gehrels, 2010).

The LA-CM-ICPMS is a two-part process (Fig. 18): (1) the laser ablation system, and (2) the ICPMS (Shoene, 2014). The sample is ablated inside a sample cell with a laser transparent window. A He carrier gas sweeps ablated particles from the cell to the plasma torch of the ICPMS instrument. Once instrument settings are optimized, samples are analyzed by standard-sampling bracketing (Gehrels, 2010). In this study, the sequence began with five standards, followed by one standard in between three to four unknown samples (with secondary standards being analyzed between each unknown), and three standards at the end of the sequence (Gehrels, 2010). Figure 19 below shows the typical signal intensities during a laser ablation analysis.

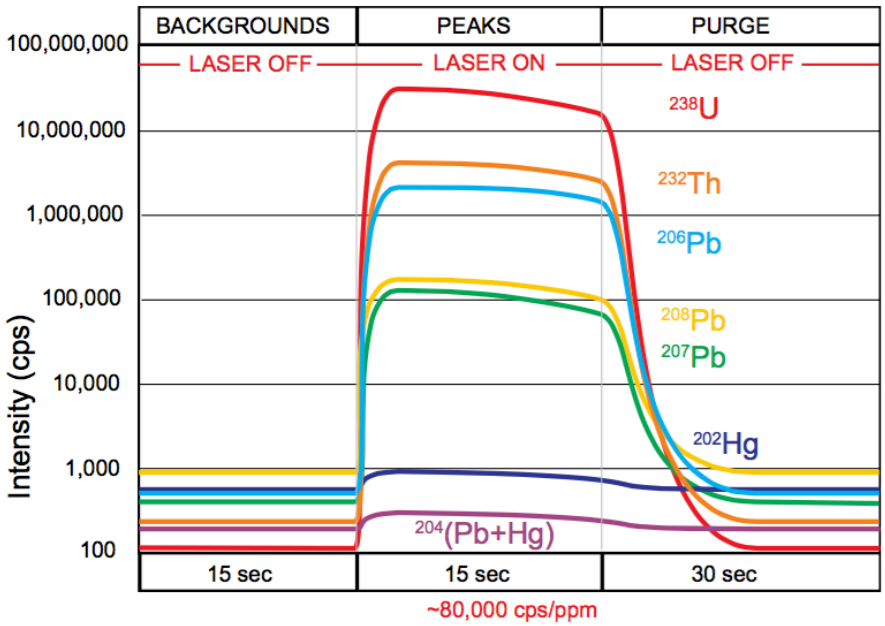

Figure 19 *Variation of ion bean intensities during a typical laser ablation analysis zircon crystal that is ~560 Ma and of typical U concentration (~500 ppm), utilizing a 30-micron beam diameter (i.e., similar to the analysis conditions of the present study) Photo courtesy of Gehrels, 2010*

To calculate true isotope ratios and U-Pb ages from the measured ion beam signals, the raw data was reduced using an excel-based data reduction program called "agecalc" (Gehrels, 2010). The raw ion intensities (intermediate 15 sec. in Figure 19) were first corrected for detector backgrounds (initial 15 sec. in Figure 19) and for any excess ^{204}Hg (Mercury) that impacted the ^{204}Pb measurement. The excess ^{204}Hg is calculated from measurements of ^{202}Hg and assuming natural isotopic abundances. The baseline and Hg-corrected intensities are then used to calculate isotope ratios (Gehrels, 2010). Fractionation of Pb/U and Pb/Th occurs during both laser ablation and during aerosol transport of the ablated material to the plasma (Gehrels et. al., 2006). Fractionation factors are determined from the ratio of the published and measured ^{206}Pb/^{238}U ratios from standard zircon SL. An analysis of standard zircon (SL) was acquired after each five analyses of unknown zircon in order to correct for Pb/U and Pb/Th fractionation. Fractionation corrections were performed using a sliding window that used results from six adjacent standards

in the time series of measurements (i.e., three previous and three subsequent standard measurements). Once intstrumental mass fractionation is accounted for in this manner, the naturally occurring "common" ^{206}Pb and ^{207}Pb was subtracted away. This correction was based upon measured ^{204}Pb values through the use of a Stacey-Kramers model that enables calculation of the composition of common Pb as a function of geologic time (Grehels, 2010). Uranium-lead $^{206}Pb/^{238}U$, $^{207}Pb/^{235}U$, and $^{207}Pb/^{206}Pb$ ages were then calculated via the age equation (Grehels, 2010). In general, $^{206}Pb/^{238}U$ ages were employed for results < ca. 800 Ma concordance of $^{206}Pb/^{238}U$ and $^{207}Pb/^{235}U$ could be demonstrated. All results discordant by greater than 10% were excluded from further analysis. Less than five percent of the measured results were negatively impacted by the U-Pb discorandace at the 10% level. Since middle and early Proterozoic zircons have higher and thus more readily measured Pb ion intensities, $^{207}Pb/^{206}Pb$ were used instead of U-Pb ages because the former are generally more accurate for ancient zircons. Finally, Th-Pb $^{208}Pb/^{232}Th$ ages produced from this analysis were not used because the Pb/Th ratios were not corrected for instrumental fractionation.

Kolmongorov-Smirnoff Statistical Analysis

The Kolmongorov-Smirnoff (K-S) test was utilized to calculate the probability that two measured detrital zircon age distributions were derived from the same population (Grehels et al., 2006). This knowledge can be in turn used to access commonality of sedimentary source region (e.g., sedimentary provenance; see Fletcher et al., 2007) The probability calculated from the K-S statistic (*P*) evaluates the statistical significance of the difference in ages as a function of sample size and the separation (D) of two age distributions in a cumulative distribution plot (Bernhardt, 2011). This is done by evaluating the null hypothesis that two samples are drawn from the same population. If *P* drops below 0.05, the null hypothesis can be rejected because the age

distributions are distinguished at 95% confidence (Bernhardt, 2011). It can then be inferred that the two samples did not come from the same source region. However, if the *P* statistic exceeds 0.05, the age distributions for the two samples cannot be distinguished at 95% confidence at the given sampling location (Bernhardt, 2011).

Particle Size Analysis

A split of each samples was sent to San Diego State and analyzed using a CAMSIZER P4 instrument (Retsch Technology). The CAMSIZER P4 particle analyzer was developed to comprehensively characterize dry, free flowing bulk materials. The CAMSIZER P4 measures both particle size and shape, whereas the traditional sieve analysis can only determine the approximate particle size. Sand is gravity fed through the CAMSIZER start measurement and photographed with high-speed digital cameras. volume.

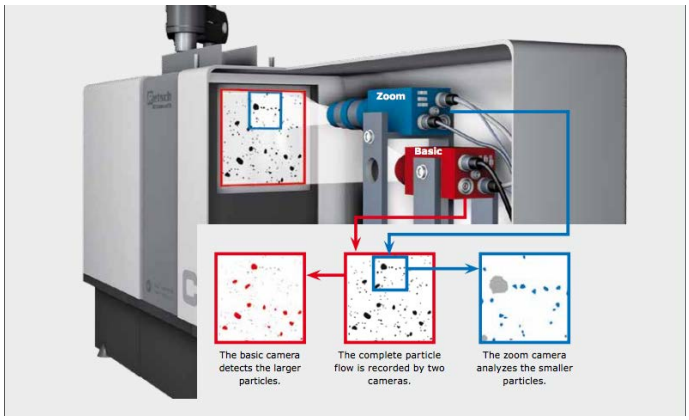

Figure 20 *The dual camera system provides optimized analysis conditions for small and large particles without compromising resolution or detection probability. The basic camera detects large particles and the zoom camera detects the small ones. Photo courtesy of Retsch Technology.*

CHAPTER III

RESULTS

Geochronology

As described in the previous section, the detrital zircon U-Pb age distributions from all eleven samples were measured to provide a quantitative measure of sedimentary provenance. Zircon U-Pb ages are generally thought to represent the time at which their host igneous rocks crystallized from magma. Thus, in cases where sediments are directly routed from igneous source regions to the depositional basin, a distribution of detrital zircon ages represents the distribution of igneous rocks within the source region of the depositional system (e.g., Gehrels, 2012). While this relationship can become obscured when sediments are reworked from previously deposited rocks, the detrital zircon age distribution of a sample can still be used to characterize the sedimentary provenance of a sample.

In this study, detrital zircon U-Pb age distributions were measured to address the three study questions I had set forth to determine: (1) what was the source of sand deposited upon Boca Chica Beach; (2) does the sedimentary provenance change moving northeastward across the Brazos Santiago Pass from Boca Chica Beach to South Padre Island; and (3) was there a temporal change in sedimentary provenance between sands sampled at the surface vs. sands sampled at shallow borehole depth on either Boca Chica Beach or South Padre Island.

In our sample suite, three samples (Playa Bagdad, Rio Grande, and the Brownsville Ship Channel) can reasonably be expected to represent end members age distributions. The modern sand from the Rio Grande River is the most important of these in that it presently derives sediments from a broad region of northeastern Mexico, Texas, and New Mexico. The modern sand from Playa Bagdad, Mexico represents a smaller depositional system in northeastern Mexico that could be transported by longshore current northwards along the coastline. Finally, the Brownsville Ship Channel sample represents older materials previously deposited in the area.

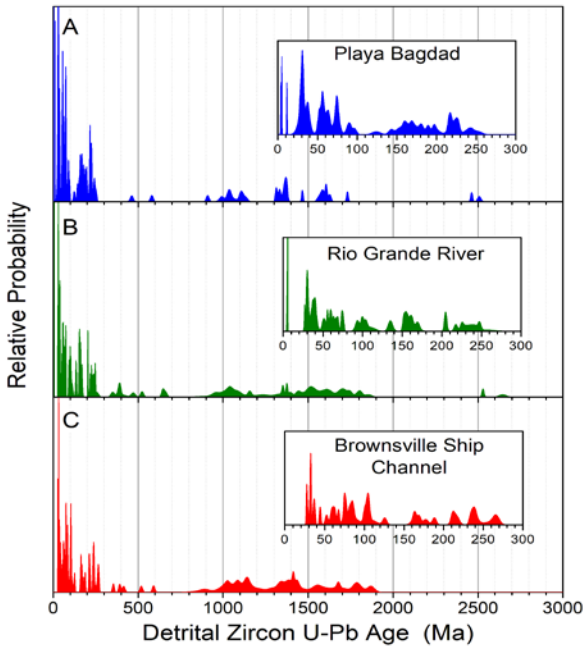

Figure 21 *The relative probability distributions for Playa Bagdad, Rio Grande River, and the Brownsville Ship Channel.*

The U-Pb detrital zircon age distributions of these three end members are shown in Figure 21 A-C as probability density functions. Probability density functions are calculated from the measured age distributions by assuming that the age uncertainty associated with each

measured U-Pb age is a Gaussian distribution. The probability density function sums up all of these individual Gaussian distributions into a single curve and then normalized the area beneath the resulting curve to unity.

As indicated in Figure 21, all three distributions reveal similar U-Pb age maxima with abundant Cenozoic and Mesozoic results less than 300 Ma and a broad distribution of Proterozoic zircon between 1-2 Ga. Because the age peaks for all three samples are rather similar, it is useful to plot cumulative probability density functions for each of the samples in Figure 22. These integrate the area beneath the probability density functions from 0-3000 Ma and express the results in terms of percent. The three bold lines plotted on Figure 22 represent the three end members. As indicated, the Playa Bagdad, Mexico sample is enriched in Cenozoic and Mesozoic zircon relative to the Rio Grande River sample while the Brownsville ship channel sample is depleted in grains of this age relative to the Rio Grande River sample. This variation can be explained by differences in the proportions of sediment supplied by different source regions in eastern Mexico, Texas, and New Mexico.

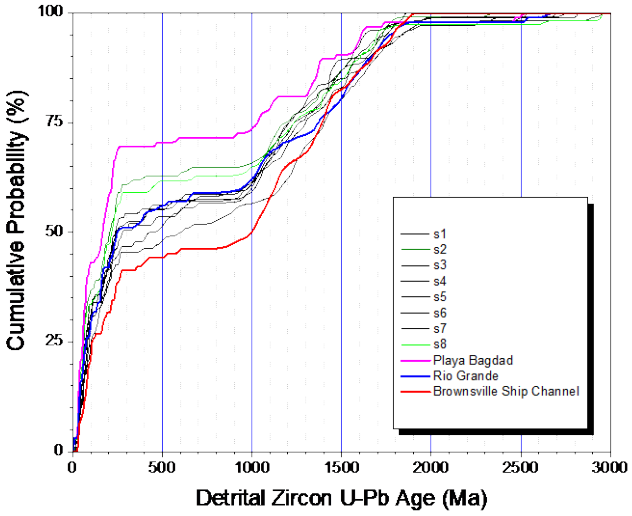

Figure 22 *Summary plot of the cumulative probability of the age distribution. See Table 1* for site location names.

Figure 22 also shows results from the beach sands and the two borehole samples (s2 and s8). As indicated, the distributions for each of the eight samples are very similar. Their cumulative probability density function curves tend to cluster around the result obtained from the Rio Grande River and are bounded by the results from the Playa Bagdad (north-eastern Mexico) and dredged sands from the Brownsville ship channel.

From Figure 22, we can qualitatively infer that the U-Pb detrital zircon age distributions measured from all eight beach sand samples received their sediment from a similarly source region. The Kolmogorov-Smirnov (K-S) test provides a means to quantitatively evaluate this relationship. The K-S test indicated the “sameness” of two independent samples from a continuous distribution by assessing whether the two distributions overlap at 95% confidence (Press et al., 1992). The K-S test depends both upon the sample size and the vertical separation of the two cumulative age distributions. The null hypothesis of the K-S test is that both

distributions were sampled from the same population. Two samples that yield a P-value greater than 0.05 in the K-S test are statistically indistinguishable (i.e., overlap at 95% confidence).

For the K-S test to indicate that a sample has a statistically significant age distribution relative to that measured for a second sample, the calculated P-value resulting from the test would be less than 0.05. A value below this threshold indicates that the distributions can be distinguished at the 95% confidence level. Such a result would indicate that the two samples are derived from different populations. Geologically, this outcome implies a statistically significant difference in the nature of the source region. The K-S test results reported here were generated using a program written by Oscar Lovera (http://sims.ess.ucla.edu/argonlab/genks/genks.htm) that implements calculations presented in Press et al. (1992). Lovera's algorithm calculates the P-value for the case in which experimental error is ignored (the conventional K-S test) and the case where experimental error is taken into account. The former calculation represents the age distribution with a cumulative distribution function with the later uses a cumulative probability density function that assumes the error associated with each age is normally distributed.

Kolmogrov-Smirnov Test Results

Comparision w/ Rio Grande River Sand		
Name	D	PROB
sample 1	0.075	0.937
sample 2	0.107	0.573
sample 3	0.097	0.727
sample 4	0.043	1.000
sample 5	0.087	0.823
sample 6	0.103	0.614
sample 7	0.070	0.961
sample 8	0.081	0.868
Playa Bagdad	0.196	0.041
Brownsville Ship Channel	0.128	0.347

Comparison w/ Playa Bagdad		
Name	D	PROB
sample 1	0.243	0.006
sample 2	0.127	0.373
sample 3	0.219	0.016
sample 4	0.182	0.081
sample 5	0.186	0.056
sample 6	0.264	0.001
sample 7	0.191	0.051
sample 8	0.134	0.298
Playa Bagdad	0.196	0.041
Brownsville Ship Channel	0.316	0.000

Comparison w/ Dredged Brownsville Ship Channel Sand		
Name	D	PROB
sample 1	0.113	0.530
sample 2	0.205	0.021
sample 3	0.109	0.571
sample 4	0.142	0.261
sample 5	0.146	0.202
sample 6	0.077	0.897
sample 7	0.133	0.311
sample 8	0.191	0.036
Playa Bagdad	0.316	0.000
Brownsville Ship Channel	0.128	0.347

Red denotes distributions indistinguishable at 95% confidence

Table 2 *A summary of the Kolmogorov-Smirnov Test results showing probability calculations that quantify the extent to which the age distributions overlap.*

Table 2 (above) presents results from the eleven samples. In regards to the comparison of the Rio Grande River sample, Table 2 above indicates that all of the eight beach sand samples are most similar to the Rio Grande River sand sample. Specifically, they are all indistinguishable from the Rio Grande River sand sample at 95% confidence. In contrast, comparison of the Playa Bagdad, Mexico sample with the Rio Grande River samples does yield a P-value of 0.04 when measurement error is taken into account and P=0.03 with no accounting for measurement error. Because the detrital zircon age distributions from the eight beach samples are statistically distinguishable from the Rio Grande River sample we can conclude that it is most likely that the beach sands were supplied by the Rio Grande River. The statistically significant contrast between the Playa Bagdad (Mexico) and Rio Grande River samples indicate that the sands originated from somewhat different sources.

K-S tests performed using the Playa Bagdad, Mexico, sample as the basis for comparison indicate that samples 2, 4, 5, 7, and 8 are indistinguishable at 95% confidence from this north-eastern Mexican system. Samples S2 (P-value of 0.373) and S8 (P-value of 0.298) are the two samples that are the most similar to Playa Badgad, Mexico. Both of these happen to be the two borehole samples collected at approximately 5 m in depth. Comparisons made between the Brownsville ship channel dredged sands reveal that only six of the eight samples overlap at 95% confidence. Thus it can be concluded that sand dredged from the Brownsville ship channel differs in some statistically meaningful way from modern Rio Grande River sand.

In summary, the detrital zircon U-Pb analysis performed indicates that the majority of the beach sand samples most strongly resemble the Rio Grande River sand (Fig. 22). K-S test results summarized in Table 2 indicates that all of the eight beach sand samples are statistically indistinguishable from the Rio Grande River sand sample at 95% confidence. The small

variability in the U-Pb age distributions exhibited by the beach sands can potentially be attributed to mixing of older and modern sands related to dredging in the Brownsville ship channel and other anthropogenic activities that impact the sediment supply on the beach on South Padre Island.

The Playa Bagdad, Mexico sample appears distinct from the Rio Grande River sample with a P-value of 0.041 when accounting for experimental error. It also appears significant that the two borehole samples from approximately 5 m in depth appear qualitatively more similar to the Playa Bagdad, Mexico sample. This implies that anthropogenic activities have altered the modern beach sand compositions related when the samples at depth were deposited.

Particle Size Analysis

As mentioned in the previous chapter, the grain size particles went to San Diego State to be analyzed using the CAMSIZER P4. The results from the CAMSIZER then went through the GRADISTAT version 4.0 program developed by Simon Blott in October 2000. The program is ideal for a rapid analysis (approximately 50 samples per hour) of unconsolidated sediments for grain size distribution and statistics using Microsoft Visual Basic that is already integrated into Microsoft Excel allowing for a tabular and graphical output (Blott, 2001). GRADISTAT Table 3 (below) is a summary of the statistical analysis of each of the samples, along with the textural group they belong in. Sample 11 (Brownsville Ship Channel) was left out of the analysis, because it somehow got lost in the shuffle between Stanford and San Diego. Sample 8 (Boca Chica Beach, bottom of core) was too fine grained for the CAMSIZER P4, meaning the sediment was <30 μm, and therefore could not be analyzed. Some of the samples had some broken shell

material mixed in, so it is believed that is why some of the samples were reported as “slightly gravelly”.

Table 3 *Summary of particle distribution results from CAMSIZER*

#	Name	Geometric Mean (µm)	Logarithmic Mean ϕ	Sorting	Skewness	Kurtosis	Sediment Mode	Textural Group
1	South Padre Island (Top Core)	236.1	2.083	1.238	0.008	1.030	Unimodal, Very Well Sorted	Sand
2	South Padre Island (Bottom Core)	235.9	2.084	1.237	0.049	1.044	Unimodal, Very Well Sorted	Slightly Gravelly Sand
3	South Padre Island Surface Sand	232.1	2.017	1.314	0.139	1.056	Unimodal, Well Sorted	Slightly Gravelly Sand
4	Boca Chica Surface Sand	232.1	2.017	1.314	0.139	1.056	Unimodal, Well Sorted	**S**lightly Gravelly Sand
5	Boca Chica Surface Sand	235	2.089	1.29	0.096	1.094	Unimodal, Well Sorted	Sand
6	Boca Chica Surface Sand	240.9	2.053	1.476	0.254	1.174	Unimodal, Moderately Well Sorted	Sand
7	Boca Chica (Top of Core)	224.5	2.155	1.276	-0.013	1.178	Unimodal, Well Sorted	Slightly Gravelly Sand
8	Boca Chica (Bottom of Core)	<30 µm	-	-	-	-	Mud	Mud
9	Mexico Playa Bagdad	224.5	2.155	1.273	0.115	1.134	Unimodal, Very Well Sorted	Slightly Gravelly Sand
10	Mexico Rio Bravo	218.9	2.192	1.369	-0.027	1.161	Unimodal, Well Sorted	Slightly Gravelly Sand

Comparing end members, S9 (Playa Bagdad) and S10 (Rio Grande River) they are almost the same in regards to distribution. Figure 23, below, shows that both samples are unimodal and well sorted amongst the different types of sediments found in each sample. From the CAMSIZER results, not much distinction can be made between the two end member samples. Other than the fact that the Rio Grande River sample, had about 0.4% of mud mixed into the sample. Which was present due to the proximity the surface sample was taken from the river.

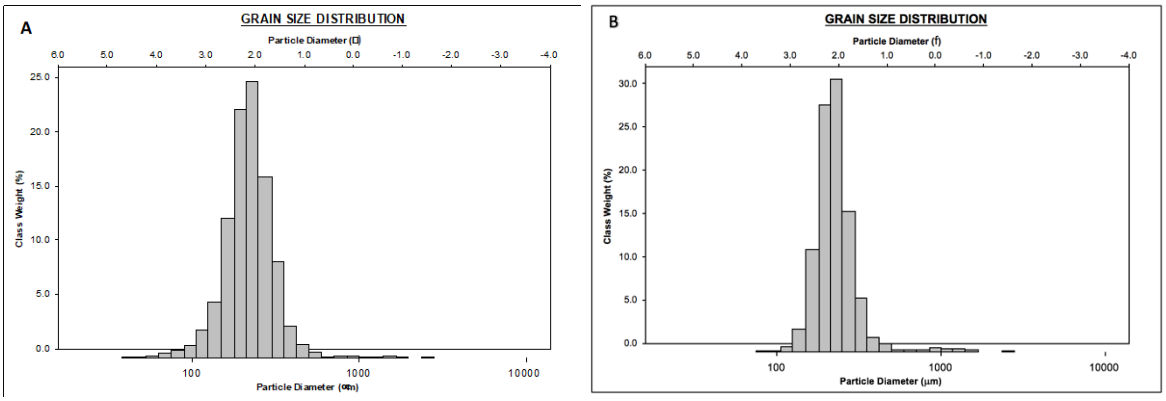

Figure 23 *Grain size distribution plots for (A) Rio Grande River sand and (B) Playa Bagdad, Mexico*

CHAPTER IV

CONCLUSION

Since detrital zircons are so stable and a common accessory mineral that crystallizes in igneous rocks, they made an excellent way to track the provenance of the Rio Grande Delta sediments. From this study, it was found that most of the sediments in the Rio Grande Delta in Texas have a similar provenance. The K-S test showed with 95% confidence that all of the surface sand samples in the United States are indistinguishable from the Rio Grande River sediment sample, meaning that they all overlap in ages and therefore come from a similar source. Some variation in the samples may be due to anthropogenic impact and dredging of the Brownsville Ship Channel.

Sediments in the Rio Grande Delta in Mexico have different origins than the sediments collected from South Padre Island, Texas. Although the long-shore drift goes from south to north in this area, the sediments from the Playa Bagdad, Mexico statistically show a different origin. The only samples that were close to the Playa Bagdad, Mexico samples were the samples collected at 5 m deep on Boca Chica Beach and Edwin King, South Padre Island. In contrast, the surface sediments are statistically significantly different from 5 m deep due to anthropogenic activities. The borehole samples were statistically significant with the Playa Bagdad, Mexico sample. This could be due to the long-shore drift from Mexico to South Padre Island, as well as anthropogenic effects of tourists and the general population. Edwin King is not

maintained by the city, and therefore anyone can drive their vehicles onto the beach. The constant driving impacts the sand sediments by compacting the sediments down and also dispersing the surface sand. Making the bottom of the core much older than the surface sand.

Currently, there is not a lot of research on the Rio Grande Delta due to being spread between the United States and Mexico. One of the main reasons for the lack of research is trying to coordinate or collaborate with Mexico. This thesis project lays the foundation for future projects in the Rio Grande Delta system. It can also provide a nice baseline for provenance along the arroyo Colorado, and different resacas in South Texas. The next step to take this project further, would be to test potential provenance sources.

REFERENCES

Benke, Arthur C., and Colbert E. Cushing. "Ch. 5 Gulf Coast Rivers of the Southwestern United States." *Rivers of North America*. Amsterdam: Elsevier/Acad., 2005. 181-231. Print.

Bernhardt, Anne, Donald R. Lowe, S. A. Graham, and Jonathan Payne. *Paleogeography and Sedimentary Development of Two Deep-marine Foreland Basins: The Cretaceous Magallanes Basin, Southern Chile, and the Tertiary Molasse Basin, Austria*. Diss. Stanford, 2011. Stanford: Stanford U, 2011. Print.

Blott, Simon J., and Kenneth Pye. "GRADISTAT: a Grain Size Distribution and Statistics Package for the Analysis of Unconsolidated Sediments." *Earth Surface Processes and Landforms*, vol. 26, no. 11, 2001, pp. 1237–1248., doi:10.1002/esp.261.

Bolourchi, Zahir "Bo", and Bill McHie. *Louisiana Statewide Perspective on Water Resources*. Apr. 2010, biotech.law.lsu.edu/blog/La_Statewide_Perspective_on_water_resources_April_2010.pdf .

"Boca Chica Beach - Lower Rio Grande Valley - U.S. Fish and Wildlife Service." *U.S. Fish & Wildlife Service*. N.p., 9 July 2012. Web. 29 Mar. 2017.

Bureau of Economic Geology. *McAllen-Brownsville Sheet* [map]. Scale: 1:250,000. Geologic Atlas of Texas. Austin, Tx: The University of Texas at Austin, 1976.

"CAMSIZER® P4." *Particle Analyzer CAMSIZER P4 - Retsch Technology*. Retsch Technology GmbH, 2017. Web. 11 Apr. 2017.

Davis, Richard A., and Duncan M. FitzGerald. *Beaches and Coasts*. Malden, MA: Blackwell Pub., 2004. Print.

Ewing, T. E., and J. L. Gonzalez, "The late Quaternary Rio Grande Delta—A distinctive, underappreciated geologic system" *Gulf Coast Association of Geological Societies Transactions*, v. 66 (2016), p. 169–180.

Faure, G. and Mensing, T.M. (2005) Isotope Principle and Applications. 3rd Edition, John Wiley & Sons, Hoboken.

Fletcher, John M., Marty Grove, David Kimbrough, Oscar Lovera, and George E. Gehrels. "Ridge-trench Interactions and the Neogene Tectonic Evolution of the Magdalena Shelf: Insights from Detrital Zircon U-Pb Ages from the Magdalena Fan and Adjacent Areas."*Geological Society of America Bulletin* 119.11/12 (2007): 1313-336. Print.

Gehrels, George, Victor Valencia, and Alex Pullen. "Detrital Zircon Geochronology by Laser-Ablation Multicollector ICPMS at the Arizona Laserchron Center." *The Paleontological Society Papers*. Ed. Thomas D. Olszewski. Vol. 12. New Haven, Connecticut: Paleontological Society, October 2006. 67-76. Print. Geochronology: Emerging Opportunities.

Gehrels, G. (2012). Detrital Zircon U-Pb Geochronology: Current Methods and New Opportunities. In Tectonics of Sedimentary Basins (eds C. Busby and A. Azor). doi: 10.1002/9781444347166.ch2

Gehrels, G. "U-Th-Pb Analytical Methods." *Arizona LaserChron Center, University of Arizona*. N.p., 12 Aug. 2010. Web. 10 Apr. 2017.

Gehrels, G. "U-Th-Pb Analytical Methods for Zircon." *Arizona LaserChron Center, University of Arizona*. N.p., 12 Aug. 2010. Web. 10 Apr. 2017.

Heise, Elizabeth A., Benavides, Jude A., Contreras, Mara, Cardenas, Andres and Lemen, Joseph, "Hurricanes Dolly and Ike damaged the Town of South Padre Island from two different directions in 2008", Shore and Beach, vol. 77 (2009), no. 2, p 30-36.

"HOME." *Wink Vibracore*. N.p., n.d. Web. 03 Apr. 2017.

Lovera, O.M., Grove, M. Cina, S.E. (2009): A generalized Kolmogorov-Smirnov statsistic for detrital zircon analysis of modern rivers. http://sims.ess.ucla.edu/argonlab/genks/genks.htm

Masselink, Gerhard, and Michael G. Hughes. "Ch. 6 Fluvial-Dominated Coastal Environments-Deltas." *Introduction to Coastal Processes & Geomorphology*. London: Hodder Arnold, 2003. 141-64. Print.

Meyer-arendt, Klaus J., "Resort Evolution Along the Gulf of Mexico Littoral: Historical, Morphological, and Environmental Aspects." *LSU Historical Dissertations and Theses*. (1987) 4411. http://digitalcommons.lsu.edu/gradschool_disstheses/4411

Morton, Robert A., and Mary J. Pieper. "Shoreline Changes on Brazos Island and South Padre Island (Mansfield Channel to Mouth of the Rio Grande)— An Analysis of Historical Changes of the Texas Gulf Shoreline." *Geological Circular* 75.2 (1975): n. pag. Web. 13 Apr. 2017.

Oko, Dan. "Boca Chica." *Texas Monthly*. N.p., May 2013. Web. 29 Mar. 2017.

"Particle Analyzer CAMSIZER P4." *Brochure* (2005): 1-16. Retsch Technology GmbH. Web. 11 Apr. 2017.

Pullen, Alex, and Martin Pepper. "Preparing & Cleaning Mounts for Analysis at the Arizona LaserChron Center." Arizona LaserChron Center, Oct. 2009. Web.

Russell, Richard Joel, and R. Dana Russell. "*Mississippi River Delta Sedimentation*." *Recent Marine Sediments: A Symposium*. Ed. Parker D. Trask. Tulsa, Oklahoma: American Association of Petroleum Geologists, 1955. 153-218. Print.

Schiller, Dane, and James Pinkerton. "Agents Feared Mexican Drug Cartel Attack on Border Dam." *Houston Chronicle*. Hearst Newspapers, LLC, 02 June 2010. Web. 13 Apr. 2017.

Schoene, Blair. "U–Th–Pb Geochronology." *Treatise on Geochemistry* (2014): 341-78. Web

Seybold, Hansjörg, José S. Andrade, and Hans J. Herrmann. "Modeling River Delta Formation." *Proceedings of the National Academy of Sciences of the United States of America*. National Academy of Sciences, 23 Oct. 2007. Web. 12 Apr. 2017.

Shuter, Eugene, and Warren E. Teasdale. "Application of Drilling, Coring, and Sampling Techniques to Test Holes and Wells." *Techniques of Water-Resource Investigations of the United States Geological Survey*. Vol. 2. Denver, CO.: U.S. Geological Survey, 1989. 1-97. PDF.

Simpson, Gayland, Mark Pecha, and George Grehels. "Mineral Separation Instruction Manual." Arizona LaserChron Center, 1 Feb. 2012. Web.

"Unit 8: Water Resources // Section 6: Depletion of Freshwater Resources." *Annenberg Learner*. N.p., n.d. Web. 8 May 2017.

W.H. Press, S.A. Teukolsky, W.T. Vetterling & B.P. Flannery (1992): *Numerical recipes in C: The art of scientific computing.* Second Edition. Cambridge University Press.

Woodroffe, C. D. “Ch. 7-Deltas and Estuaries." *Coasts: Form, Process, and Evolution*. Cambridge: Cambridge UP, 2002. 321-377. Print.

APPENDIX A

APPENDIX A

U-PB DATA TABLES

Sample 1: South Padre Island (Edwin King, Top of Core)

#	U (ppm)	U/Th	$^{206}Pb/^{238}U$	± 2s	$^{207}Pb/^{235}U$	± 2s	$^{207}Pb/^{206}Pb$	± 2s	U-Pb Age	± 2s
1	59	1.44	1498.7	20.4	1483.2	12.6	1486.1	25.3	1486.1	25.3
2	330	1.03	478.0	12.0	474.6	9.2	450.0	16.0	478.0	12.0
3	68	1.30	107.7	2.6	110.5	4.0	150.7	84.6	107.7	2.6
4	101	1.31	406.6	9.3	408.5	9.4	425.7	56.2	406.6	9.3
5	295	1.05	31.5	0.6	32.9	1.3	304.0	57.0	31.5	0.6
6	37	0.45	502.7	12.0	502.7	16.0	491.7	84.0	502.7	12.0
7	351	0.82	95.9	1.8	96.3	2.6	128.5	65.2	95.9	1.8
8	24	2.34	1016.1	21.8	1013.1	15.8	1006.2	50.5	1006.2	50.5
9	115	1.18	56.8	1.7	57.3	3.6	81.7	132.8	56.8	1.7
10	111	1.73	1168.5	23.8	1168.5	12.4	1196.4	32.0	1196.4	32.0
11	59	0.82	78.9	3.2	81.4	7.1	182.7	192.8	78.9	3.2
12	83	1.51	239.6	6.4	239.7	8.6	252.2	89.1	239.6	6.4
13	565	1.59	71.4	1.2	71.8	1.7	112.9	51.9	71.4	1.2
14	78	1.45	626.0	12.0	622.0	14.0	590.0	72.0	626.0	12.0
15	332	2.20	1647.0	21.0	1654.0	10.0	1679.0	22.0	1679.0	22.0
16	118	1.32	1434.3	22.4	1426.1	12.2	1434.3	27.4	1434.3	27.4
17	164	0.36	28.6	0.6	29.0	1.2	262.0	56.0	28.6	0.6
18	76	0.84	81.2	2.4	81.6	4.0	150.6	120.5	81.2	2.4
19	260	0.77	1430.5	9.4	1435.1	7.3	1438.7	15.5	1438.7	15.5
20	312	5.82	266.8	3.7	269.9	4.8	276.6	52.0	266.8	3.7
21	83	15.95	61.9	1.9	62.8	4.3	90.8	131.1	61.9	1.9
22	61	1.32	653.3	10.2	644.9	8.1	607.5	48.9	653.3	10.2
23	166	0.79	1475.5	22.9	1477.6	12.5	1479.7	22.9	1479.7	22.9
24	319	0.73	98.9	2.4	98.2	2.9	65.0	59.9	98.9	2.4
25	92	0.93	108.1	2.0	109.5	3.3	159.5	74.1	108.1	2.0
26	11	1.17	1081.7	18.6	1075.5	15.5	1035.2	44.5	1035.2	44.5
27	54	1.57	1351.1	29.5	1343.2	19.7	1337.3	29.5	1337.3	29.5
28	30	1.14	34.1	2.3	34.3	5.5	9.7	299.4	34.1	2.3

29	56	1.03	994.3	12.5	1003.0	10.6	1019.4	31.9	1019.4	31.9
30	176	1.12	162.3	2.1	163.4	3.6	176.5	46.4	162.3	2.1
31	146	1.02	84.4	4.0	82.7	6.7	71.4	193.9	84.4	4.0
32	164	0.94	83.0	1.6	82.5	2.9	181.0	34.0	83.0	1.6
33	303	1.53	92.2	1.9	91.9	2.7	91.4	74.1	92.2	1.9
34	180	1.17	1407.0	18.0	1413.9	9.0	1412.0	22.0	1412.0	22.0
35	510	3.31	46.6	1.0	46.8	1.1	114.5	62.2	46.6	1.0
36	350	0.60	63.5	1.3	62.7	1.8	66.5	74.2	63.5	1.3
37	111	0.86	165.1	5.1	167.7	6.8	220.6	89.7	165.1	5.1
38	79	1.93	1024.9	15.3	1034.5	12.4	1060.3	32.5	1060.3	32.5
39	256	0.63	171.8	2.0	173.2	2.8	177.0	27.0	171.8	2.0
40	190	1.25	58.8	1.0	60.9	2.0	207.0	41.0	58.8	1.0
41	486	0.99	5.2	0.8	5.2	1.2	117.0	26.0	5.2	0.8
42	75	1.14	1122.0	16.0	1123.0	13.0	1148.0	11.0	1148.0	11.0
43	19	1.49	1407.2	20.3	1407.2	16.4	1403.3	39.5	1403.3	39.5
44	28	0.47	67.5	2.2	71.0	4.9	249.3	143.8	67.5	2.2
45	64	0.34	97.5	3.7	101.5	7.0	182.4	152.0	97.5	3.7
46	294	2.98	102.1	6.7	101.3	6.2	103.0	113.3	102.1	6.7
47	16	1.43	1215.4	24.3	1207.6	22.4	1198.9	40.8	1198.9	40.8
48	52	1.13	550.1	9.8	557.4	10.3	594.5	60.9	550.1	9.8
49	128	1.51	179.5	3.8	185.4	6.0	290.3	70.0	179.5	3.8
50	75	1.20	1603.0	27.0	1620.0	12.0	1645.0	32.0	1645.0	32.0
51	103	0.73	969.4	23.9	992.4	17.7	1043.4	47.9	1043.4	47.9
52	13	0.84	1039.0	31.0	1053.0	34.0	1123.0	45.0	1123.0	45.0
53	56	1.31	37.0	2.0	39.0	3.4	270.3	218.3	37.0	2.0
54	95	1.38	1541.0	26.0	1593.0	15.0	1657.0	40.0	1657.0	40.0
55	235	1.71	1757.0	13.0	1747.2	6.2	1742.0	6.0	1742.0	6.0
56	150	1.08	256.5	2.4	252.8	4.6	246.0	22.0	256.5	2.4
57	121	0.69	1033.9	12.5	1024.6	6.6	1031.9	21.2	1031.9	21.2
58	125	1.30	338.5	6.0	335.0	6.6	351.9	53.8	338.5	6.0
59	162	1.79	1718.0	18.0	1705.0	8.7	1698.0	18.0	1698.0	18.0
60	156	1.92	1052.3	15.6	1103.3	13.5	1209.6	29.2	1209.6	29.2
61	178	1.93	598.7	10.7	596.6	8.7	594.8	33.2	598.7	10.7
62	23	1.54	1212.1	43.0	1296.0	35.7	1426.0	97.5	1426.0	97.5
63	12	1.02	1343.3	25.8	1375.0	16.8	1396.7	34.7	1396.7	34.7
64	132	0.96	58.6	1.8	57.6	3.3	80.3	130.5	58.6	1.8
65	91	0.76	12.7	2.7	13.2	6.7	510.0	220.0	12.7	2.7

66	25	0.77	1351.4	18.3	1362.9	10.6	1381.2	26.0	1381.2	26.0
67	28	1.01	1050.3	13.7	1055.1	10.8	1076.7	32.3	1076.7	32.3
68	85	0.31	175.8	3.9	176.5	5.0	175.0	89.6	175.8	3.9
69	236	1.25	98.2	1.6	97.7	2.7	139.0	29.0	98.2	1.6
70	290	2.14	208.9	1.7	209.6	2.5	209.0	17.0	208.9	1.7
71	47	0.90	1165.2	20.5	1174.4	12.3	1172.3	38.9	1172.3	38.9
72	203	5.28	4.7	1.0	4.9	2.3	257.0	37.0	4.7	1.0
73	109	1.82	519.5	8.6	524.4	7.8	544.5	45.9	519.5	8.6
74	46	0.75	90.2	3.0	91.1	4.6	95.3	104.8	90.2	3.0
75	126	0.97	1690.2	26.0	1691.2	12.0	1698.2	22.0	1698.2	22.0
76	13	0.70	110.1	5.5	115.8	13.3	205.0	245.9	110.1	5.5
77	198	0.40	37.2	1.4	39.7	2.3	219.8	129.9	37.2	1.4
78	116	0.44	214.5	4.0	210.5	4.6	206.1	59.5	214.5	4.0
79	50	0.74	2499.6	31.5	2488.7	12.8	2475.0	19.7	2475.0	19.7
80	322	5.49	1880.0	26.0	1840.0	12.0	1801.0	22.0	1801.0	22.0
81	176	1.62	2610.0	25.0	2655.0	14.0	2685.0	11.0	2685.0	11.0
82	100	0.87	1521.5	27.3	1511.0	14.7	1508.9	27.3	1508.9	27.3
83	285	0.61	161.8	1.5	160.3	2.3	163.0	22.0	161.8	1.5
84	26	0.94	966.7	13.8	971.6	10.8	990.3	35.4	990.3	35.4
85	58	0.69	1591.6	14.6	1612.9	8.3	1630.6	18.5	1630.6	18.5
86	126	1.98	1690.0	22.5	1696.8	10.8	1697.8	16.6	1697.8	16.6
87	34	0.83	405.9	12.6	405.9	15.5	427.3	86.4	405.9	12.6
88	50	2.49	954.9	10.4	964.8	9.1	974.7	29.2	974.7	29.2
89	179	1.57	58.9	1.1	59.2	1.7	187.0	32.0	58.9	1.1
90	53	0.94	1181.5	8.8	1195.9	8.9	1218.0	12.0	1218.0	12.0
91	221	2.05	1236.3	14.6	1246.8	9.1	1277.9	21.9	1277.9	21.9
92	12	0.58	996.1	21.8	1020.8	15.9	1075.3	48.6	1075.3	48.6
93	51	0.25	28.6	1.2	28.8	3.3	580.0	120.0	28.6	1.2
94	162	0.82	169.2	3.2	168.3	4.3	169.2	66.9	169.2	3.2

Sample 2: South Padre Island (Edwin King, Bottom of Core)

#	U (ppm)	U/Th	$^{206}Pb/^{238}U$	± 2s	$^{207}Pb/^{235}U$	± 2s	$^{207}Pb/^{206}Pb$	± 2s	U-Pb Age	± 2s
1	762	2.70	1300.1	17.0	1335.1	7.7	1540.6	13.6	1540.6	13.6
2	19	1.35	899.1	15.9	905.1	20.7	1069.0	74.2	1069.0	74.2
3	27	0.75	936.2	20.7	1016.6	15.0	1008.1	46.5	1008.1	46.5
4	69	6.04	1128.4	13.1	1112.5	9.5	1210.5	10.3	1210.5	10.3
5	603	1.57	213.4	2.3	239.5	2.3	249.2	17.9	213.4	2.3
6	128	1.23	1096.5	15.1	1144.9	8.6	1086.8	33.5	1086.8	33.5
7	188	1.16	95.3	2.0	98.6	3.1	216.1	44.2	95.3	2.0
8	206	2.89	942.7	5.4	1010.3	4.5	1086.5	8.7	1086.5	8.7
9	92	0.94	597.6	7.1	611.4	8.7	622.0	30.0	597.6	7.1
10	86	0.56	73.9	1.8	73.4	3.0	260.0	42.2	73.9	1.8
11	596	6.12	270.7	3.5	245.7	4.4	286.9	47.2	270.7	3.5
12	307	1.10	9.9	0.6	9.6	1.4	319.9	57.4	9.9	0.6
13	131	14.23	64.5	2.0	67.0	4.2	93.3	133.5	64.5	2.0
14	148	1.01	57.5	1.0	56.3	2.0	183.8	33.3	57.5	1.0
15	42	0.89	1445.7	25.3	1473.5	16.0	1307.4	42.5	1307.4	42.5
16	152	1.01	238.3	2.6	243.4	4.3	229.0	22.6	238.3	2.6
17	823	3.22	98.3	6.2	97.8	6.3	97.3	104.8	98.3	6.2
18	107	1.54	987.0	18.2	1076.3	10.4	1119.3	31.9	1119.3	31.9
19	154	0.95	77.3	1.6	76.0	3.1	175.1	35.9	77.3	1.6
20	60	0.82	1162.9	10.5	1222.1	7.5	1150.2	12.0	1150.2	12.0
21	308	2.11	201.3	1.6	223.5	2.5	209.1	18.2	201.3	1.6
22	322	3.68	1478.0	34.2	1531.5	12.9	1637.4	14.5	1637.4	14.5
23	527	2.07	226.2	3.1	221.6	3.3	247.0	18.0	226.2	3.1
24	314	1.89	1284.4	12.2	1294.6	6.4	1370.7	4.8	1370.7	4.8
25	382	0.70	322.6	9.5	354.7	12.7	342.0	93.4	322.6	9.5
26	199	1.24	57.6	0.9	57.5	2.1	198.9	40.5	57.6	0.9
27	434	3.04	79.3	1.2	74.2	1.9	170.1	31.2	79.3	1.2
28	151	0.35	153.2	6.6	163.5	7.2	138.4	128.7	153.2	6.6
29	30	0.32	26.7	1.6	27.6	4.7	713.1	138.9	26.7	1.6
30	128	0.66	121.1	2.4	119.5	3.7	238.4	45.9	121.1	2.4
31	239	1.86	33.3	0.6	30.4	0.9	156.7	39.0	33.3	0.6
32	54	1.23	1342.1	23.9	1401.0	13.7	1383.6	33.9	1383.6	33.9
33	238	0.60	158.5	2.0	168.3	2.7	187.4	25.0	158.5	2.0
34	140	1.01	62.7	1.6	58.9	2.2	313.4	74.7	62.7	1.6
35	1131	3.70	1311.8	9.6	1345.4	5.6	1371.1	6.3	1371.1	6.3
36	109	0.61	1570.3	17.8	1578.1	7.6	1700.7	13.1	1700.7	13.1
37	155	1.05	34.9	0.8	36.8	1.5	296.0	55.1	34.9	0.8
38	120	0.65	393.7	12.6	437.8	17.3	456.2	83.0	393.7	12.6
39	153	0.98	1738.8	20.7	1625.6	9.4	1792.6	23.3	1792.6	23.3

40	133	1.20	87.2	1.7	84.7	3.0	214.7	36.9	87.2	1.7
41	335	1.30	1579.1	21.8	1714.7	8.0	1759.5	18.4	1759.5	18.4
42	72	0.67	2433.0	32.7	2570.0	13.1	2315.6	20.9	2315.6	20.9
43	200	1.12	53.1	0.8	57.9	1.7	192.2	36.4	53.1	0.8
44	364	4.72	58.6	1.0	55.9	1.4	151.7	27.3	58.6	1.0
45	129	0.90	237.7	2.8	212.5	3.5	260.9	29.1	237.7	2.8
46	128	1.78	206.1	2.9	234.6	4.7	247.1	31.0	206.1	2.9
47	183	1.22	29.4	0.6	30.2	1.3	265.3	49.4	29.4	0.6
48	172	1.68	63.0	1.8	61.5	3.1	78.6	128.6	63.0	1.8
49	158	0.60	1297.1	16.6	1357.6	11.3	1472.4	13.1	1472.4	13.1
50	72	1.23	1675.7	28.5	1712.1	12.1	1724.3	30.5	1724.3	30.5
51	118	0.86	214.6	3.1	208.2	5.7	282.8	30.5	214.6	3.1
52	195	1.39	58.0	1.0	51.6	1.6	183.8	34.7	58.0	1.0
53	18	0.59	44.5	2.2	42.9	7.3	754.3	166.4	44.5	2.2
54	35	0.91	52.9	4.8	50.2	9.2	547.6	183.6	52.9	4.8
55	261	1.27	1645.6	25.5	1532.7	12.8	1740.6	16.8	1740.6	16.8
56	211	1.58	1091.1	23.3	1060.4	11.9	1145.8	29.5	1145.8	29.5
57	189	1.41	64.7	1.0	64.3	1.8	180.0	28.3	64.7	1.0
58	63	1.11	33.9	1.9	35.3	3.5	421.0	92.0	33.9	1.9
59	471	1.80	1199.6	14.1	1278.9	8.4	1313.7	19.5	1313.7	19.5
60	150	0.40	35.2	0.8	31.5	1.3	222.2	54.0	35.2	0.8
61	82	0.88	271.1	3.8	252.0	5.3	251.6	33.1	271.1	3.8
62	148	0.97	248.4	2.2	233.4	3.7	273.7	20.1	248.4	2.2
63	194	5.64	70.4	1.0	78.2	2.4	256.4	38.9	70.4	1.0
64	44	0.87	1566.8	13.2	1594.7	6.6	1679.3	12.4	1679.3	12.4
65	195	1.68	1356.5	10.3	1451.8	5.2	1521.2	6.1	1521.2	6.1
66	51	0.63	119.9	3.1	132.9	5.9	322.8	54.3	119.9	3.1
67	237	0.63	178.2	2.8	178.6	4.1	181.5	31.1	178.2	2.8
68	14	0.80	1059.4	30.0	1045.5	33.1	1128.4	45.1	1128.4	45.1
69	100	1.19	32.8	2.0	39.3	3.3	264.0	208.3	32.8	2.0
70	174	1.53	55.8	1.2	60.0	1.8	180.3	30.1	55.8	1.2
71	168	1.62	55.2	1.2	58.6	2.0	231.5	42.1	55.2	1.2
72	220	1.65	1468.3	14.4	1341.7	7.1	1443.6	12.4	1443.6	12.4
73	248	1.64	1770.1	13.4	1717.7	6.5	1728.7	6.3	1728.7	6.3
74	51	0.25	29.9	1.3	30.8	3.1	568.2	117.9	29.9	1.3
75	229	1.05	165.0	1.7	180.1	2.4	192.1	20.7	165.0	1.7
76	288	3.11	61.1	2.5	61.5	1.9	183.4	46.4	61.1	2.5
77	330	0.95	175.1	2.1	179.2	5.4	196.9	45.8	175.1	2.1
78	493	14.76	37.1	2.4	41.8	4.0	256.0	88.7	37.1	2.4
79	278	2.80	66.8	1.3	74.8	1.5	128.6	30.9	66.8	1.3
80	85	0.66	38.9	1.4	33.0	2.8	369.0	85.2	38.9	1.4

81	125	0.51	31.1	0.8	31.8	1.8	478.4	80.1	31.1	0.8
82	318	1.65	646.1	10.3	563.0	9.3	634.0	32.7	646.1	10.3
83	55	0.64	1804.0	29.8	1605.9	18.0	1721.2	41.7	1721.2	41.7
84	103	1.06	232.2	2.5	225.2	5.0	235.8	38.0	232.2	2.5
85	76	1.31	1128.3	12.4	1007.8	8.1	1112.0	13.0	1112.0	13.0
86	84	0.80	1097.4	13.2	1161.6	11.8	1113.4	32.1	1113.4	32.1
87	291	0.83	179.3	2.0	183.8	3.2	222.3	31.3	179.3	2.0
88	319	1.74	243.6	4.2	242.0	6.5	224.6	71.9	243.6	4.2
89	143	0.98	237.3	2.4	242.8	3.5	280.4	27.8	237.3	2.4
90	172	1.07	946.7	22.2	1005.1	16.1	993.0	44.6	993.0	44.6
91	84	0.63	40.4	1.2	42.5	3.2	252.6	53.9	40.4	1.2
92	195	1.38	1318.9	14.3	1500.9	7.7	1484.5	6.2	1484.5	6.2
93	87	13.89	185.0	4.2	189.3	8.2	292.7	56.8	185.0	4.2
94	427	3.42	1842.3	42.1	1663.6	13.9	1578.2	21.6	1578.2	21.6
95	50	0.99	1110.9	8.2	1170.0	9.4	1230.2	11.7	1230.2	11.7
96	80	0.82	27.6	1.2	30.3	3.0	501.1	117.7	27.6	1.2
97	117	1.93	198.8	2.2	200.4	4.5	202.4	29.8	198.8	2.2
98	212	1.46	166.2	3.5	170.2	4.6	189.1	69.2	166.2	3.5
99	270	0.64	159.0	1.5	147.6	2.4	161.1	23.4	159.0	1.5
100	155	1.19	28.4	0.8	32.2	1.5	281.8	68.7	28.4	0.8
101	148	1.19	1494.7	26.2	1519.9	13.5	1335.2	26.0	1335.2	26.0
102	53	1.66	1358.6	22.4	1427.4	15.9	1510.1	40.7	1510.1	40.7
103	66	0.99	1362.7	27.6	1324.5	16.5	1456.7	10.0	1456.7	10.0
104	78	2.16	70.9	1.4	79.3	3.0	343.1	43.7	70.9	1.4
105	120	0.69	37.4	1.1	40.3	2.2	279.2	81.8	37.4	1.1

Sample 3: South Padre Island (Isla Blanca Park, Surface Sand)

#	U (ppm)	U/Th	$^{206}Pb/^{238}U$	± 2s	$^{207}Pb/^{235}U$	± 2s	$^{207}Pb/^{206}Pb$	± 2s	U-Pb Age	± 2s
1	302	0.57	161.3	2.2	150.1	1.5	178.5	20.4	161.3	2.2
2	145	2.04	1061.5	9.3	1012.5	14.1	949.8	12.0	949.8	12.0
3	501	3.05	213.3	1.8	245.5	2.2	230.1	13.1	213.3	1.8
4	17	0.63	42.9	7.1	44.3	2.3	715.2	157.4	42.9	7.1
5	21	1.38	927.9	19.8	952.8	18.6	958.2	68.7	958.2	68.7
6	178	1.27	336.9	6.4	356.3	5.6	372.7	57.1	336.9	6.4
7	515	2.61	1381.5	6.7	1332.0	9.8	1426.1	5.2	1426.1	5.2
8	119	1.17	81.5	2.7	92.8	1.7	233.8	40.2	81.5	2.7
9	216	1.54	1037.3	11.8	996.5	16.2	1076.3	30.4	1076.3	30.4
10	166	1.15	29.2	1.5	30.3	0.9	301.3	69.5	29.2	1.5
11	40	0.67	1066.1	9.1	1194.5	10.9	1234.4	20.8	1234.4	20.8
12	130	0.69	129.9	3.8	138.2	2.5	221.6	44.1	129.9	3.8
13	221	1.53	1205.7	12.7	1096.6	24.6	1192.0	32.0	1192.0	32.0
14	303	5.63	2001.8	11.8	2060.7	24.5	1829.2	22.0	1829.2	22.0
15	271	1.30	1671.9	12.6	1559.5	23.3	1728.6	19.7	1728.6	19.7
16	839	5.62	4.8	1.0	5.1	1.1	123.1	67.3	4.8	1.0
17	102	0.79	4.6	0.5	4.8	0.2	246.0	35.3	4.6	0.5
18	154	1.74	56.3	2.3	56.6	1.2	204.5	45.5	56.3	2.3
19	114	0.61	458.9	15.3	412.7	12.7	433.0	82.5	458.9	15.3
20	85	0.92	598.7	8.8	596.8	7.9	602.2	30.9	598.7	8.8
21	214	1.40	49.9	1.6	51.1	0.9	176.3	32.9	49.9	1.6
22	190	1.54	1493.2	9.1	1517.3	13.5	1302.7	5.6	1302.7	5.6
23	303	0.96	276.3	5.0	257.0	4.7	301.9	72.4	276.3	5.0
24	567	1.38	213.8	2.5	229.5	2.2	234.0	17.6	213.8	2.5
25	370	2.63	1796.8	14.8	1573.2	30.9	1711.5	24.6	1711.5	24.6
26	142	1.03	936.3	10.2	1072.6	14.2	1005.2	34.3	1005.2	34.3
27	246	2.80	65.5	1.5	73.3	1.4	119.1	30.4	65.5	1.5
28	136	1.42	1088.0	9.3	995.2	13.2	1185.9	29.0	1185.9	29.0
29	1200	1.77	220.2	1.8	237.0	1.5	248.4	10.9	220.2	1.8
30	217	1.19	52.0	1.9	55.4	0.8	168.5	37.6	52.0	1.9
31	196	2.41	1547.9	23.8	1800.6	45.0	1714.2	29.4	1714.2	29.4
32	37	0.65	1115.8	15.0	1211.1	19.3	1226.8	23.6	1226.8	23.6
33	152	0.40	29.3	1.3	31.0	0.7	234.4	51.6	29.3	1.3
34	53	1.24	1378.5	12.1	1439.4	26.3	1318.3	33.3	1318.3	33.3
35	1135	3.32	1397.5	6.0	1356.3	9.3	1432.0	5.6	1432.0	5.6
36	510	1.60	85.8	2.6	96.8	2.1	89.6	68.8	85.8	2.6
37	213	0.99	180.4	6.4	173.8	5.5	229.9	82.4	180.4	6.4
38	147	1.13	1118.4	11.3	1239.1	18.8	1080.0	37.0	1080.0	37.0

39	60	2.32	1132.1	21.3	1374.3	25.4	1177.5	38.5	1177.5	38.5
40	94	0.95	40.3	2.8	38.5	1.4	517.6	129.9	40.3	2.8
41	91	0.80	33.7	5.5	38.0	2.3	10.3	313.7	33.7	5.5
42	177	1.09	1000.7	15.6	965.1	23.9	1040.1	46.3	1040.1	46.3
43	231	1.57	193.3	4.6	169.9	3.3	175.6	70.6	193.3	4.6
44	272	0.48	42.3	2.2	35.4	1.4	214.6	120.8	42.3	2.2
45	247	1.00	451.1	9.0	382.1	10.0	421.0	58.4	451.1	9.0
46	209	2.22	1391.7	15.7	1425.3	26.5	1442.5	26.0	1442.5	26.0
47	105	1.04	223.7	4.6	204.0	2.5	221.4	42.9	223.7	4.6
48	21	0.64	40.3	6.0	43.8	2.0	729.7	121.0	40.3	6.0
49	79	0.52	77.4	3.4	69.8	1.8	261.8	48.2	77.4	3.4
50	83	0.60	40.4	3.5	41.8	1.1	238.4	58.3	40.4	3.5
51	183	1.12	1416.1	8.4	1395.5	18.4	1333.7	23.3	1333.7	23.3
52	80	2.07	63.4	3.2	61.8	1.7	316.3	55.5	63.4	3.2
53	282	1.90	33.8	0.9	33.5	0.6	147.7	37.7	33.8	0.9
54	251	0.33	97.8	7.1	89.6	3.7	187.5	163.6	97.8	7.1
55	206	1.66	1720.5	10.4	1583.1	21.6	1709.8	16.3	1709.8	16.3
56	234	1.77	1673.8	5.9	1629.6	14.2	1846.4	5.9	1846.4	5.9
57	194	1.05	1565.2	12.6	1763.9	23.9	1801.3	22.7	1801.3	22.7
58	300	0.83	162.5	3.3	170.2	1.9	161.3	41.5	162.5	3.3
59	845	1.11	65.5	1.9	65.8	1.3	64.1	83.7	65.5	1.9
60	177	1.07	1521.2	11.6	1455.0	22.4	1411.4	20.4	1411.4	20.4
61	83	0.93	1297.6	10.9	1464.7	19.0	1452.6	29.2	1452.6	29.2
62	591	2.14	230.4	3.6	215.3	3.0	284.5	16.3	230.4	3.6
63	147	1.10	33.9	1.5	38.8	0.7	262.0	50.6	33.9	1.5
64	225	4.40	1802.3	12.4	1673.0	23.0	1755.5	22.6	1755.5	22.6
65	209	1.08	55.1	3.3	56.3	1.8	75.0	122.7	55.1	3.3
66	170	1.41	61.7	1.7	61.4	1.1	182.8	30.0	61.7	1.7
67	125	1.20	1159.4	9.3	1065.2	14.6	1100.8	34.6	1100.8	34.6
68	148	0.64	1376.2	10.4	1409.0	16.9	1369.8	13.1	1369.8	13.1
69	39	0.95	229.1	13.0	250.9	10.6	395.3	138.5	229.1	13.0
70	183	1.26	34.8	1.4	31.7	0.6	299.4	47.5	34.8	1.4
71	69	0.93	1528.1	15.2	1323.4	28.5	1461.6	9.3	1461.6	9.3
72	201	2.87	254.1	3.0	264.3	3.4	274.5	21.2	254.1	3.0
73	48	1.99	1259.1	34.7	1055.6	43.0	1421.0	100.5	1421.0	100.5
74	50	0.72	140.2	6.3	116.3	3.1	308.2	54.3	140.2	6.3
75	80	1.16	1111.3	12.8	1125.2	17.4	1053.1	10.7	1053.1	10.7
76	161	1.06	270.2	4.3	234.2	2.5	229.7	23.9	270.2	4.3
77	92	0.77	78.8	7.1	71.7	2.6	552.2	236.6	78.8	7.1
78	175	1.33	1847.5	5.3	1751.1	10.2	1680.9	4.6	1680.9	4.6
79	111	1.24	585.3	10.4	564.1	8.9	640.3	45.4	585.3	10.4

80	321	2.34	1672.3	10.3	1767.4	22.3	1782.8	22.0	1782.8	22.0
81	252	0.59	187.2	2.9	158.0	2.1	194.6	29.6	187.2	2.9
82	28	1.12	1059.0	14.9	1081.2	17.0	1028.5	19.1	1028.5	19.1
83	850	3.24	104.1	6.5	89.7	6.0	93.1	116.8	104.1	6.5
84	450	1.81	1249.5	8.5	1287.9	13.1	1246.6	19.1	1246.6	19.1
85	51	0.88	1299.9	9.6	1496.8	13.8	1414.8	13.2	1414.8	13.2
86	126	0.85	250.9	3.4	224.1	3.0	247.6	28.5	250.9	3.4
87	160	1.07	97.5	3.0	87.7	2.0	205.6	41.3	97.5	3.0
88	251	1.52	1339.5	7.7	1396.9	15.5	1431.8	11.9	1431.8	11.9
89	97	1.05	1021.1	13.5	1173.0	15.2	1054.0	34.9	1054.0	34.9
90	84	1.15	691.4	7.5	637.4	10.7	606.3	46.6	691.4	7.5
91	54	1.01	1149.6	8.8	1292.8	8.9	1152.8	12.7	1152.8	12.7
92	192	5.30	76.1	2.5	76.0	1.1	254.7	40.1	76.1	2.5
93	313	2.23	206.9	2.3	212.0	1.8	200.3	16.0	206.9	2.3
94	96	0.80	1045.3	11.5	981.4	14.4	1059.2	30.0	1059.2	30.0
95	153	0.33	172.5	6.8	174.0	7.3	128.9	127.2	172.5	6.8
96	202	1.65	54.8	3.3	55.5	1.7	82.0	124.0	54.8	3.3
97	320	1.92	1354.3	7.1	1410.1	12.9	1429.6	5.5	1429.6	5.5

Sample 4: Boca Chica Beach (Beach near Brazos Santiago Pass, Surface Sand)

#	U (ppm)	U/Th	$^{206}Pb/^{238}U$	± 2s	$^{207}Pb/^{235}U$	± 2s	$^{207}Pb/^{206}Pb$	± 2s	U-Pb Age	± 2s
1	84	0.54	66.9	1.9	71.1	2.8	237.5	46.6	66.9	1.9
2	127	1.20	1064.2	14.5	1040.6	8.3	1044.5	30.1	1044.5	30.1
3	435	1.48	86.1	1.9	94.0	2.9	82.5	68.3	86.1	1.9
4	109	1.34	583.7	10.2	516.2	10.7	619.5	45.3	583.7	10.2
5	79	0.78	76.0	2.2	75.3	5.4	248.1	162.5	76.0	2.2
6	641	6.24	238.4	3.8	237.2	4.5	284.3	45.1	238.4	3.8
7	478	4.99	977.9	12.2	988.0	7.1	935.3	17.3	935.3	17.3
8	182	1.10	1721.9	25.0	1799.3	11.0	1691.9	17.0	1691.9	17.0
9	220	1.63	209.5	2.5	253.2	2.8	216.6	18.0	209.5	2.5
10	108	1.03	224.8	2.3	230.9	5.2	234.4	38.0	224.8	2.3
11	70	1.17	1178.1	17.3	1186.4	12.1	1179.3	10.9	1179.3	10.9
12	295	3.02	4.4	0.2	5.9	0.1	181.5	46.2	4.4	0.2
13	93	0.88	36.6	1.3	34.3	3.1	503.6	122.8	36.6	1.3
14	143	0.90	1730.5	14.7	1710.0	7.9	1565.4	19.8	1565.4	19.8
15	328	1.01	1360.5	23.2	1414.3	12.5	1328.4	20.8	1328.4	20.8
16	77	0.65	37.1	1.2	37.4	3.1	265.4	55.9	37.1	1.2
17	232	3.17	288.7	3.3	288.7	2.9	258.0	19.0	288.7	3.3
18	188	1.49	1700.7	17.1	1840.9	7.8	1656.4	9.7	1656.4	9.7
19	293	1.33	1705.2	23.8	1762.5	11.0	1638.1	17.4	1638.1	17.4
20	185	1.00	1338.9	22.2	1424.5	11.2	1377.7	19.8	1377.7	19.8
21	94	1.07	1017.3	15.8	1084.5	12.9	1197.0	33.3	1197.0	33.3
22	388	0.81	8.5	0.4	8.5	0.7	66.2	191.0	8.5	0.4
23	49	0.97	1422.1	13.4	1558.0	9.2	1412.4	12.7	1412.4	12.7
24	316	0.96	32.1	0.6	35.8	1.4	275.1	62.4	32.1	0.6
25	44	0.83	1498.3	13.8	1778.4	7.8	1556.5	11.8	1556.5	11.8
26	175	1.10	949.2	23.2	913.6	18.5	1069.2	47.1	1069.2	47.1
27	91	0.83	33.5	2.3	34.7	6.1	10.8	289.6	33.5	2.3
28	148	0.90	233.5	2.3	204.9	3.9	297.1	31.1	233.5	2.3
29	31	0.31	27.4	1.5	28.9	5.0	675.5	161.0	27.4	1.5
30	274	1.89	33.1	0.7	32.3	1.0	157.2	39.6	33.1	0.7
31	566	2.15	252.4	3.2	251.2	3.7	255.9	18.0	252.4	3.2
32	101	0.66	15.0	0.2	15.4	0.5	228.7	33.6	15.0	0.2
33	285	2.61	64.7	1.3	69.0	1.7	118.6	29.0	64.7	1.3
34	101	0.84	617.5	7.4	599.7	8.8	567.1	30.5	617.5	7.4
35	82	1.39	565.7	12.9	660.2	13.3	614.9	74.1	565.7	12.9
36	216	1.00	54.3	1.6	57.3	3.6	72.5	136.3	54.3	1.6
37	165	1.17	58.6	1.3	53.0	1.7	163.2	40.4	58.6	1.3
38	186	1.11	1409.6	17.3	1376.6	9.1	1532.4	23.0	1532.4	23.0
39	308	4.96	1929.0	23.5	1872.6	11.2	1773.3	20.6	1773.3	20.6

40	206	5.63	72.2	1.0	73.2	2.4	248.2	34.0	72.2	1.0
41	44	0.76	1075.8	12.5	1187.6	7.9	1240.4	17.6	1240.4	17.6
42	76	1.10	1829.7	27.9	1638.3	19.5	1545.5	26.8	1545.5	26.8
43	356	1.37	188.4	1.6	180.3	2.1	169.6	19.1	188.4	1.6
44	282	0.61	173.7	1.5	170.5	2.4	161.0	21.8	173.7	1.5
45	389	5.46	63.3	0.9	55.6	1.4	164.0	28.3	63.3	0.9
46	169	1.53	53.9	1.2	63.0	2.2	217.7	43.8	53.9	1.2
47	175	1.52	2380.0	24.3	2699.1	15.4	2525.3	11.5	2525.3	11.5
48	307	1.88	1734.5	17.0	1713.4	10.1	1599.1	9.7	1599.1	9.7
49	90	14.27	178.4	3.8	204.6	8.2	251.4	56.6	178.4	3.8
50	72	1.05	1494.6	23.6	1492.0	16.7	1442.4	10.4	1442.4	10.4
51	550	1.09	377.2	8.2	454.6	6.9	519.0	42.1	377.2	8.2
52	93	0.77	1040.5	12.9	998.0	10.7	1188.7	32.5	1188.7	32.5
53	434	3.30	1686.3	41.2	1544.0	13.9	1764.8	24.4	1764.8	24.4
54	199	1.59	949.8	15.1	1143.1	12.2	1175.3	28.3	1175.3	28.3
55	37	0.88	244.7	10.0	256.3	12.0	358.7	142.7	244.7	10.0
56	44	0.68	122.0	2.7	121.9	5.6	365.2	56.5	122.0	2.7
57	144	12.11	59.5	1.9	63.3	4.5	87.4	142.7	59.5	1.9
58	184	0.47	196.6	3.5	201.2	4.2	193.8	58.4	196.6	3.5
59	173	1.07	62.3	1.0	62.3	1.9	178.8	30.9	62.3	1.0
60	211	0.91	110.7	2.7	108.3	3.9	145.6	74.0	110.7	2.7
61	908	3.21	103.5	6.9	90.7	5.4	98.2	118.0	103.5	6.9
62	533	0.92	106.4	1.9	106.9	2.9	121.6	64.5	106.4	1.9
63	148	0.72	165.5	2.9	161.6	3.3	181.0	25.2	165.5	2.9
64	519	1.37	213.8	2.3	250.7	2.1	262.4	16.8	213.8	2.3
65	54	1.63	1321.0	20.1	1445.5	17.2	1531.0	39.8	1531.0	39.8
66	151	1.15	29.0	0.9	31.7	1.7	312.7	66.2	29.0	0.9
67	70	0.73	2488.8	33.3	2395.7	13.1	2335.4	19.2	2335.4	19.2
68	166	0.40	35.4	0.9	30.6	1.3	232.9	54.7	35.4	0.9
69	32	0.67	1091.9	18.2	1064.6	15.0	1197.1	27.3	1197.1	27.3
70	46	0.99	1124.7	18.2	1094.8	15.8	981.3	38.8	981.3	38.8
71	91	2.10	60.4	1.8	61.0	3.2	321.3	54.2	60.4	1.8
72	259	5.68	78.8	1.0	71.1	1.4	131.3	21.7	78.8	1.0
73	82	0.70	33.0	1.3	38.6	2.9	360.6	86.7	33.0	1.3
74	52	1.81	988.3	12.1	1190.4	9.8	1098.6	14.0	1098.6	14.0
75	117	1.24	82.0	1.6	81.1	2.5	199.9	41.7	82.0	1.6
76	360	0.81	1304.4	8.7	1314.5	7.0	1284.5	14.7	1284.5	14.7
77	164	1.12	101.2	3.5	96.1	5.2	93.5	109.4	101.2	3.5
78	133	1.07	33.8	0.7	40.1	1.6	269.6	54.5	33.8	0.7
79	321	2.14	1768.8	21.2	1697.4	9.2	1533.8	19.8	1533.8	19.8
80	1169	3.81	1367.1	9.4	1483.3	5.0	1529.0	5.4	1529.0	5.4

81	218	1.42	1513.0	13.0	1403.9	7.8	1299.4	6.3	1299.4	6.3
82	39	0.93	1369.4	24.4	1325.6	15.4	1418.0	45.8	1418.0	45.8
83	118	0.68	1607.3	20.6	1683.7	10.9	1784.0	22.4	1784.0	22.4
84	288	2.10	212.1	1.6	201.6	2.3	199.7	16.2	212.1	1.6
85	59	2.05	1126.8	24.6	1118.6	21.1	1287.0	39.2	1287.0	39.2
86	1007	5.53	44.6	0.9	47.0	1.0	117.4	69.1	44.6	0.9
87	248	1.54	193.2	3.3	191.9	4.5	162.8	70.6	193.2	3.3
88	158	1.04	239.0	2.5	242.9	4.2	252.2	21.0	239.0	2.5
89	79	1.37	1070.7	12.5	1122.1	8.5	1015.7	12.0	1015.7	12.0
90	143	0.99	972.4	13.8	958.2	11.3	985.4	31.0	985.4	31.0
91	157	0.35	168.4	7.3	152.9	7.7	136.3	128.2	168.4	7.3
92	152	0.69	1374.5	16.6	1446.2	10.5	1440.3	13.7	1440.3	13.7

Sample 5: Boca Chica Beach (Midpoint, Surface Sand)

#	U (ppm)	U/Th	$^{206}Pb/^{238}U$	± 2s	$^{207}Pb/^{235}U$	± 2s	$^{207}Pb/^{206}Pb$	± 2s	U-Pb Age	± 2s
1	462	0.78	88.9	2.4	102.6	2.6	64.6	52.5	88.9	2.4
2	249	1.70	1535.9	16.8	1305.9	7.7	1528.4	13.4	1528.4	13.4
3	152	0.27	24.5	1.6	29.9	4.4	766.8	166.9	24.5	1.6
4	123	0.83	208.3	2.4	240.0	3.8	250.7	27.6	208.3	2.4
5	70	1.13	1798.4	30.1	1574.1	19.5	1626.6	28.8	1626.6	28.8
6	324	2.02	1320.2	10.5	1205.1	6.6	1563.6	5.1	1563.6	5.1
7	465	2.90	68.3	1.1	75.3	2.1	159.1	30.7	68.3	1.1
8	221	1.36	104.1	1.7	94.5	2.8	124.7	29.2	104.1	1.7
9	115	0.63	41.1	1.1	35.4	2.1	334.4	89.7	41.1	1.1
10	77	0.84	1119.9	13.3	1079.8	9.9	1041.6	33.1	1041.6	33.1
11	141	2.07	947.2	8.9	810.8	8.3	856.1	25.5	856.1	25.5
12	133	1.23	59.2	2.0	61.6	2.3	138.9	41.3	59.2	2.0
13	198	1.17	1560.4	9.6	1577.7	4.8	1602.3	5.3	1602.3	5.3
14	38	0.78	1034.6	18.6	1098.3	16.9	1204.5	22.1	1204.5	22.1
15	518	1.12	5.5	0.8	6.0	1.3	105.0	24.8	5.5	0.8
16	45	1.86	1022.7	21.3	893.1	17.0	1147.4	55.8	1147.4	55.8
17	499	3.22	221.8	1.8	252.2	1.6	261.3	11.6	221.8	1.8
18	283	5.63	2092.1	28.6	1739.8	11.0	1615.0	19.3	1615.0	19.3
19	330	0.87	16.8	0.2	18.1	0.5	180.0	41.2	16.8	0.2
20	49	2.28	1304.0	44.1	1326.8	35.0	1489.3	102.3	1489.3	102.3
21	247	0.70	1122.4	11.8	1025.3	6.4	1146.3	23.1	1146.3	23.1
22	86	2.12	76.3	1.4	77.5	3.5	370.9	47.0	76.3	1.4
23	63	0.75	2441.8	36.1	2234.7	14.6	2731.7	19.4	2731.7	19.4
24	143	1.03	1047.4	21.5	1268.8	13.3	1169.2	35.4	1169.2	35.4
25	52	1.12	1224.0	25.4	1306.0	11.7	1509.8	31.3	1509.8	31.3
26	87	0.77	84.1	2.8	71.1	6.8	447.0	244.5	84.1	2.8
27	106	0.66	396.1	13.5	421.8	17.6	420.4	96.8	396.1	13.5
28	117	0.91	39.7	1.0	41.7	3.3	436.6	111.4	39.7	1.0
29	142	1.03	55.4	1.7	53.9	2.2	354.9	68.1	55.4	1.7
30	132	0.91	206.6	2.5	211.1	3.9	266.1	27.3	206.6	2.5
31	100	0.70	1390.7	16.0	1666.7	6.3	1740.9	12.5	1740.9	12.5
32	397	0.62	293.4	10.7	357.0	14.1	319.7	92.5	293.4	10.7
33	129	1.16	1556.4	28.7	1581.0	15.8	1304.1	28.5	1304.1	28.5
34	116	0.89	218.5	2.4	191.9	5.0	234.7	35.7	218.5	2.4
35	152	0.34	163.4	6.0	166.7	7.6	155.7	131.4	163.4	6.0
36	86	1.31	1034.1	12.2	896.2	12.1	1057.1	36.9	1057.1	36.9
37	88	1.41	695.1	11.7	605.2	12.7	527.0	65.8	695.1	11.7
38	46	1.47	1512.0	18.5	1537.1	16.9	1484.0	38.0	1484.0	38.0
39	64	0.63	1536.0	30.3	1562.5	15.8	1968.5	44.7	1968.5	44.7

40	75	1.02	1205.7	17.8	1262.0	14.5	1136.1	11.7	1136.1	11.7
41	230	1.50	949.4	14.3	1093.9	12.4	1045.6	25.1	1045.6	25.1
42	123	0.93	258.7	2.1	258.9	4.2	266.8	16.8	258.7	2.1
43	182	0.34	31.7	0.6	30.5	1.1	247.5	52.1	31.7	0.6
44	243	1.23	96.8	1.9	111.4	3.3	152.8	74.6	96.8	1.9
45	293	5.49	84.3	0.9	68.5	1.5	133.8	23.9	84.3	0.9
46	93	0.56	81.6	2.0	69.0	3.3	238.6	38.7	81.6	2.0
47	73	2.44	1441.1	33.0	1280.2	17.5	1232.4	27.2	1232.4	27.2
48	262	0.96	29.5	0.6	33.8	1.4	287.8	55.7	29.5	0.6
49	328	0.72	140.4	2.2	161.2	3.3	195.9	46.2	140.4	2.2
50	302	1.95	558.1	10.2	690.6	8.4	686.4	36.0	558.1	10.2
51	61	2.30	1191.4	23.7	1375.2	23.5	1240.0	43.1	1240.0	43.1
52	74	5.38	1216.9	11.7	1122.2	9.5	1021.3	12.3	1021.3	12.3
53	206	1.40	187.8	3.3	157.7	4.7	178.3	78.6	187.8	3.3
54	102	0.61	43.0	2.0	41.7	6.0	626.1	142.6	43.0	2.0
55	122	1.05	82.7	2.5	86.7	4.0	159.6	106.6	82.7	2.5
56	231	1.39	1213.0	20.9	1064.5	11.0	1034.4	31.6	1034.4	31.6
57	14	0.75	948.9	31.8	978.6	32.1	1128.9	47.1	1128.9	47.1
58	156	0.46	31.6	0.8	32.5	1.2	231.0	54.0	31.6	0.8
59	270	2.20	217.5	1.9	232.5	2.5	186.6	16.6	217.5	1.9
60	124	0.69	112.3	2.8	125.9	3.4	207.7	46.2	112.3	2.8
61	169	0.94	52.0	0.9	55.6	2.0	175.7	33.3	52.0	0.9
62	176	1.76	63.6	1.1	60.9	1.6	187.7	35.1	63.6	1.1
63	184	1.14	1568.1	23.5	1644.8	11.5	1565.1	22.0	1565.1	22.0
64	178	1.76	88.4	1.8	107.7	2.3	158.6	24.1	88.4	1.8
65	178	2.52	936.1	5.6	872.7	4.5	984.7	9.3	984.7	9.3
66	84	0.97	1360.8	20.9	1351.7	11.0	1299.7	26.8	1299.7	26.8
67	485	4.48	1004.2	11.3	1090.2	6.9	1057.5	19.3	1057.5	19.3
68	344	1.18	1413.0	21.3	1270.8	13.2	1473.3	20.0	1473.3	20.0
69	490	1.67	1083.8	13.0	1111.2	7.7	1191.5	23.2	1191.5	23.2
70	39	0.85	223.9	10.1	230.4	12.1	321.3	133.8	223.9	10.1
71	643	1.51	241.7	2.4	237.1	2.6	267.6	16.6	241.7	2.4
72	236	1.39	435.3	7.3	445.2	7.7	509.8	43.8	435.3	7.3
73	135	0.30	175.0	4.0	188.9	5.3	225.3	81.7	175.0	4.0
74	838	1.17	69.0	1.2	61.3	1.9	69.4	69.4	69.0	1.2
75	365	0.66	44.7	2.5	35.9	8.2	767.2	174.9	44.7	2.5
76	786	3.51	98.0	5.8	96.8	5.5	92.4	121.5	98.0	5.8
77	250	1.74	193.5	3.5	182.0	5.8	259.4	76.4	193.5	3.5
78	160	1.09	1360.4	23.5	1597.2	13.0	1344.9	19.8	1344.9	19.8
79	189	1.35	58.5	0.9	50.1	1.5	173.0	29.6	58.5	0.9
80	35	0.82	97.5	4.8	104.1	11.5	179.8	215.7	97.5	4.8

81	71	1.04	1320.9	28.9	1300.9	14.7	1289.0	11.2	1289.0	11.2
82	129	1.99	209.4	2.5	212.2	4.2	220.0	25.4	209.4	2.5
83	52	0.91	1037.3	23.0	1000.8	26.7	1008.5	89.9	1008.5	89.9
84	53	0.61	138.7	3.3	122.3	5.9	327.1	63.2	138.7	3.3
85	83	0.77	73.9	2.3	66.1	4.9	292.3	147.5	73.9	2.3
86	284	0.46	180.1	3.6	160.3	4.4	184.5	77.7	180.1	3.6
87	257	3.03	65.1	2.3	58.2	1.9	176.5	49.6	65.1	2.3
88	235	1.15	415.3	9.4	368.6	10.3	431.9	51.3	415.3	9.4
89	175	1.59	56.7	1.7	57.0	3.0	78.9	145.7	56.7	1.7
90	1114	3.70	1482.2	9.8	1518.7	5.7	1358.8	5.9	1358.8	5.9
91	252	1.63	27.4	0.6	32.3	0.8	155.7	35.1	27.4	0.6
92	153	0.67	1147.0	17.0	1335.0	11.6	1558.6	14.3	1558.6	14.3
93	395	1.02	409.8	6.7	419.8	6.1	589.4	38.7	409.8	6.7
94	172	1.08	165.5	5.7	162.9	6.2	218.0	87.0	165.5	5.7
95	68	1.23	1722.0	26.9	1787.8	11.9	1800.4	28.1	1800.4	28.1
96	92	1.97	53.0	1.8	59.7	3.2	292.6	57.5	53.0	1.8
97	74	0.93	1142.5	28.5	1307.3	18.8	1064.5	53.4	1064.5	53.4
98	46	0.81	1664.3	11.4	1811.2	6.3	1621.0	13.3	1621.0	13.3
99	183	2.20	1293.9	30.3	1534.9	16.8	1446.1	22.9	1446.1	22.9
100	49	1.16	1107.8	20.8	1237.0	15.2	1047.7	39.8	1047.7	39.8
101	867	2.32	80.1	1.1	66.2	1.7	109.0	49.7	80.1	1.1
102	57	0.93	1457.0	11.6	1514.5	9.6	1303.7	13.8	1303.7	13.8
103	561	2.02	205.6	3.0	236.7	3.3	257.6	15.4	205.6	3.0

Sample 6: Boca Chica Beach (Beach near mouth of Rio Grande, Surface Sand)

#	U (ppm)	U/Th	$^{206}Pb/^{238}U$	± 2s	$^{207}Pb/^{235}U$	± 2s	$^{207}Pb/^{206}Pb$	± 2s	U-Pb Age	± 2s
1	357	0.64	80.1	3.5	81.7	6.6	62.7	161.2	80.1	3.5
2	257	0.98	137.8	1.7	150.1	3.4	183.5	54.8	137.8	1.7
3	42	2.04	1073.1	37.7	1234.5	35.7	1222.7	111.1	1222.7	111.1
4	239	1.32	104.5	1.7	87.2	2.6	142.9	29.1	104.5	1.7
5	96	0.64	142.2	2.5	121.3	3.1	236.8	35.1	142.2	2.5
6	23	0.52	46.5	1.8	39.8	7.4	750.6	112.6	46.5	1.8
7	350	2.58	1512.5	27.8	1678.9	12.9	1686.6	25.5	1686.6	25.5
8	208	1.79	2989.0	23.0	2995.0	12.4	2948.1	12.3	2948.1	12.3
9	411	5.74	1040.8	12.7	1136.7	6.6	899.6	17.6	899.6	17.6
10	164	1.01	109.1	3.8	82.2	5.2	96.2	106.8	109.1	3.8
11	32	0.85	128.2	6.3	125.7	10.9	188.1	269.1	128.2	6.3
12	99	1.26	871.8	17.9	1010.0	12.4	1198.2	26.5	1198.2	26.5
13	153	2.32	909.8	11.9	1024.9	7.6	806.0	29.0	806.0	29.0
14	825	3.27	89.1	7.7	92.3	6.4	80.0	103.6	89.1	7.7
15	144	1.09	233.4	2.2	210.2	3.4	314.8	27.5	233.4	2.2
16	98	0.89	583.0	11.8	606.9	8.6	647.0	39.7	583.0	11.8
17	112	1.02	42.3	1.9	42.2	3.4	235.9	240.4	42.3	1.9
18	113	1.28	886.5	12.4	1118.5	8.3	910.2	35.6	910.2	35.6
19	284	2.30	1826.0	18.1	1935.0	8.9	1919.7	19.3	1919.7	19.3
20	50	1.12	2004.3	23.0	1529.1	16.1	1864.8	35.3	1864.8	35.3
21	307	1.00	16.3	0.5	16.8	1.3	323.4	57.4	16.3	0.5
22	228	1.74	147.7	3.0	179.3	4.1	172.9	83.1	147.7	3.0
23	383	1.64	1351.2	23.8	1682.2	18.0	1334.2	25.2	1334.2	25.2
24	171	1.16	57.2	1.3	65.5	1.6	166.0	34.2	57.2	1.3
25	136	0.73	262.6	2.3	241.5	3.8	271.4	28.0	262.6	2.3
26	109	0.88	1552.2	12.5	1970.7	9.2	1513.9	21.1	1513.9	21.1
27	141	12.35	58.2	2.3	51.8	4.3	81.0	139.6	58.2	2.3
28	209	1.67	1495.5	10.9	1654.6	5.0	1544.7	6.1	1544.7	6.1
29	841	1.19	61.1	1.2	73.9	1.8	74.6	63.5	61.1	1.2
30	142	0.96	1079.6	20.6	922.9	14.6	1148.1	41.6	1148.1	41.6
31	97	1.12	1249.5	15.1	1013.9	13.3	1262.6	37.6	1262.6	37.6
32	110	0.79	616.4	6.9	725.3	10.0	605.3	34.0	616.4	6.9
33	144	1.15	97.2	2.3	111.6	2.7	185.8	36.0	97.2	2.3
34	145	0.68	128.7	2.3	180.7	3.5	208.2	27.2	128.7	2.3
35	350	1.91	661.4	10.3	609.1	9.9	567.9	33.6	661.4	10.3
36	94	1.19	857.7	14.2	1003.6	12.7	1041.2	33.2	1041.2	33.2
37	21	0.61	39.5	2.0	40.2	6.6	840.6	184.5	39.5	2.0
38	218	2.65	1873.5	44.0	1985.6	28.2	1369.7	35.2	1369.7	35.2
39	147	0.50	26.3	0.9	27.7	2.0	480.2	87.1	26.3	0.9

40	78	1.28	1283.6	30.3	1805.0	17.2	1419.2	37.5	1419.2	37.5
41	88	1.05	490.0	9.4	533.4	8.5	543.9	53.3	490.0	9.4
42	107	0.61	39.5	1.1	46.0	2.5	245.2	78.5	39.5	1.1
43	47	0.89	1496.2	29.5	1293.1	18.4	1377.5	37.2	1377.5	37.2
44	264	2.16	29.7	0.6	27.7	0.9	175.5	41.0	29.7	0.6
45	71	0.63	2597.7	36.7	3014.0	11.2	2880.9	21.3	2880.9	21.3
46	254	0.62	154.0	2.9	198.2	5.3	165.8	32.2	154.0	2.9
47	271	0.83	148.3	2.5	149.1	2.5	191.2	30.4	148.3	2.5
48	211	1.09	1511.4	19.5	1428.4	13.5	1685.8	23.8	1685.8	23.8
49	756	4.58	46.4	1.1	50.6	1.0	107.2	51.4	46.4	1.1
50	76	0.96	1231.5	37.1	1064.0	17.6	1163.5	51.7	1163.5	51.7
51	219	1.07	262.1	3.5	282.9	5.5	244.5	64.3	262.1	3.5
52	265	2.94	60.1	2.3	77.3	1.6	153.2	52.2	60.1	2.3
53	525	1.48	216.8	2.5	265.5	2.5	286.3	18.9	216.8	2.5
54	185	5.41	77.0	1.1	74.6	2.2	253.5	42.1	77.0	1.1
55	57	0.89	31.9	1.7	28.1	3.3	466.1	96.0	31.9	1.7
56	34	0.82	218.6	10.3	246.1	15.1	368.8	158.6	218.6	10.3
57	275	0.58	42.7	1.4	47.5	2.0	195.8	144.8	42.7	1.4
58	336	2.09	213.1	1.9	230.4	2.0	195.3	19.1	213.1	1.9
59	548	14.48	31.8	2.7	38.5	4.0	238.6	76.5	31.8	2.7
60	830	2.23	1330.6	17.5	1263.7	7.9	1595.3	12.1	1595.3	12.1
61	46	1.30	1409.7	26.0	1253.2	19.7	1422.3	49.3	1422.3	49.3
62	151	1.07	1462.2	23.6	1888.6	11.7	1724.9	17.9	1724.9	17.9
63	57	1.07	1313.8	10.0	1157.8	7.3	1228.5	10.4	1228.5	10.4
64	309	0.99	1337.7	22.6	1596.0	11.0	1158.1	18.6	1158.1	18.6
65	204	1.59	1239.9	23.3	1202.3	8.3	1662.5	21.3	1662.5	21.3
66	168	1.00	1358.1	7.1	1597.1	4.1	1422.5	7.5	1422.5	7.5
67	79	1.78	1677.3	36.1	1424.8	17.5	1519.6	30.7	1519.6	30.7
68	120	0.72	31.7	0.8	40.6	3.0	450.3	111.5	31.7	0.8
69	22	1.50	791.6	16.5	1098.0	23.7	1139.1	74.5	1139.1	74.5
70	97	0.56	1378.4	18.7	1860.1	7.0	1731.8	10.9	1731.8	10.9
71	60	1.19	1448.7	21.1	1416.8	13.7	1171.9	40.7	1171.9	40.7
72	339	1.23	201.6	1.4	154.8	2.0	212.1	17.2	201.6	1.4
73	334	0.84	1470.2	10.6	1295.4	8.5	1280.6	16.5	1280.6	16.5
74	202	1.24	1587.0	21.5	1489.5	14.2	1374.5	27.3	1374.5	27.3
75	76	1.38	876.3	17.6	961.1	16.5	891.9	57.5	891.9	57.5
76	63	0.73	1260.7	21.2	1531.9	14.5	1641.5	47.4	1641.5	47.4
77	230	0.97	96.9	1.7	114.3	2.9	151.9	78.0	96.9	1.7
78	125	1.22	64.2	2.4	53.9	2.7	165.6	46.7	64.2	2.4
79	320	0.84	378.8	10.6	305.2	11.8	324.6	105.0	378.8	10.6
80	88	1.00	30.8	1.6	40.3	2.7	522.5	123.7	30.8	1.6

81	400	0.81	99.3	2.5	104.5	3.1	54.0	60.5	99.3	2.5
82	252	1.27	981.7	20.6	992.0	11.1	1242.8	27.4	1242.8	27.4
83	166	1.11	92.0	1.4	85.3	2.5	185.0	32.4	92.0	1.4
84	226	1.00	457.1	10.5	356.5	8.4	392.4	66.5	457.1	10.5
85	65	6.34	1205.0	15.1	1253.9	11.2	1235.6	13.0	1235.6	13.0
86	378	1.07	511.6	10.4	418.1	10.2	525.6	16.6	511.6	10.4
87	50	0.97	1113.0	18.3	967.4	13.2	818.4	45.2	818.4	45.2
88	327	2.90	1648.5	28.6	1613.4	14.5	1797.5	13.7	1797.5	13.7
89	127	0.37	169.5	4.1	189.2	4.6	243.8	66.7	169.5	4.1
90	81	1.66	1386.4	25.1	1274.0	14.7	1790.0	24.6	1790.0	24.6
91	260	3.09	257.3	2.8	254.0	3.0	236.4	18.7	257.3	2.8
92	267	1.86	1655.5	17.8	1461.0	6.4	1631.9	12.8	1631.9	12.8
93	514	2.31	1094.6	8.5	1303.7	7.4	1396.6	4.4	1396.6	4.4
94	67	0.94	58.4	2.2	68.5	4.5	217.9	124.2	58.4	2.2
95	93	0.99	1436.4	10.8	1969.8	5.9	1833.8	7.8	1833.8	7.8
96	111	0.86	191.7	3.2	211.1	6.5	264.1	34.5	191.7	3.2
97	170	0.61	1115.1	15.6	1170.3	11.0	1633.3	12.6	1633.3	12.6
98	42	1.89	1623.0	19.5	1411.3	16.1	1502.3	33.5	1502.3	33.5
99	500	3.79	1869.4	42.3	1674.0	15.0	1440.0	19.1	1440.0	19.1
100	159	0.37	169.5	7.8	135.2	6.0	138.7	117.8	169.5	7.8
101	123	1.24	79.3	2.4	96.0	4.1	172.0	125.1	79.3	2.4
102	74	0.85	1698.7	29.4	1356.3	12.9	1581.6	8.7	1581.6	8.7
103	107	2.29	1007.3	18.8	1030.3	9.0	1269.3	30.6	1269.3	30.6
104	302	1.01	190.8	1.2	156.1	2.0	164.8	21.4	190.8	1.2
105	51	2.53	1454.8	25.2	1252.8	21.5	1465.5	34.1	1465.5	34.1
106	492	1.44	1242.1	12.7	1337.1	9.7	1279.1	22.2	1279.1	22.2
107	360	0.41	177.9	4.4	186.3	4.9	193.2	78.4	177.9	4.4
108	66	0.92	3149.5	17.1	2684.6	6.3	2255.6	5.2	2255.6	5.2

Sample 7: Boca Chica Beach (Beach near mouth of Rio Grande, Top of Core)

#	U (ppm)	U/Th	$^{206}Pb/^{238}U$	± 2s	$^{207}Pb/^{235}U$	± 2s	$^{207}Pb/^{206}Pb$	± 2s	U-Pb Age	± 2s
1	185	2.67	942.0	5.7	1010.8	5.3	936.5	8.9	936.5	8.9
2	251	1.05	385.1	9.7	436.1	9.0	379.7	48.2	385.1	9.7
3	1017	1.06	203.3	2.7	214.6	2.9	227.9	20.6	203.3	2.7
4	481	5.57	968.3	13.5	953.7	7.9	1079.5	20.0	1079.5	20.0
5	47	1.81	1210.1	43.4	1247.0	37.0	1529.2	91.8	1529.2	91.8
6	57	0.79	1244.4	10.8	1064.1	8.2	1268.1	11.0	1268.1	11.0
7	56	0.87	1031.6	25.6	948.2	26.6	1028.6	86.7	1028.6	86.7
8	204	1.46	1373.1	17.2	1198.6	8.2	1313.6	12.3	1313.6	12.3
9	355	0.76	192.7	2.4	153.3	4.6	190.7	49.0	192.7	2.4
10	211	1.21	1813.6	22.8	1919.9	13.2	1932.5	24.3	1932.5	24.3
11	184	1.70	64.6	1.1	58.5	1.9	193.6	30.8	64.6	1.1
12	178	0.95	61.9	0.9	66.9	2.3	163.7	31.7	61.9	0.9
13	365	0.75	83.2	3.3	77.9	5.6	60.0	169.5	83.2	3.3
14	80	0.85	26.5	1.2	34.4	3.2	540.8	107.4	26.5	1.2
15	166	1.35	1705.2	17.6	1465.1	8.4	1457.0	10.0	1457.0	10.0
16	886	5.80	41.9	0.9	53.5	1.3	118.1	59.0	41.9	0.9
17	482	1.80	1141.1	13.0	1043.0	9.0	1334.0	24.3	1334.0	24.3
18	121	0.44	33.5	0.9	27.1	1.8	422.0	87.2	33.5	0.9
19	93	0.58	38.6	1.4	35.2	2.9	291.9	50.5	38.6	1.4
20	173	1.18	27.5	0.8	29.8	1.4	279.5	65.4	27.5	0.8
21	23	0.93	1210.1	16.5	1033.3	14.6	1041.3	18.1	1041.3	18.1
22	45	1.06	1238.5	20.5	1589.1	13.2	1201.9	35.3	1201.9	35.3
23	360	3.49	1660.7	28.1	1649.5	13.7	1853.0	13.7	1853.0	13.7
24	86	2.19	76.5	1.4	78.6	3.1	331.5	48.6	76.5	1.4
25	51	0.92	1435.8	12.7	1320.5	8.5	1380.8	15.2	1380.8	15.2
26	63	0.99	1219.7	23.7	1369.0	15.4	1658.1	44.8	1658.1	44.8
27	193	1.23	60.0	1.3	53.1	1.9	178.1	34.1	60.0	1.3
28	268	1.68	222.4	1.9	208.5	3.0	241.7	16.5	222.4	1.9
29	118	0.96	191.2	2.2	203.0	5.7	229.7	36.5	191.2	2.2
30	77	15.52	165.3	4.3	161.5	7.3	322.3	62.0	165.3	4.3
31	56	0.98	1363.8	9.7	1015.6	9.6	1141.9	13.5	1141.9	13.5
32	175	1.18	49.8	1.1	61.2	1.9	175.8	40.7	49.8	1.1
33	326	4.80	54.2	0.8	68.2	1.1	180.4	24.6	54.2	0.8
34	240	1.32	156.8	1.6	178.8	2.7	182.7	18.9	156.8	1.6
35	41	0.81	62.3	5.7	46.4	9.8	502.7	172.3	62.3	5.7
36	233	1.37	91.2	1.7	111.1	2.3	124.2	29.7	91.2	1.7
37	159	2.11	107.8	1.6	104.6	2.5	166.6	25.7	107.8	1.6
38	177	0.40	31.5	0.7	33.4	1.1	247.6	62.5	31.5	0.7
39	253	0.92	191.4	1.3	211.9	2.1	215.2	17.7	191.4	1.3

40	177	1.07	165.9	4.3	162.6	7.7	243.8	99.8	165.9	4.3
41	303	2.04	1399.6	11.1	1307.4	6.1	1233.6	5.1	1233.6	5.1
42	57	0.57	1405.3	31.7	1910.7	18.5	1756.8	51.7	1756.8	51.7
43	880	3.11	85.9	6.8	101.8	5.4	98.1	126.9	85.9	6.8
44	72	1.27	1058.1	16.2	1093.5	14.3	1148.9	9.8	1148.9	9.8
45	481	3.68	1487.5	36.2	1852.6	13.1	1626.6	20.8	1626.6	20.8
46	332	1.19	33.6	0.5	34.0	1.1	296.7	58.9	33.6	0.5
47	398	0.96	89.1	2.3	100.3	3.2	58.8	64.7	89.1	2.3
48	171	0.39	165.0	7.2	172.5	6.9	141.1	135.8	165.0	7.2
49	114	0.84	233.7	3.0	205.7	3.9	232.8	25.9	233.7	3.0
50	197	0.93	237.9	3.8	216.0	5.3	317.3	49.2	237.9	3.8
51	257	1.86	1904.8	25.1	1692.4	11.2	1888.5	19.4	1888.5	19.4
52	246	0.62	18.6	0.1	14.7	0.2	166.5	19.9	18.6	0.1
53	123	0.59	407.4	13.9	472.2	16.3	380.6	82.7	407.4	13.9
54	75	0.93	523.5	8.8	524.3	9.1	623.1	67.8	523.5	8.8
55	176	1.53	1507.9	19.3	1265.2	13.9	1611.9	24.3	1611.9	24.3
56	37	0.80	1189.4	13.1	1188.3	8.4	998.5	20.1	998.5	20.1
57	169	1.81	1802.8	16.9	1525.5	8.4	1461.5	18.8	1461.5	18.8
58	235	1.68	1101.7	14.9	1217.3	13.5	1062.8	23.7	1062.8	23.7
59	99	0.68	1152.2	13.1	942.0	9.5	1019.0	32.2	1019.0	32.2
60	86	1.51	1929.4	27.6	1874.3	18.9	1631.8	28.6	1631.8	28.6
61	345	1.42	1531.9	24.4	1769.3	18.0	1683.6	22.9	1683.6	22.9
62	453	2.83	245.7	1.9	228.0	1.6	212.3	10.5	245.7	1.9
63	476	1.09	411.1	7.2	432.1	6.1	526.2	32.1	411.1	7.2
64	146	0.87	1638.0	13.9	1523.1	9.0	1784.2	21.7	1784.2	21.7
65	234	1.58	1198.6	21.8	1210.8	10.5	1155.2	27.6	1155.2	27.6
66	185	1.45	1609.3	13.2	1195.8	7.2	1538.8	5.2	1538.8	5.2
67	113	1.64	1072.4	18.4	881.0	10.1	1163.4	30.4	1163.4	30.4
68	226	5.81	6.8	0.1	6.8	0.2	262.8	33.4	6.8	0.1
69	225	2.52	311.1	3.1	278.8	3.3	290.6	19.4	311.1	3.1
70	147	0.98	249.9	2.7	255.8	4.7	272.1	21.7	249.9	2.7
71	15	0.73	43.5	2.1	39.4	6.5	798.6	188.0	43.5	2.1
72	80	1.33	1098.9	14.4	991.8	12.6	1160.1	34.1	1160.1	34.1
73	269	3.17	55.1	2.2	60.3	1.9	177.6	41.4	55.1	2.2
74	353	1.04	549.2	11.0	521.6	9.9	518.2	15.6	549.2	11.0
75	52	0.76	2422.8	15.7	2444.0	8.0	2814.0	6.7	2814.0	6.7
76	273	0.32	85.6	4.2	114.1	5.9	195.4	145.8	85.6	4.2
77	14	0.78	985.5	33.1	1166.5	37.0	978.2	38.1	978.2	38.1
78	87	0.72	40.5	1.2	38.1	2.6	307.4	69.2	40.5	1.2
79	70	0.91	67.8	2.6	74.9	4.4	221.1	149.1	67.8	2.6
80	82	1.10	1120.4	12.5	1180.9	8.0	1163.0	13.8	1163.0	13.8

81	846	2.64	75.7	1.1	65.3	1.7	105.8	53.4	75.7	1.1
82	132	1.38	1127.7	14.1	1081.7	8.0	1113.9	27.1	1113.9	27.1
83	33	0.68	957.9	23.5	913.0	16.8	921.3	49.6	921.3	49.6
84	177	1.26	31.4	0.5	34.9	1.3	283.6	51.1	31.4	0.5
85	123	1.03	4.3	0.1	3.5	0.2	309.3	51.9	4.3	0.1
86	32	0.91	118.8	4.6	96.1	13.9	174.3	248.6	118.8	4.6
87	124	1.30	87.7	1.9	89.0	2.5	194.3	45.1	87.7	1.9
88	302	2.09	192.1	1.9	241.9	2.6	182.7	15.7	192.1	1.9
89	81	0.79	1343.1	34.6	1205.9	22.9	1237.6	50.3	1237.6	50.3
90	148	1.02	58.9	1.7	65.1	2.4	321.1	62.0	58.9	1.7
91	20	0.52	37.6	1.9	38.9	5.8	581.3	122.4	37.6	1.9
92	132	2.17	214.6	3.0	222.5	4.9	300.2	26.2	214.6	3.0
93	73	1.12	1908.1	28.8	1850.5	18.3	1942.4	23.2	1942.4	23.2
94	158	1.91	1495.1	8.6	1364.6	5.5	1361.9	5.1	1361.9	5.1
95	98	0.87	1574.5	11.2	1831.5	6.8	1775.4	10.3	1775.4	10.3
96	160	1.65	1080.8	9.4	895.3	6.7	1118.4	11.4	1118.4	11.4
97	134	1.12	71.1	2.5	80.9	4.2	162.0	113.7	71.1	2.5
98	192	1.10	57.7	0.9	54.1	1.9	199.2	33.4	57.7	0.9

Sample 8: Boca Chica Beach (Beach near mouth of Rio Grande, Bottom of Core)

#	U (ppm)	U/Th	$^{206}Pb/^{238}U$	± 2s	$^{207}Pb/^{235}U$	± 2s	$^{207}Pb/^{206}Pb$	± 2s	U-Pb Age	± 2s
1	78	2.60	1416.1	30.2	1473.9	20.6	1309.3	30.5	1309.3	30.5
2	209	1.54	1512.5	13.5	1335.3	7.6	1385.0	5.5	1385.0	5.5
3	80	0.68	39.8	1.3	34.6	2.8	369.2	77.6	39.8	1.3
4	406	1.37	173.9	1.8	176.7	2.4	181.4	18.3	173.9	1.8
5	116	0.64	135.9	2.6	119.3	4.1	230.0	43.6	135.9	2.6
6	144	0.68	148.5	2.8	147.8	3.2	170.9	27.4	148.5	2.8
7	45	0.87	1662.2	14.3	1789.1	7.8	1686.4	12.7	1686.4	12.7
8	132	0.85	223.8	2.9	219.1	3.7	255.1	27.3	223.8	2.9
9	1001	5.56	47.2	1.0	51.7	1.1	111.0	59.8	47.2	1.0
10	171	1.59	1314.9	9.4	1368.2	5.4	1391.8	5.8	1391.8	5.8
11	124	1.81	187.9	2.3	189.9	4.8	216.6	30.5	187.9	2.3
12	429	2.95	221.2	2.1	214.2	1.8	258.6	13.0	221.2	2.1
13	177	2.60	447.0	23.0	374.9	17.0	418.3	150.3	447.0	23.0
14	180	1.60	55.7	1.8	57.9	3.0	81.6	141.2	55.7	1.8
15	71	0.65	2329.2	30.5	2670.0	13.3	2626.6	18.8	2626.6	18.8
16	270	2.05	29.1	0.7	29.9	0.9	171.0	39.1	29.1	0.7
17	79	2.40	70.6	1.2	73.2	3.5	365.4	42.8	70.6	1.2
18	13	0.84	1061.9	29.5	959.1	36.7	1156.3	42.4	1156.3	42.4
19	51	0.27	30.0	1.3	30.8	3.4	525.0	128.2	30.0	1.3
20	101	0.97	668.2	7.2	552.4	9.8	581.2	32.0	668.2	7.2
21	542	2.59	1401.9	9.1	1501.0	6.8	1388.9	4.9	1388.9	4.9
22	117	1.72	244.1	3.1	226.8	4.6	265.1	30.0	244.1	3.1
23	1082	1.95	211.2	1.4	231.3	1.9	220.5	11.3	211.2	1.4
24	147	0.93	38.5	0.7	40.0	1.6	285.5	54.0	38.5	0.7
25	147	1.15	1760.9	21.0	1708.5	8.8	1708.3	22.7	1708.3	22.7
26	288	0.82	166.3	1.9	170.4	3.2	219.6	31.3	166.3	1.9
27	64	0.91	1432.0	26.5	1521.5	17.6	1509.8	10.7	1509.8	10.7
28	23	0.55	40.6	2.1	41.8	6.7	642.4	136.1	40.6	2.1
29	518	13.07	40.3	2.4	36.8	3.8	262.3	89.0	40.3	2.4
30	74	1.23	1039.1	17.2	1063.4	14.0	1066.1	10.2	1066.1	10.2
31	249	1.13	437.0	9.4	389.5	9.3	389.6	61.8	437.0	9.4
32	31	0.31	27.1	1.6	28.7	5.0	647.2	154.6	27.1	1.6
33	52	0.71	124.8	3.1	137.6	6.2	357.3	59.8	124.8	3.1
34	18	1.44	985.6	15.5	1043.3	23.0	1053.0	74.4	1053.0	74.4
35	84	0.85	33.3	2.5	36.3	5.9	10.5	290.1	33.3	2.5
36	222	1.32	106.7	1.8	103.3	2.6	138.5	29.6	106.7	1.8
37	477	0.97	55.6	0.8	53.9	1.1	107.7	27.2	55.6	0.8
38	52	0.95	1508.1	13.2	1335.5	10.0	1548.4	14.5	1548.4	14.5
39	19	0.63	42.6	2.5	41.8	6.7	736.1	174.4	42.6	2.5

40	59	0.81	2548.7	15.3	2953.5	7.3	2952.6	6.0	2952.6	6.0
41	120	0.98	233.1	2.8	210.2	5.4	257.1	28.6	233.1	2.8
42	156	2.07	1030.1	9.1	1010.1	6.7	976.3	12.6	976.3	12.6
43	210	1.21	29.3	0.6	31.9	1.3	272.7	54.7	29.3	0.6
44	179	1.23	56.5	0.9	60.1	2.0	195.2	38.8	56.5	0.9
45	72	1.38	998.1	12.5	1046.8	9.1	1122.7	13.9	1122.7	13.9
46	51	1.92	991.6	11.7	1161.8	9.0	1211.9	14.1	1211.9	14.1
47	101	0.69	38.6	1.1	39.3	2.2	325.1	76.0	38.6	1.1
48	66	5.57	1038.8	14.0	1109.8	9.4	1088.2	10.3	1088.2	10.3
49	205	1.23	61.9	1.0	62.7	2.1	181.5	30.9	61.9	1.0
50	55	0.81	1262.5	11.7	1074.6	7.6	1239.6	12.2	1239.6	12.2
51	109	1.57	1047.5	16.3	1046.1	11.2	1179.7	31.2	1179.7	31.2
52	262	1.17	161.9	1.7	185.5	2.2	194.8	21.0	161.9	1.7
53	295	0.65	165.6	1.5	165.1	2.4	167.5	20.6	165.6	1.5
54	41	1.70	1420.0	25.4	1385.4	17.4	1543.8	32.0	1543.8	32.0
55	38	0.94	1350.7	25.9	1525.0	15.6	1301.6	42.7	1301.6	42.7
56	590	1.42	244.6	2.2	249.5	2.5	270.9	18.4	244.6	2.2
57	179	1.64	2868.9	26.0	2471.4	15.0	2939.3	11.2	2939.3	11.2
58	153	1.68	59.8	1.2	63.7	2.4	244.5	41.9	59.8	1.2
59	146	0.60	1212.9	15.2	1240.7	10.1	1390.3	12.6	1390.3	12.6
60	126	1.19	1127.2	15.8	1088.1	8.9	1116.4	34.9	1116.4	34.9
61	232	0.62	174.0	1.9	180.8	2.6	169.4	25.9	174.0	1.9
62	184	2.77	1054.3	5.9	993.2	4.4	1043.3	8.2	1043.3	8.2
63	988	0.95	187.6	2.7	206.7	2.6	275.6	20.9	187.6	2.7
64	263	0.49	38.3	1.4	37.4	2.3	208.1	133.3	38.3	1.4
65	257	0.80	177.4	1.5	176.7	2.2	198.4	17.6	177.4	1.5
66	196	1.24	1856.2	11.2	1597.5	5.4	1694.7	4.9	1694.7	4.9
67	150	1.17	62.0	1.0	56.9	2.0	168.2	33.3	62.0	1.0
68	233	2.73	266.1	3.2	296.2	3.1	238.7	20.1	266.1	3.2
69	39	0.92	58.2	5.2	49.8	8.8	468.2	175.8	58.2	5.2
70	352	3.69	1564.0	32.7	1672.8	11.8	1598.0	13.3	1598.0	13.3
71	598	1.81	208.5	3.1	233.0	3.8	286.7	17.2	208.5	3.1
72	149	1.07	273.2	2.5	248.3	4.4	251.6	24.1	273.2	2.5
73	170	2.01	88.9	1.7	91.8	2.1	140.9	23.1	88.9	1.7
74	64	1.04	29.2	1.8	32.0	3.3	417.2	102.5	29.2	1.8
75	89	0.69	71.5	2.5	73.5	6.8	491.1	221.7	71.5	2.5
76	169	1.07	1335.9	7.6	1365.0	4.8	1487.2	7.0	1487.2	7.0
77	287	2.02	213.6	1.8	193.6	2.5	217.4	15.8	213.6	1.8
78	120	0.31	177.1	4.4	166.8	5.2	231.2	78.0	177.1	4.4
79	233	0.62	177.9	3.1	158.3	4.0	194.4	33.6	177.9	3.1
80	342	0.81	160.5	2.2	181.7	5.2	178.3	42.8	160.5	2.2

81	82	1.43	976.9	19.1	867.8	14.0	976.1	60.5	976.1	60.5
82	126	0.45	31.5	0.8	32.2	1.9	529.5	76.2	31.5	0.8
83	671	2.39	1503.3	16.3	1356.7	6.8	1434.7	12.8	1434.7	12.8
84	301	1.63	1490.5	18.4	1711.0	9.3	1665.1	9.7	1665.1	9.7
85	89	0.64	4.1	0.1	3.9	0.3	260.6	54.0	4.1	0.1
86	112	0.63	1527.9	18.6	1659.3	7.4	1545.2	14.1	1545.2	14.1
87	189	1.52	1755.9	16.0	1769.5	8.3	1646.2	9.0	1646.2	9.0
88	253	1.60	229.3	2.3	212.3	2.5	224.1	17.1	229.3	2.3
89	128	1.12	53.7	1.5	59.6	2.4	304.0	68.1	53.7	1.5
90	167	0.99	57.8	1.2	58.1	1.8	180.2	36.6	57.8	1.2
91	167	0.33	31.1	0.6	28.5	1.3	274.6	51.4	31.1	0.6
92	439	4.00	1719.2	40.4	1662.7	13.6	1776.2	23.1	1776.2	23.1
93	90	0.98	1613.8	10.2	1560.8	6.7	1690.7	8.4	1690.7	8.4
94	86	0.88	267.5	4.3	267.3	5.6	273.5	34.6	267.5	4.3
95	950	2.53	64.9	1.3	68.2	1.6	104.0	49.3	64.9	1.3
96	135	0.98	230.2	2.3	261.3	4.1	259.1	19.4	230.2	2.3
97	56	1.07	1121.6	24.5	1044.7	24.7	998.3	91.3	998.3	91.3
98	200	1.09	5.7	0.1	5.2	0.2	172.6	32.1	5.7	0.1
99	211	1.76	1403.1	15.7	1482.8	7.3	1538.7	11.2	1538.7	11.2
100	142	0.39	32.6	0.8	32.6	1.3	230.7	54.8	32.6	0.8
101	457	3.03	77.4	1.2	74.5	1.9	147.5	29.9	77.4	1.2
102	129	1.05	86.7	1.8	87.8	2.7	233.8	39.6	86.7	1.8
103	252	1.65	1768.9	14.1	1823.6	5.9	1606.7	5.7	1606.7	5.7
104	361	1.08	473.4	12.5	485.8	8.3	406.8	16.6	473.4	12.5
105	248	3.55	61.9	2.6	59.3	2.0	196.3	48.8	61.9	2.6
106	125	2.18	1061.7	17.6	1219.6	9.6	1253.1	26.1	1253.1	26.1
107	36	0.63	1068.4	19.8	1233.8	16.2	1187.7	23.1	1187.7	23.1
108	214	1.55	5.1	0.1	5.0	0.2	171.0	34.1	5.1	0.1
109	162	1.12	31.6	0.7	29.9	1.6	306.4	69.7	31.6	0.7
110	1185	3.35	1234.5	9.9	1248.0	5.9	1443.3	5.9	1443.3	5.9

Sample 9: Playa Bagdad, Mexico (Surface Sand)

#	U (ppm)	U/Th	$^{206}Pb/^{238}U$	± 2s	$^{207}Pb/^{235}U$	± 2s	$^{207}Pb/^{206}Pb$	± 2s	U-Pb Age	± 2s
1	184	5.25	75.1	2.3	69.5	0.9	246.0	35.4	75.1	2.3
2	161	1.69	90.5	2.2	92.6	1.6	151.7	23.0	90.5	2.2
3	101	0.97	218.7	4.7	219.1	2.2	231.9	38.8	218.7	4.7
4	60	0.70	1153.7	7.0	1146.9	10.8	1109.8	11.7	1109.8	11.7
5	211	1.54	1331.0	7.4	1303.2	13.5	1363.3	10.9	1363.3	10.9
6	134	0.96	243.8	3.5	240.4	2.1	245.2	18.7	243.8	3.5
7	101	0.60	1465.0	6.9	1558.8	16.3	1563.5	11.8	1563.5	11.8
8	41	0.81	1499.0	6.6	1554.7	13.0	1604.6	11.1	1604.6	11.1
9	46	1.64	1104.8	9.3	1080.4	10.0	1133.3	12.4	1133.3	12.4
10	282	0.86	167.2	3.1	156.3	1.9	201.9	31.5	167.2	3.1
11	181	1.24	62.2	1.8	59.7	1.0	178.9	26.6	62.2	1.8
12	83	0.87	28.9	2.8	28.5	1.2	499.3	106.7	28.9	2.8
13	33	0.68	1077.4	13.9	1092.6	17.9	1059.8	25.0	1059.8	25.0
14	139	0.61	142.9	3.2	147.2	2.8	172.0	25.5	142.9	3.2
15	234	0.80	189.5	2.2	189.5	1.3	182.2	16.8	189.5	2.2
16	169	1.19	1582.4	4.9	1619.6	10.1	1605.7	4.9	1605.7	4.9
17	75	0.67	34.9	2.5	34.1	1.3	338.8	78.1	34.9	2.5
18	81	0.59	4.0	0.3	3.8	0.1	243.1	50.9	4.0	0.3
19	274	5.21	74.1	1.4	72.9	1.0	122.9	20.9	74.1	1.4
20	44	0.63	124.1	5.2	123.6	2.9	336.5	56.8	124.1	5.2
21	706	2.42	1382.8	7.2	1348.9	15.8	1359.3	12.7	1359.3	12.7
22	159	0.34	28.5	1.1	28.4	0.6	250.9	54.4	28.5	1.1
23	156	0.86	76.2	2.6	78.8	1.6	169.9	30.8	76.2	2.6
24	453	2.83	217.9	1.7	222.6	1.8	223.6	11.7	217.9	1.7
25	101	0.65	39.4	2.2	35.0	1.0	272.2	73.9	39.4	2.2
26	479	0.94	55.9	1.1	53.4	0.8	111.8	25.8	55.9	1.1
27	167	1.06	88.3	2.7	85.3	2.0	207.4	38.0	88.3	2.7
28	147	1.82	961.4	6.4	979.8	9.8	1037.7	12.1	1037.7	12.1
29	195	1.35	5.1	0.2	5.5	0.1	178.2	30.1	5.1	0.2
30	305	1.01	462.5	8.9	442.3	11.6	437.6	15.4	462.5	8.9
31	246	3.34	62.5	1.9	63.7	2.2	169.3	48.5	62.5	1.9
32	320	1.78	1304.9	6.8	1226.0	11.9	1376.0	4.8	1376.0	4.8
33	144	2.00	936.5	8.8	978.3	13.6	992.3	12.7	992.3	12.7
34	113	1.86	178.9	4.7	178.2	2.1	200.3	28.3	178.9	4.7
35	540	1.49	227.2	2.1	225.5	2.3	236.0	16.7	227.2	2.1
36	261	2.70	64.6	1.6	64.7	1.3	120.4	28.7	64.6	1.6
37	243	1.72	223.3	2.6	220.9	2.3	230.7	16.4	223.3	2.6
38	236	1.09	162.8	2.3	162.2	1.7	185.3	20.5	162.8	2.3
39	300	3.13	1485.2	11.8	1429.5	29.6	1585.1	14.0	1585.1	14.0

40	176	2.59	909.2	4.7	921.2	5.3	909.9	8.5	909.9	8.5
41	84	14.00	187.1	8.1	171.4	4.1	265.4	50.7	187.1	8.1
42	414	2.82	73.8	1.9	72.3	1.1	152.2	27.7	73.8	1.9
43	85	0.48	69.0	2.9	70.4	1.6	234.4	42.8	69.0	2.9
44	93	0.92	35.9	3.0	35.0	1.4	453.8	119.1	35.9	3.0
45	137	0.63	1342.5	10.8	1181.4	15.7	1365.4	12.9	1365.4	12.9
46	64	0.92	1421.4	15.5	1418.7	26.0	1320.7	9.1	1320.7	9.1
47	264	0.58	159.3	2.1	152.9	1.4	152.2	20.9	159.3	2.1
48	144	1.03	30.6	1.5	27.6	0.8	275.1	63.7	30.6	1.5
49	545	1.83	225.8	3.3	228.3	3.0	235.3	16.4	225.8	3.3
50	87	0.92	580.8	8.5	556.5	7.3	602.2	29.9	580.8	8.5
51	17	0.57	38.6	7.1	43.0	2.1	699.1	157.9	38.6	7.1
52	286	0.96	30.3	1.3	30.4	0.6	285.2	51.5	30.3	1.3
53	60	0.95	31.3	3.2	32.1	1.8	405.4	95.2	31.3	3.2
54	115	0.64	11.5	0.3	11.4	0.2	216.1	41.3	11.5	0.3
55	110	0.89	219.0	4.9	213.6	2.8	249.4	28.6	219.0	4.9
56	1032	1.78	215.9	1.7	217.9	1.3	222.3	11.9	215.9	1.7
57	13	0.76	1028.9	33.7	995.1	30.6	1023.4	40.5	1023.4	40.5
58	210	1.06	52.3	1.8	55.7	0.8	173.3	34.2	52.3	1.8
59	154	1.01	57.6	1.8	52.2	0.9	168.9	31.6	57.6	1.8
60	316	0.85	154.3	4.6	161.5	2.0	179.4	40.7	154.3	4.6
61	46	0.25	26.3	3.2	27.4	1.2	530.4	113.7	26.3	3.2
62	343	1.16	168.7	2.3	170.4	1.5	162.6	18.8	168.7	2.3
63	147	1.07	238.2	4.4	250.5	2.3	232.2	20.9	238.2	4.4
64	1008	3.22	1309.6	5.0	1231.9	9.4	1367.0	5.8	1367.0	5.8
65	171	1.39	1627.3	8.3	1671.3	15.3	1583.8	8.6	1583.8	8.6
66	90	0.91	1505.4	6.1	1572.2	9.9	1627.8	8.2	1627.8	8.2
67	126	1.02	52.4	2.6	57.6	1.8	129.1	37.6	52.4	2.6
68	26	0.28	27.1	4.8	26.7	1.5	663.2	149.3	27.1	4.8
69	72	1.06	1108.2	11.8	1053.4	15.9	1035.6	10.4	1035.6	10.4
70	84	0.71	73.0	6.3	75.6	2.5	479.3	219.9	73.0	6.3
71	263	1.94	196.9	2.3	202.8	1.6	204.6	16.5	196.9	2.3
72	215	1.63	1674.0	6.2	1748.9	12.4	1731.1	5.5	1731.1	5.5
73	185	1.69	1385.1	4.9	1382.1	9.6	1312.9	5.5	1312.9	5.5
74	148	0.40	32.1	1.2	33.1	0.8	205.8	46.8	32.1	1.2
75	65	5.96	1122.4	9.6	1093.1	12.0	1105.8	10.1	1105.8	10.1
76	77	0.88	252.5	5.0	250.8	3.7	230.4	32.2	252.5	5.0
77	174	0.98	52.2	1.7	55.9	1.1	148.7	34.0	52.2	1.7
78	234	1.68	30.7	0.8	28.9	0.6	142.5	36.0	30.7	0.8
79	528	2.53	1276.9	6.2	1313.6	9.5	1465.5	4.7	1465.5	4.7
80	135	0.97	37.4	1.5	33.1	0.7	283.0	50.1	37.4	1.5

81	179	1.10	31.1	1.3	31.2	0.5	267.2	47.8	31.1	1.3
82	129	0.97	57.6	2.2	54.5	1.5	330.4	67.1	57.6	2.2
83	57	0.86	2609.7	6.6	2553.8	14.6	2462.6	5.8	2462.6	5.8
84	1054	0.95	180.7	2.6	178.0	2.4	266.6	19.1	180.7	2.6
85	163	1.45	55.8	1.6	55.4	1.0	169.5	30.6	55.8	1.6
86	152	1.47	58.6	2.2	58.6	1.2	220.9	41.0	58.6	2.2
87	243	0.60	173.0	2.8	161.1	1.8	160.1	26.9	173.0	2.8
88	80	2.17	74.4	3.0	71.0	1.3	318.7	42.3	74.4	3.0
89	202	1.44	1413.2	7.9	1325.2	12.7	1334.2	5.6	1334.2	5.6
90	175	1.49	2439.3	13.9	2521.4	24.5	2507.5	10.1	2507.5	10.1
91	114	0.76	37.7	2.8	34.0	0.9	426.6	99.5	37.7	2.8
92	235	1.21	96.5	2.6	90.1	1.5	128.1	27.9	96.5	2.6
93	120	0.49	28.7	1.8	27.4	0.8	454.9	70.9	28.7	1.8
94	119	1.79	201.1	4.3	214.9	2.8	264.2	29.6	201.1	4.3
95	92	0.66	153.9	4.4	149.9	2.5	234.6	31.9	153.9	4.4

Sample 10: Rio Bravo (Grande) (Mexico, Surface Sand)

#	U (ppm)	U/Th	$^{206}Pb/^{238}U$	± 2s	$^{207}Pb/^{235}U$	± 2s	$^{207}Pb/^{206}Pb$	± 2s	U-Pb Age	± 2s
1	89	0.95	36.2	2.5	35.4	5.3	9.8	299.5	36.2	2.5
2	97	1.20	34.8	2.0	40.6	3.3	257.2	228.2	34.8	2.0
3	55	0.88	2911.8	14.5	2944.4	6.5	2529.4	6.3	2529.4	6.3
4	143	0.52	28.9	0.9	30.9	1.7	521.3	69.8	28.9	0.9
5	128	1.12	52.8	2.0	59.3	2.5	136.9	37.8	52.8	2.0
6	187	1.81	103.9	1.9	97.4	2.2	146.0	23.2	103.9	1.9
7	344	1.84	1352.7	11.7	1436.7	7.3	1375.7	4.6	1375.7	4.6
8	1130	1.86	204.4	1.5	236.5	1.9	250.5	11.3	204.4	1.5
9	100	1.42	1406.4	20.6	1570.0	12.6	1627.6	27.2	1627.6	27.2
10	149	1.00	6.0	0.1	6.1	0.2	167.2	32.3	6.0	0.1
11	47	0.92	1367.1	12.1	1554.6	9.7	1439.3	14.4	1439.3	14.4
12	37	0.92	111.9	5.5	110.4	12.8	217.7	230.6	111.9	5.5
13	79	1.32	958.1	18.8	870.4	15.5	909.9	61.4	909.9	61.4
14	475	1.01	392.5	6.8	407.6	6.4	648.0	38.0	392.5	6.8
15	299	0.64	151.8	1.4	152.6	2.3	160.1	20.7	151.8	1.4
16	76	2.21	1509.7	27.9	1381.3	18.0	1342.8	27.2	1342.8	27.2
17	143	1.40	1083.2	13.5	1168.8	9.0	1012.1	28.0	1012.1	28.0
18	89	1.13	1038.9	15.8	993.8	12.7	1033.8	36.8	1033.8	36.8
19	253	0.94	50.2	1.8	51.0	3.3	81.9	133.4	50.2	1.8
20	335	0.82	154.7	2.2	176.2	3.1	224.1	31.2	154.7	2.2
21	75	0.90	31.7	1.1	33.4	2.8	482.0	105.5	31.7	1.1
22	265	0.65	154.8	1.8	161.6	3.1	171.6	24.8	154.8	1.8
23	412	3.74	1840.6	43.1	1601.7	16.4	1604.0	24.9	1604.0	24.9
24	209	4.95	73.7	0.9	84.4	2.5	235.2	35.8	73.7	0.9
25	70	0.72	2367.4	32.8	2349.9	13.3	2645.5	21.2	2645.5	21.2
26	405	2.77	1834.7	30.7	1817.7	14.8	1577.1	23.7	1577.1	23.7
27	307	0.51	160.8	3.7	179.7	4.8	158.2	86.3	160.8	3.7
28	142	0.96	1487.0	16.0	1705.2	8.2	1699.9	19.5	1699.9	19.5
29	74	1.11	1799.5	25.0	1774.8	17.6	1528.6	24.2	1528.6	24.2
30	118	0.72	37.2	1.2	41.5	2.1	321.0	87.4	37.2	1.2
31	187	1.59	5.5	0.2	5.4	0.4	83.6	136.3	5.5	0.2
32	223	1.14	161.9	2.0	164.1	2.5	194.4	22.2	161.9	2.0
33	83	1.00	523.2	9.4	495.5	10.1	521.3	59.2	523.2	9.4
34	253	0.72	978.7	13.7	1042.7	7.2	1088.4	24.2	1088.4	24.2
35	171	0.36	26.9	0.6	29.7	1.1	274.6	59.6	26.9	0.6
36	52	1.10	1676.9	24.5	1560.6	13.5	1727.6	32.7	1727.6	32.7
37	174	1.15	93.3	2.3	96.1	2.9	213.1	43.1	93.3	2.3
38	307	3.48	1701.2	33.6	1699.8	14.2	1805.7	13.5	1805.7	13.5
39	108	0.63	134.9	2.5	117.6	3.8	235.9	41.4	134.9	2.5

40	21	0.56	42.0	2.0	37.4	6.2	686.8	129.9	42.0	2.0
41	168	1.81	1364.1	9.2	1393.3	5.0	1352.9	5.7	1352.9	5.7
42	267	0.31	94.7	3.9	98.1	7.5	194.3	161.3	94.7	3.9
43	424	4.76	1060.5	11.8	971.8	7.0	953.6	19.0	953.6	19.0
44	184	1.36	60.4	1.1	60.6	2.0	175.5	31.5	60.4	1.1
45	72	5.80	1131.8	13.8	1213.7	9.0	1157.2	10.6	1157.2	10.6
46	357	0.65	350.4	10.9	343.2	13.3	324.6	99.4	350.4	10.9
47	45	0.96	1272.1	25.1	1431.5	16.5	1511.6	45.0	1511.6	45.0
48	210	4.35	1543.1	21.9	1755.5	12.1	1519.8	22.9	1519.8	22.9
49	927	3.58	103.9	6.0	105.1	6.4	95.9	111.6	103.9	6.0
50	115	1.89	1060.5	16.4	1230.7	9.3	1239.6	30.0	1239.6	30.0
51	442	3.12	247.6	1.9	218.7	1.9	232.7	11.0	247.6	1.9
52	785	1.08	66.2	1.3	69.6	2.0	70.2	71.0	66.2	1.3
53	46	1.92	1221.8	26.7	1358.0	18.0	1521.6	33.5	1521.6	33.5
54	200	1.03	55.8	0.8	59.0	1.8	189.8	34.1	55.8	0.8
55	69	0.79	1364.4	23.1	1451.5	13.1	1522.5	38.2	1522.5	38.2
56	216	1.23	99.7	1.5	101.7	2.8	136.5	29.9	99.7	1.5
57	313	1.03	30.4	0.6	35.5	1.3	287.3	52.0	30.4	0.6
58	158	1.90	1686.0	18.2	1703.9	8.6	1686.4	17.7	1686.4	17.7
59	97	1.50	1410.2	27.4	1618.1	13.6	1630.1	42.3	1630.1	42.3
60	109	0.66	1588.9	21.8	1538.0	12.0	1619.1	24.0	1619.1	24.0
61	345	1.09	471.6	12.1	457.2	8.6	420.8	14.5	471.6	12.1
62	340	5.94	2064.9	25.1	1822.9	12.1	1854.0	20.9	1854.0	20.9
63	40	0.96	5.2	0.5	4.9	1.0	467.4	164.5	5.2	0.5
64	111	0.86	230.0	3.1	241.5	5.3	268.6	32.8	230.0	3.1
65	43	0.89	256.6	10.8	223.9	13.3	376.3	156.3	256.6	10.8
66	246	3.06	68.8	1.2	73.1	1.5	129.8	31.5	68.8	1.2
67	135	1.36	1018.3	16.4	1025.6	7.9	1076.9	30.4	1076.9	30.4
68	140	0.94	225.3	2.0	229.1	3.9	278.3	29.6	225.3	2.0
69	242	1.84	29.5	0.6	32.1	1.0	170.0	38.4	29.5	0.6
70	106	0.65	158.4	2.5	158.8	5.0	245.8	37.0	158.4	2.5
71	330	0.86	169.6	2.3	148.8	3.8	163.6	45.1	169.6	2.3
72	272	0.96	205.2	1.5	193.1	2.3	176.1	19.6	205.2	1.5
73	30	0.83	1073.2	22.7	1034.7	16.6	1040.0	49.4	1040.0	49.4
74	85	0.69	40.3	1.3	42.4	3.6	257.1	54.9	40.3	1.3
75	13	0.91	1081.2	33.7	1149.3	31.6	1055.6	42.1	1055.6	42.1
76	155	2.67	406.6	25.7	398.0	16.7	402.3	139.5	406.6	25.7
77	146	1.09	30.9	0.8	33.0	1.7	270.8	61.5	30.9	0.8
78	192	1.37	58.9	1.1	58.3	1.6	192.8	34.2	58.9	1.1
79	94	0.99	661.0	10.3	650.7	8.4	618.1	47.9	661.0	10.3
80	263	1.34	1493.1	24.8	1655.4	12.1	1793.4	18.7	1793.4	18.7

81	539	1.98	241.9	3.1	233.0	3.5	287.0	18.4	241.9	3.1
82	256	0.53	39.7	1.4	40.0	2.5	209.5	133.6	39.7	1.4
83	181	1.61	63.3	1.1	61.3	1.8	201.2	32.0	63.3	1.1
84	66	1.26	1089.2	11.8	1167.8	8.3	1040.4	13.8	1040.4	13.8
85	170	1.02	978.5	21.1	1025.2	15.8	1008.6	42.4	1008.6	42.4
86	183	1.04	1748.6	25.3	1671.7	11.3	1715.7	16.7	1715.7	16.7
87	235	1.02	387.3	9.4	408.7	8.6	469.3	54.1	387.3	9.4
88	100	0.61	1457.3	16.4	1583.9	7.0	1746.1	12.5	1746.1	12.5
89	452	15.43	37.8	2.3	39.5	4.3	250.0	79.1	37.8	2.3
90	93	0.84	644.9	7.8	670.8	9.9	637.4	28.8	644.9	7.8
91	58	1.19	1256.4	24.9	1376.2	14.1	1321.5	35.7	1321.5	35.7
92	45	1.26	1141.9	22.9	1326.2	16.9	1185.0	46.9	1185.0	46.9
93	353	1.02	1307.1	22.1	1377.5	11.1	1453.5	23.0	1453.5	23.0
94	127	2.05	217.7	2.2	205.4	4.6	199.9	28.1	217.7	2.2
95	44	0.72	135.6	3.2	134.3	6.0	350.9	57.6	135.6	3.2
96	186	1.00	1487.7	21.2	1454.5	11.1	1505.3	20.1	1505.3	20.1
97	121	1.71	236.1	3.2	239.8	4.3	242.9	30.9	236.1	3.2
98	195	1.02	167.4	5.3	160.5	6.1	237.3	96.2	167.4	5.3
99	283	5.62	75.5	1.0	70.3	1.5	129.5	24.2	75.5	1.0
100	153	0.60	1344.8	15.1	1335.0	11.4	1395.8	12.4	1395.8	12.4

Sample 11: Brownsville Ship Channel (Surface Sand)

#	U (ppm)	U/Th	$^{206}Pb/^{238}U$	± 2s	$^{207}Pb/^{235}U$	± 2s	$^{207}Pb/^{206}Pb$	± 2s	U-Pb Age	± 2s
1	175	0.93	903.2	23.9	906.9	17.7	1027.3	47.7	1027.3	47.7
2	110	1.78	211.5	2.2	206.6	4.9	217.1	29.7	211.5	2.2
3	446	3.18	76.9	1.2	82.5	1.8	163.7	29.6	76.9	1.2
4	81	1.82	58.5	1.6	60.0	2.9	297.1	60.0	58.5	1.6
5	165	0.93	1094.2	13.8	1035.0	11.8	1068.8	33.7	1068.8	33.7
6	341	0.78	80.4	4.1	80.0	6.8	65.4	179.5	80.4	4.1
7	229	1.30	105.2	1.6	93.3	2.8	129.0	28.9	105.2	1.6
8	47	2.04	1015.8	21.3	975.9	17.1	1047.9	48.2	1047.9	48.2
9	263	1.32	1695.0	22.6	1514.4	11.5	1667.1	18.5	1667.1	18.5
10	183	1.40	354.2	5.8	322.6	6.6	327.1	55.9	354.2	5.8
11	164	1.76	1806.9	18.4	1786.9	8.3	1797.0	19.0	1797.0	19.0
12	573	1.95	239.3	3.1	245.5	3.4	273.5	15.8	239.3	3.1
13	226	1.63	1221.4	23.5	1188.5	12.1	1208.3	29.7	1208.3	29.7
14	237	1.66	177.6	3.3	165.3	4.2	176.4	69.9	177.6	3.3
15	330	1.48	1523.9	24.2	1579.2	14.8	1553.4	26.3	1553.4	26.3
16	130	0.91	1736.3	14.7	1529.6	8.1	1708.5	18.2	1708.5	18.2
17	450	1.83	1113.1	15.0	1171.0	8.0	1285.7	20.4	1285.7	20.4
18	178	1.01	1385.7	23.0	1366.6	12.1	1407.0	21.6	1407.0	21.6
19	445	3.00	234.6	2.1	247.4	1.8	218.7	11.5	234.6	2.1
20	89	0.87	1678.3	11.8	1726.1	5.9	1678.6	8.9	1678.6	8.9
21	363	0.82	1447.1	9.5	1481.3	7.6	1338.7	15.9	1338.7	15.9
22	56	1.00	1140.2	24.7	1188.3	23.0	1139.8	94.0	1139.8	94.0
23	261	0.32	89.7	3.9	103.8	6.9	186.8	153.3	89.7	3.9
24	43	1.17	1187.4	23.5	1141.5	16.6	1242.2	45.3	1242.2	45.3
25	259	1.90	32.2	0.6	29.2	0.8	169.4	38.6	32.2	0.6
26	28	0.83	1019.1	23.2	1018.9	14.7	1158.8	47.5	1158.8	47.5
27	869	5.49	44.2	1.0	49.7	1.2	125.0	61.9	44.2	1.0
28	140	1.37	1514.8	26.1	1449.3	14.1	1437.8	27.3	1437.8	27.3
29	119	0.65	125.8	2.6	134.0	3.9	217.2	44.3	125.8	2.6
30	564	6.72	268.1	3.7	253.2	4.9	271.9	50.1	268.1	3.7
31	121	0.63	37.0	1.1	40.7	2.2	302.2	73.9	37.0	1.1
32	178	2.24	1370.4	28.5	1493.3	15.3	1398.5	25.0	1398.5	25.0
33	880	3.18	102.9	6.7	92.4	5.6	105.9	104.6	102.9	6.7
34	237	1.63	518.6	7.9	530.5	7.9	508.7	41.2	518.6	7.9
35	159	1.00	84.9	1.7	82.7	2.9	171.4	32.9	84.9	1.7
36	79	1.47	913.6	17.7	970.9	15.5	862.7	58.3	862.7	58.3
37	133	1.35	1122.8	12.2	1128.4	8.3	1140.0	25.6	1140.0	25.6
38	152	0.98	1636.2	19.2	1694.9	8.4	1789.5	23.7	1789.5	23.7
39	330	1.26	1702.9	21.7	1621.7	8.1	1778.5	16.8	1778.5	16.8

40	363	1.76	1323.3	11.8	1377.2	6.5	1412.2	5.1	1412.2	5.1
41	121	1.28	1107.6	14.0	1037.9	9.1	1133.5	32.2	1133.5	32.2
42	119	0.34	162.6	4.0	175.7	5.6	240.3	77.8	162.6	4.0
43	157	0.42	31.6	0.8	34.5	1.3	228.4	53.2	31.6	0.8
44	50	0.25	28.4	1.2	29.9	3.1	611.3	127.9	28.4	1.2
45	333	1.03	241.6	4.8	267.7	4.8	283.5	71.2	241.6	4.8
46	50	1.01	1193.0	8.2	1192.2	9.4	1142.6	12.3	1142.6	12.3
47	109	1.55	1059.4	16.2	1064.8	11.4	1139.0	30.5	1139.0	30.5
48	75	1.14	1543.8	25.9	1601.4	18.2	1601.9	26.7	1601.9	26.7
49	192	5.27	74.9	1.0	81.6	2.3	254.2	36.5	74.9	1.0
50	93	1.32	1620.9	27.8	1706.3	15.4	1541.0	40.3	1541.0	40.3
51	319	2.13	1775.2	21.9	1769.5	10.5	1568.1	23.5	1568.1	23.5
52	200	4.50	1738.8	22.6	1763.0	11.9	1542.1	23.6	1542.1	23.6
53	151	0.36	27.4	0.6	30.7	1.3	268.0	55.2	27.4	0.6
54	165	1.80	100.4	1.7	93.0	2.2	153.7	23.1	100.4	1.7
55	39	0.72	1096.1	12.4	1093.8	8.4	1140.2	20.3	1140.2	20.3
56	409	0.96	391.8	6.3	448.2	7.0	634.2	38.6	391.8	6.3
57	404	2.54	1729.5	32.1	1813.9	14.1	1843.6	26.9	1843.6	26.9
58	180	1.08	1476.8	19.3	1450.3	9.4	1361.8	23.3	1361.8	23.3
59	150	1.09	1217.1	20.7	1100.4	11.4	1134.0	40.4	1134.0	40.4
60	462	0.80	105.1	1.9	100.2	2.6	125.7	73.2	105.1	1.9
61	199	0.89	217.0	3.4	220.9	5.1	297.7	61.1	217.0	3.4
62	163	1.06	85.2	2.2	89.5	3.1	221.7	40.8	85.2	2.2
63	345	1.02	1421.7	23.2	1421.7	12.9	1337.7	21.8	1337.7	21.8
64	290	0.82	169.2	2.2	168.8	3.8	184.0	49.2	169.2	2.2
65	198	1.76	62.8	1.8	58.3	3.1	79.2	130.9	62.8	1.8
66	142	2.01	929.0	10.8	868.5	9.3	890.0	26.6	890.0	26.6
67	78	1.40	1066.7	12.6	1032.0	8.0	1027.8	12.8	1027.8	12.8
68	53	1.74	1386.8	21.3	1532.3	16.3	1467.0	43.9	1467.0	43.9
69	209	1.67	1592.8	21.7	1690.2	11.6	1867.9	16.2	1867.9	16.2
70	110	0.68	1496.7	20.9	1712.3	10.7	1792.9	24.5	1792.9	24.5
71	328	0.89	163.5	2.0	180.4	5.1	183.7	40.3	163.5	2.0
72	89	1.46	1635.1	19.7	1632.1	12.5	1625.5	24.5	1625.5	24.5
73	26	1.07	1083.7	16.6	1099.0	13.1	1074.4	18.6	1074.4	18.6
74	36	0.95	111.1	5.8	116.5	12.0	187.2	231.8	111.1	5.8
75	43	1.00	1352.5	26.8	1500.5	16.6	1389.9	40.5	1389.9	40.5
76	76	1.01	1486.8	19.6	1457.1	11.7	1409.8	25.1	1409.8	25.1
77	98	1.03	238.7	2.3	211.1	5.0	250.1	37.2	238.7	2.3
78	77	2.39	1318.1	30.4	1445.2	19.2	1324.0	30.3	1324.0	30.3
79	256	0.49	35.9	1.5	37.9	2.4	217.4	124.4	35.9	1.5
80	128	1.22	81.3	1.6	85.9	2.9	213.8	37.6	81.3	1.6

81	88	1.76	1785.9	30.9	1815.4	15.9	1672.9	30.6	1672.9	30.6
82	82	0.80	74.5	2.3	78.5	5.4	260.4	139.5	74.5	2.3
83	21	1.36	926.3	17.1	973.9	21.2	974.6	71.9	974.6	71.9
84	1005	0.94	188.4	2.5	204.0	2.7	247.3	19.7	188.4	2.5
85	145	2.08	993.5	13.2	1015.9	9.3	1088.6	12.4	1088.6	12.4
86	919	2.73	67.5	1.2	72.5	1.7	113.1	55.0	67.5	1.2
87	497	1.12	415.0	8.2	443.5	7.2	486.0	40.1	415.0	8.2
88	249	0.74	1053.0	13.2	1112.7	7.2	1007.5	22.4	1007.5	22.4
89	239	1.18	103.3	1.9	103.3	3.0	165.0	75.7	103.3	1.9
90	188	0.45	214.2	3.8	206.1	4.7	205.3	56.1	214.2	3.8
91	196	1.50	1453.9	20.5	1460.2	12.4	1350.9	28.2	1350.9	28.2
92	64	1.28	258.0	6.7	231.2	11.1	256.3	105.4	258.0	6.7
93	417	3.44	1796.4	41.4	1737.8	14.0	1750.6	22.9	1750.6	22.9
94	41	1.64	1461.4	25.2	1449.4	17.9	1449.9	36.4	1449.9	36.4
95	77	0.95	264.6	3.6	275.5	5.7	244.0	34.8	264.6	3.6
96	296	1.01	32.6	0.6	33.7	1.2	305.3	54.3	32.6	0.6
97	96	0.88	591.2	7.5	651.6	9.0	656.1	28.2	591.2	7.5
98	148	13.14	61.1	2.0	63.6	4.2	84.6	121.0	61.1	2.0
99	53	0.94	1441.0	13.3	1388.8	9.7	1382.8	15.0	1382.8	15.0
100	65	0.96	1498.0	27.3	1509.1	17.2	1435.3	10.7	1435.3	10.7
101	340	5.53	1864.6	24.7	1814.5	12.0	1880.9	20.8	1880.9	20.8
102	45	1.01	1117.0	18.2	965.7	14.0	1017.1	41.3	1017.1	41.3
103	94	1.12	1011.6	16.0	1066.8	12.9	1022.1	35.3	1022.1	35.3
104	244	1.07	52.4	1.8	60.2	3.7	75.5	121.0	52.4	1.8

APPENDIX B

APPENDIX B

CAMSIZER P4 Histograms

Sample 1: South Padre Island (Top of Core)

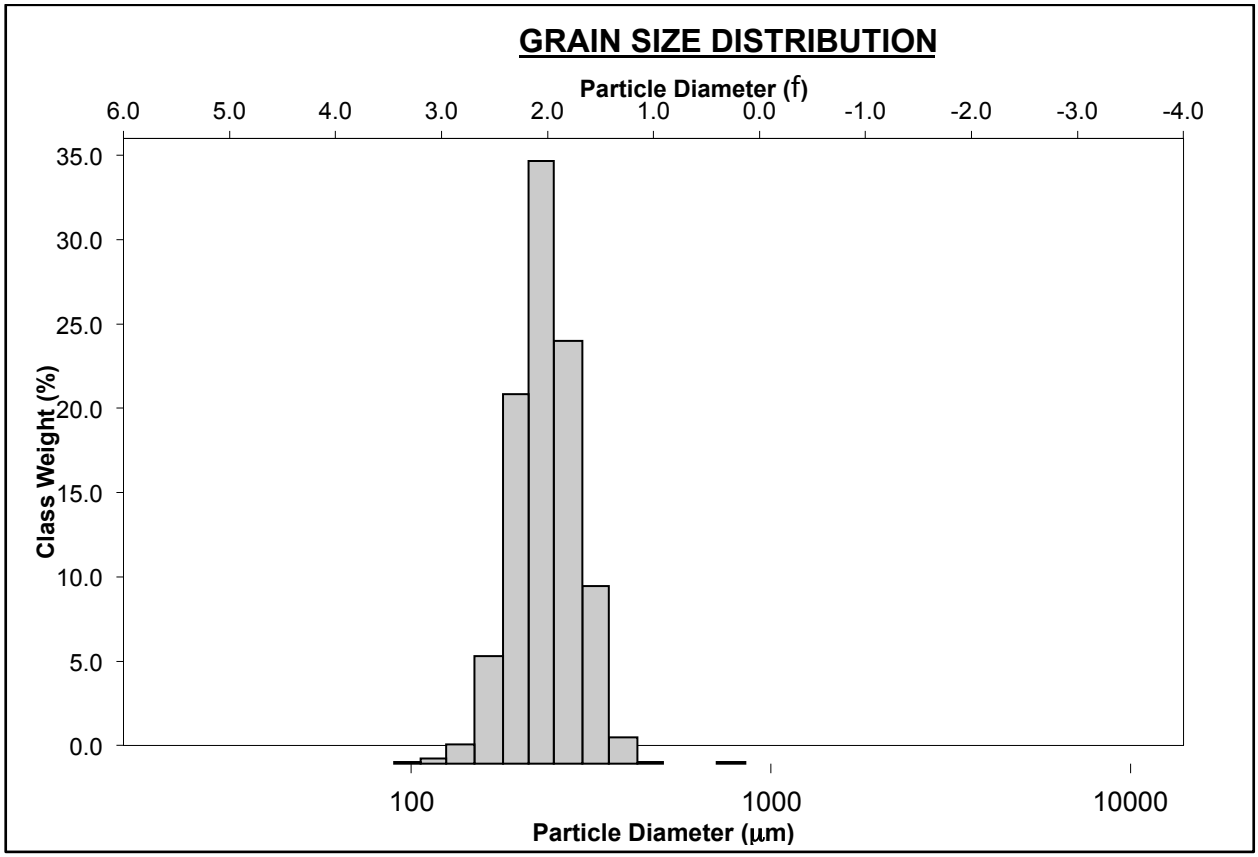

Sample 2: South Padre Island (Bottom of Core)

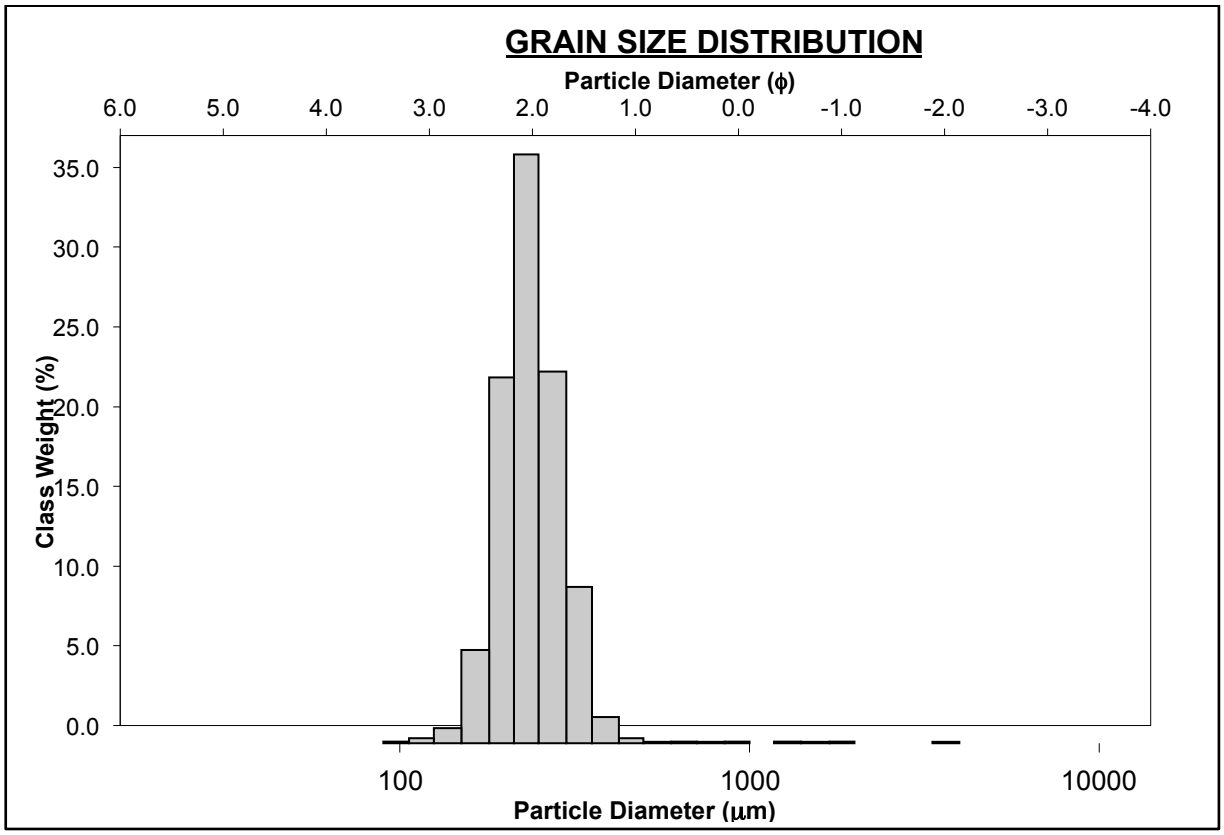

Sample 3: South Padre Island (Isla Blanca Park, Surface Sand)

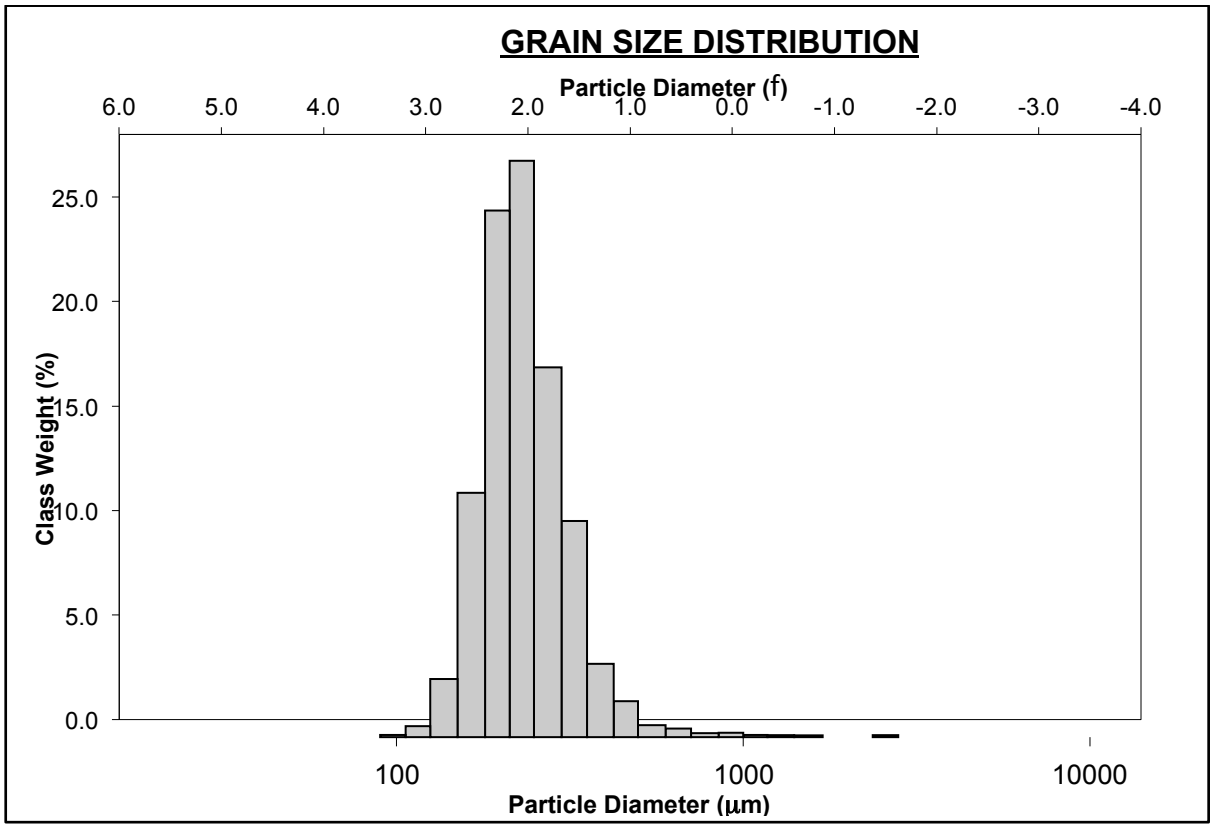

Sample 4: Boca Chica Beach (Near Brazos Santiago Pass, Surface Sand)

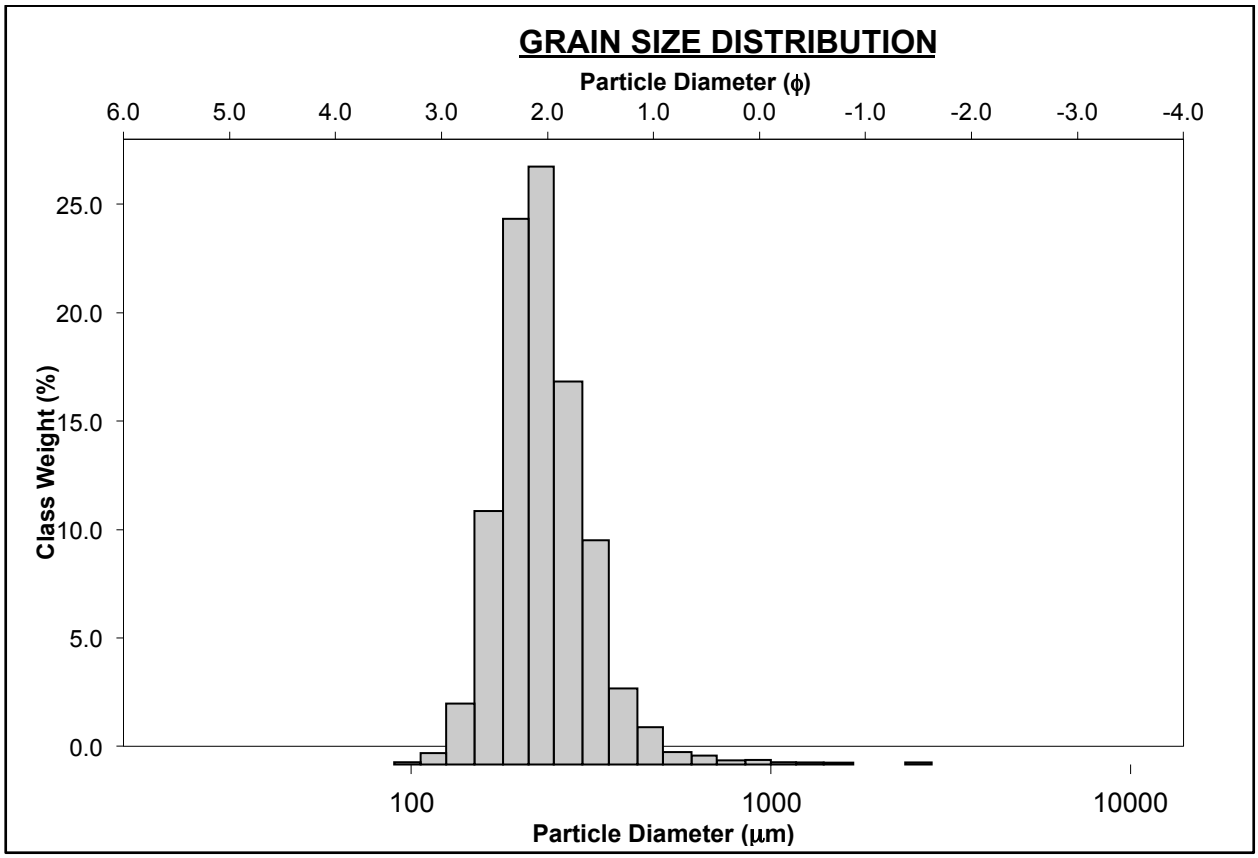

Sample 5: Boca Chica Beach (Midpoint, Surface Sand)

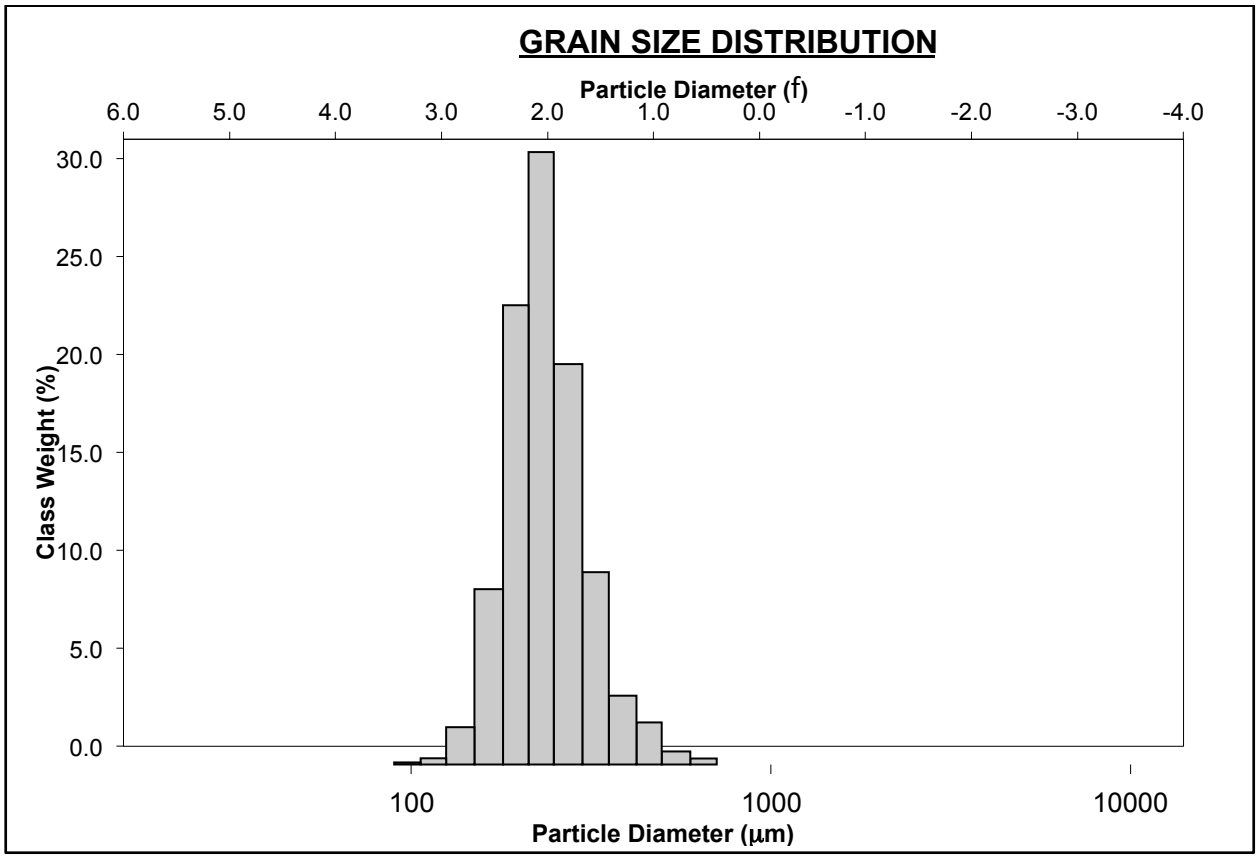

Sample 6: Boca Chica Beach (Near Mouth of River, Surface Sand)

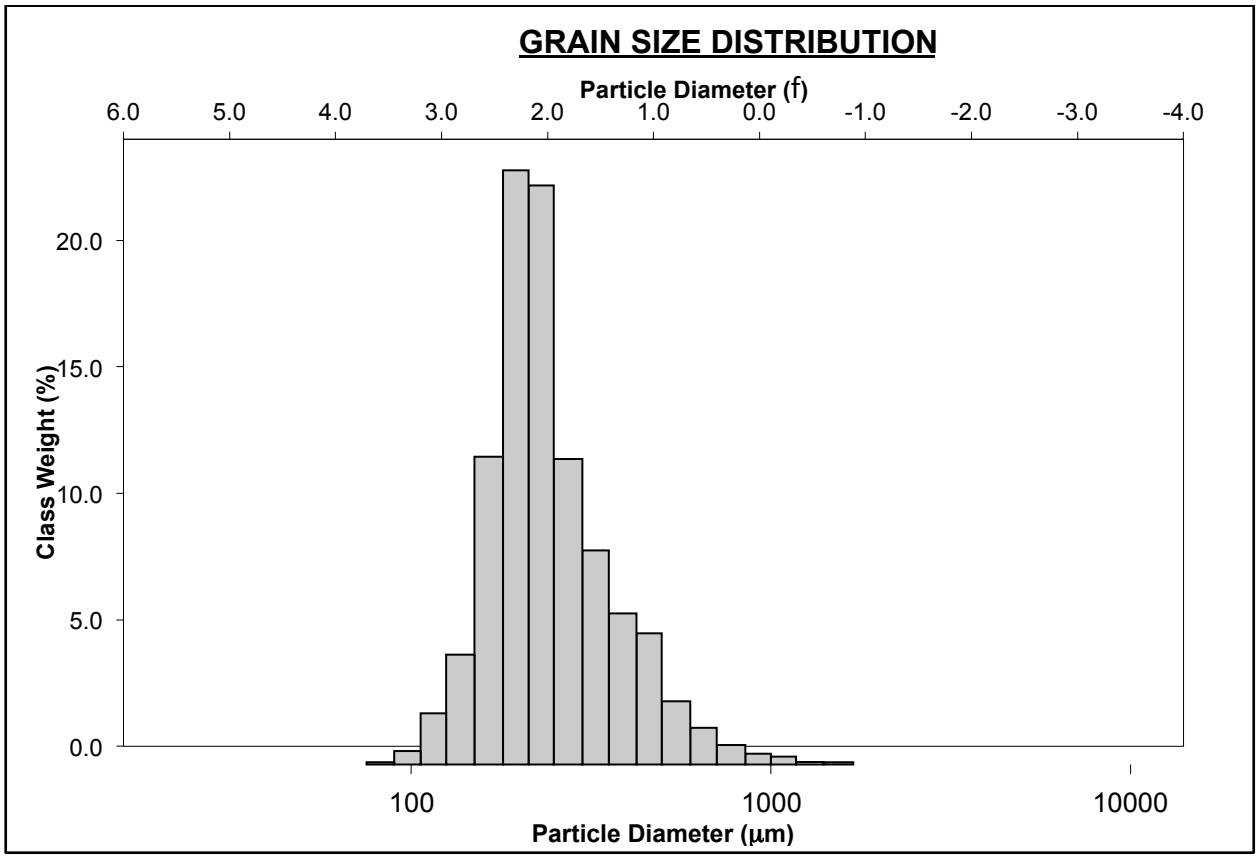

Sample 7: Boca Chica Beach (Near Mouth of River, Top of Core)

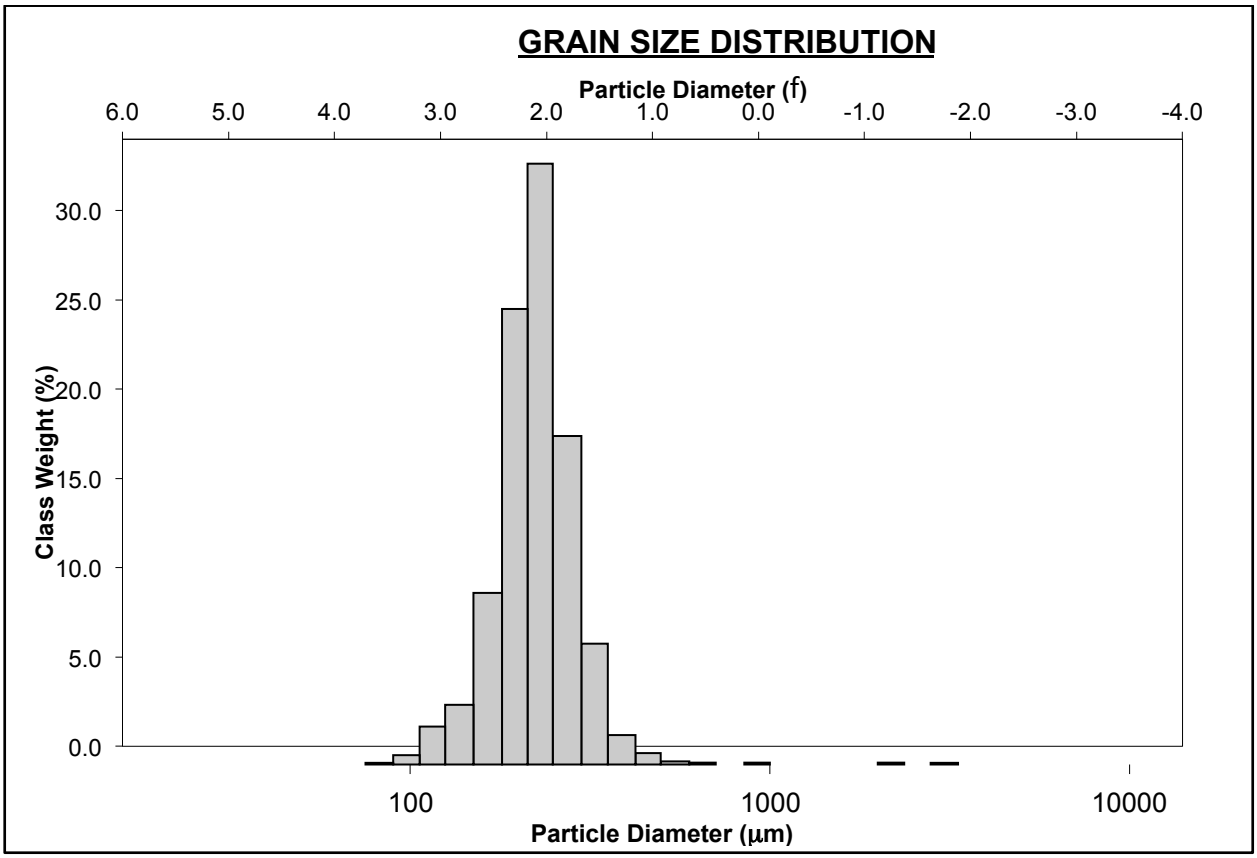

Sample 8: Boca Chica Beach (Near Mouth of River, Bottom of Core)

Too fine grained for CAMSIZER P4

Sample 9: Playa Bagdad (Mexico, Surface Sand)

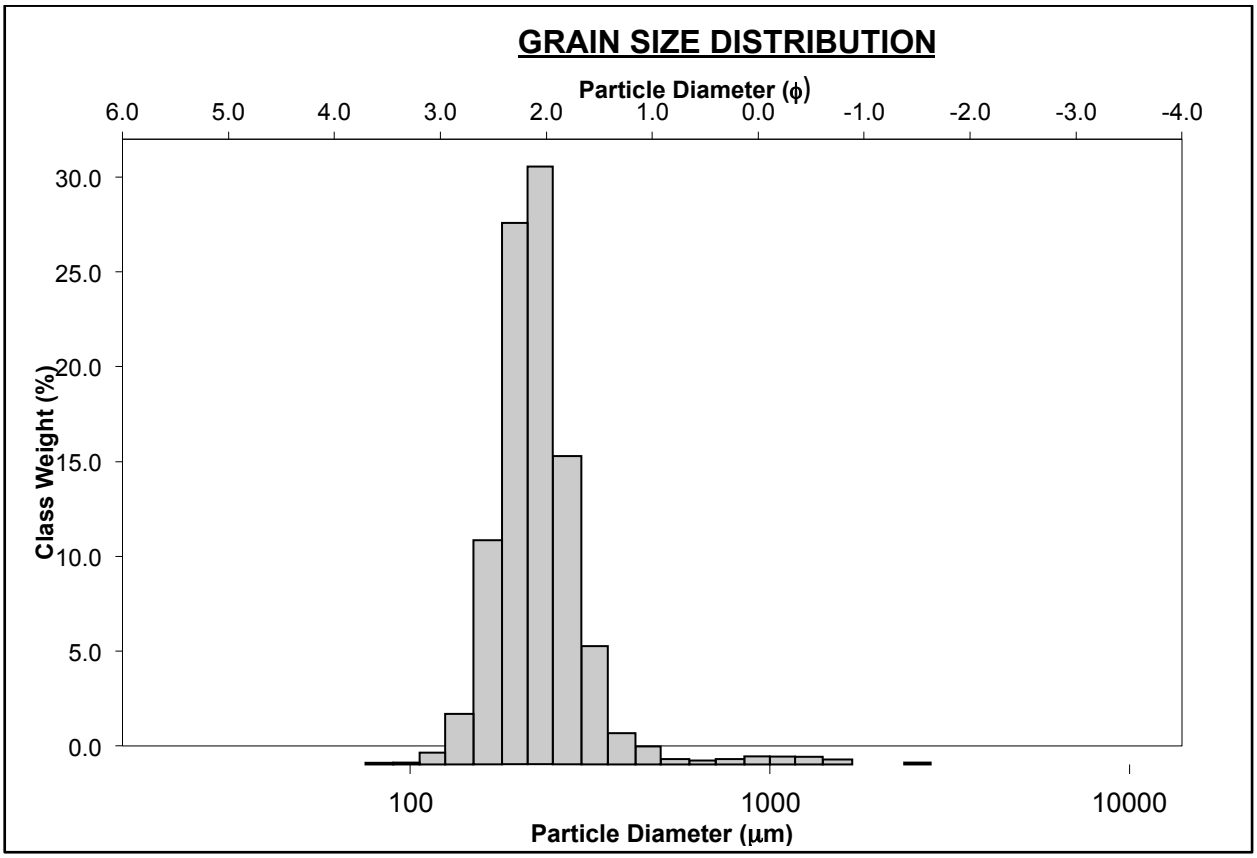

Sample 10: Rio Grande River Sand (Surface Sand)

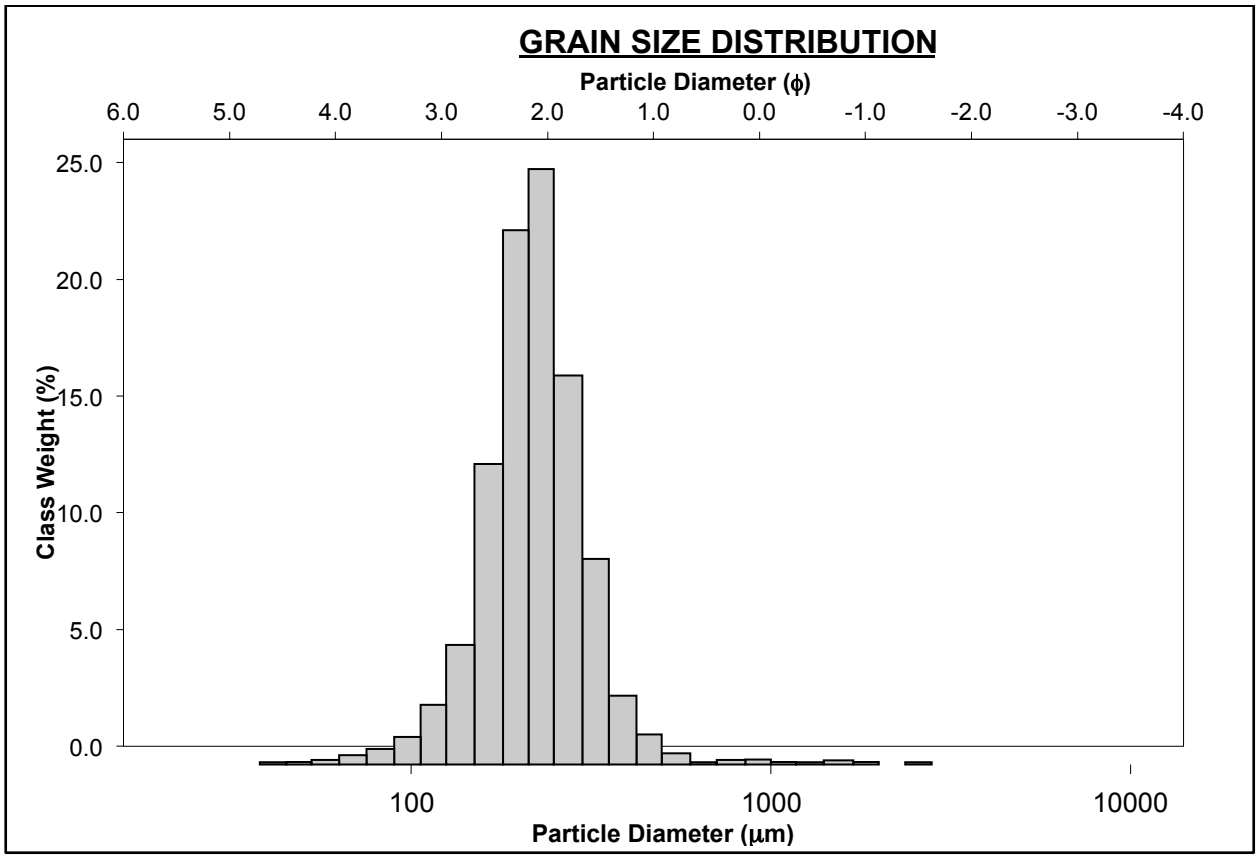

BIOGRAPHICAL SKETCH

Samantha B. Moore graduated with her undergraduate degree in 2012 with a Bachelor's of Arts in Biology with a Chemistry and Dance minor from Columbia College in Columbia, South Carolina. She earned her Master's of Science degree in Ocean, Coastal, and Environmental Science from the School of Earth, Environmental, and Marine Science at the University of Rio Grande Valley in December 2018. Prior to starting her masters, Samantha worked for two years in an environmental lab where she first began an interest in environmental science. She also has experience as a laboratory and outreach coordinator for environmental science at the University of Texas at Brownsville.

Samantha is a member of the Geological Sciences of America since 2016.

If you have any questions, please contact me at sbmoore532@gmail.com.